



SAPIENZA
UNIVERSITÀ DI ROMA

Exploring Data Aggregation and Transformations to Generalize across Visual Domains

Department of Computer, Control and Management Engineering "Antonio Ruberti", Sapienza - University of Rome

Dottorato di Ricerca in Ingegneria Informatica – XXXIII Ciclo

Candidate

Antonio D'Innocente

ID number 1792918

Thesis Advisor

Prof. Barbara Caputo

A thesis submitted in partial fulfillment of the requirements for the
degree of Doctor of Philosophy in Computer Science

January 2021

Exploring Data Aggregation and Transformations to Generalize across Visual Domains

Ph.D. thesis. Sapienza – University of Rome

© 2020 Antonio D’Innocente. All rights reserved

This thesis has been typeset by L^AT_EX and the Sapthesis class.

Author’s email: ant.dinnocente@gmail.com

Acknowledgments

Ringrazio la mia advisor, la professoressa Barbara Caputo, per avermi accolto nel suo laboratorio ed avermi fatto lavorare in prima linea nei problemi della Computer Vision. La professoressa Caputo ha una grande attitudine nel trasmettere la dedizione, mi ha insegnato cos'è e come si fa la ricerca e mi ha sempre incoraggiato a lavorare su quegli argomenti che di più mi appassionavano. Ringrazio la professoressa Tatiana Tommasi per la perfetta supervisione e per aver sempre ascoltato e valorizzato le mie idee. La professoressa Tommasi ha dato di gran lunga i più grandi contributi nei nostri lavori, in ogni aspetto, senza di lei quasi tutte le pubblicazioni descritte in questa tesi non sarebbero state possibili.

La fortuna di lavorare in diverse realtà mi ha portato a conoscere molti colleghi ed amici con cui ho condiviso un fantastico percorso: Arjan, Chiara, Fabio M. C., Fabio C., Massimiliano, Mirco, Nizar, Paolo, Silvia, Valentina, vi ricordo tutti con affetto. Una speciale menzione va al gruppo di Milano: Valentina, Chiara e Arjan, siete grandi ragazzi, è impossibile pensarvi e non ricordare qualcosa di esilarante, spero che ci rivedremo presto. A tutti gli altri amici e colleghi di Torino che si sono nel tempo aggiunti al lab, sono contentissimo di avervi incontrati e mi dispiace che non abbiamo avuto più tempo per conoscerci meglio, state formando un gran gruppo, continuate così.

Abstract

Computer vision has flourished in recent years thanks to Deep Learning advancements, fast and scalable hardware solutions and large availability of structured image data. Convolutional Neural Networks trained on supervised tasks with backpropagation learn to extract meaningful representations from raw pixels automatically, and surpass shallow methods in image understanding. Though convenient, data-driven feature learning is prone to dataset bias: a network learns its parameters from training signals alone, and will usually perform poorly if train and test distribution differ. To alleviate this problem, research on Domain Generalization (DG), Domain Adaptation (DA) and their variations is increasing.

This thesis contributes to these research topics by presenting novel and effective ways to solve the dataset bias problem in its various settings. We propose new frameworks for Domain Generalization and Domain Adaptation which make use of feature aggregation strategies and visual transformations via data-augmentation and multi-task integration of self-supervision. We also design an algorithm that adapts an object detection model to any out of distribution sample at test time.

With thorough experimentation, we show how our proposed solutions outperform competitive state-of-the-art approaches in established DG and DA benchmarks.

Contents

1	Introduction	1
1.1	Contributions	3
1.2	Outline	5
1.3	Publications	6
2	Related Works	7
2.1	Domain Generalization	8
2.1.1	Literature Overview	8
2.2	Unsupervised Domain Adaptation	10
2.2.1	Literature Overview	10
2.3	Self-Supervised Learning	15
2.3.1	Literature Overview	15
2.4	Multi-Task Learning	17
2.4.1	Literature Overview	17
2.5	Datasets	19
2.5.1	Image Classification Datasets	19
2.5.2	Object Detection Datasets	22
3	Domain Generalization-specific approaches	24
3.1	DSAM: a model based approach to Domain Generalization	25
3.1.1	Domain Specific Aggregation Modules	26
3.1.1.1	Aggregation Module	27
3.1.1.2	D-SAM Architecture for Domain Generalization	28
3.1.1.3	Training and Testing	28
3.1.2	Experiments	29
3.1.2.1	Model setup	29
3.1.2.2	Training setup	30
3.1.2.3	Results	30
3.1.3	Conclusions	32
3.2	Rethinking Domain Generalization Baselines	33
3.2.1	Source augmentation by style transfer	34
3.2.1.1	Training the Style Transfer Model	34
3.2.1.2	Style Transfer as Data Augmentation	36
3.2.2	Experiments	36
3.2.2.1	Experimental Setting	36
3.2.2.2	Comparison methods	37

3.2.2.3	Training Setup	39
3.2.2.4	Results analysis	40
3.2.2.5	Analysis of AdaIN hyperparameters	41
3.2.2.6	Style transfer from external data vs source data	41
3.2.3	Conclusions	44
4	Self-Supervised approaches for Domain Generalization and Domain Adaptation	45
4.1	Domain Generalization by solving jigsaw puzzles	46
4.1.1	The JiGen approach	48
4.1.1.1	Extension to Unsupervised Domain Adaptation	49
4.1.1.2	Implementation Details	49
4.1.2	Experiments	50
4.1.2.1	Patch-Based Convolutional Models for Jigsaw Puzzles	50
4.1.2.2	Multi-Source Domain Generalization	52
4.1.2.3	Ablation	54
4.1.2.4	Single Source Domain Generalization	55
4.1.2.5	Unsupervised Domain Adaptation	57
4.1.3	Conclusions	58
4.2	Tackling PDA with self-supervision	59
4.2.1	Solving jigsaw puzzles for Partial Domain Adaptation	60
4.2.1.1	Problem Setting	60
4.2.1.2	Jigsaw Puzzle Closed Set Adaptation	61
4.2.1.3	Jigsaw Puzzle for Partial Domain Adaptation	61
4.2.2	Combining Self-Supervision with other PDA Strategies	62
4.2.3	Experiments	62
4.2.3.1	Implementation Details	62
4.2.3.2	Results of SSPDA	63
4.2.3.3	Results of SSPDA combined with other PDA strategies	63
4.2.4	Conclusions	65
4.3	One-Shot unsupervised cross-domain detection	66
4.3.1	Method	67
4.3.2	Experiments	71
4.3.2.1	Datasets	71
4.3.2.2	Performance analysis	71
4.3.2.3	Comparison with One-Shot Style Transfer	76
4.3.2.4	Ablation Study	76
4.3.3	Conclusions	78
5	Conclusions and Future Work	79
5.1	Conclusions	79
5.2	Future Work	80

Chapter 1

Introduction

The release of AlexNet [68] in 2012 ended a thirty year long AI winter and changed computer vision history. Thanks to fast, parallel implementation on graphic processing units and clever design, training a deep learning model with millions of parameters on a large scale database became a reality and, as a result, a Convolutional Neural Network was winning the ILSVRC [30] and reducing error rates by 10 points over previous state of the art approaches using Fisher Vectors. Since then, Deep Learning research dominated the computer vision field with several new ground breaking approaches. Generative adversarial networks [49] for content generation, Deep Residual Learning [52] for training deeper models, Faster-RCNN [106] for real-time object detection to name a few, all these methods built on top of Deep Learning, Convolutions, new hardware advancements and the increasing availability of image data.

The rise of Deep Learning marked a turning point in industry as well. Thanks to the performance reached by these new models, companies started to integrate computer vision solutions in their products. Face recognition for surveillance tasks, detection for robots and navigation, semantic segmentation and counting for product inspection, ranked retrieval for visual search and indexing, anomaly detection for medical image analysis. Industrial interest in Deep Learning shifted the focus of research: from ideas to applications, from theoretical investigation to practical problem solving.

While proven to be the best approach for many Computer Vision applications, Deep Learning is far from perfect. At the time of writing this thesis, dataset bias is one of the most difficult challenges. Consider a model trained for detecting objects and people in an urban scenario (i.e. camera mounted on a moving car). If the training data is biased, as in the case of containing all images taken during a sunny day, then this model will fail when test data is acquired on a different setting, such as night images or bad weather. Backpropagation learns all the cues for minimizing errors on the training set, ignoring which of these cues are specific to the training set. This leads to poor performances when conditions change. An oracle solution for this problem consists of collecting training data from the same distribution where test data comes from. However, this approach might be unfeasible: Convolutional Neural Networks require large amounts of labeled data to be trained effectively, and collecting these annotations for all possible inference settings is often too expensive.

Furthermore, we might not be able to anticipate how test conditions will shift after deployment.

To alleviate this issue we employ Domain Generalization and Domain Adaptation. *Domain Generalization* (DG) is a challenging setting, used when we want train a model to predict effectively on any unseen target distribution. It often assumes multiple distributions (domains) available at training time. We use *Domain Adaptation* (DA) when we have some, often unlabeled, test distribution data at training time, and need to adapt the model to that specific distribution.

Many DA and DG solution use feature based approaches for separating domain-specific from domain-agnostic features (DG) or aligning features from train and test data with adversarial learning (DA). In this thesis, we take a different route, and explore alternative approaches for learning domain invariant representations that leverage data aggregations and transformations. In particular, we propose to use the self-supervised learning paradigm for solving generalization and adaptation problem. We show how the joint training of an auxiliary self-supervised task on unlabeled data can be used to bridge the gap between train and test, learn domain invariant representation, and provide auxiliary targets for adapting deep learning models on one sample at test time. Furthermore, we introduce a novel Domain Generalization framework, and study the effect of refined data augmentation on state-of-the-art DG methods.

1.1 Contributions

The contribution of this thesis is to propose novel Domain Adaptation and Domain Generalization solutions by exploring data aggregation and visual transformation strategies. In three of our works, we show how a novel self-supervised-based approach can achieve solid generalization and adaptation results without explicit loss functions. We also present a DG framework which models an agnostic backbone within its architecture, and show how most state-of-the-art DG solutions become ineffective when we apply strong data augmentation to our sources. We present:

- **A novel model-based approach for Domain Generalization [32].** This algorithm leverages a multi-branch architecture and feature aggregation strategy to achieve a separation between domain-specific and agnostic information. We demonstrate how principled feature extraction from this model has led us to achieve state-of-the-art results in two Domain Generalization benchmarks.
- **A novel self-supervised based approach for Domain Generalization and Domain Adaptation [18].** We design a multi-task algorithm integrating supervised and self-supervised signals from the training samples. We show for the first time how an auxiliary self-supervised objective broadens the semantic understanding across domains, gaining state-of-the-art results in Domain Generalization. Furthermore, it is shown the use of self-supervision alone can prime adaptation on the unlabeled target in the unsupervised Domain Adaptation setting.
- **A self-supervised based algorithm for Partial Domain Adaptation [11].** By expanding on the method proposed in [18], we integrate our self-supervised based approach into Partial Domain Adaptation algorithm, and improve over the state-of-the-art in the difficult PDA setting.
- **A novel cross-domain object detection algorithm able to perform adaptation without a target [33].** All existing cross-domain approaches need a sizable amount of unlabeled target data during training. Here, we introduce the one-shot cross-domain setting and present the first approach specifically designed for adapting a model without the need to anticipate and collect the target set. Our OSHOT algorithm performs adaptation on the fly to each test sample by exploiting self-supervised signals from the sample itself. We compare our algorithm with top performing approaches for cross-domain detection and the most recent one-shot style-transfer technique, achieving state-of-the-art results in our new setting.
- **An extensive study on the real effectiveness of state-of-the-art Domain Generalization methods when strong regularization is used on the sources [9].** All existing DG algorithms are tested using weakly-augmented labeled data. By applying powerful data-augmentation techniques, we are able to reach state-of-the-art results with the naive Deep All algorithm. Furthermore, we show how improvements of top performing methods are negated when strong data augmentation is applied on the sources. In light of

this, we have to rethink Domain Generalization benchmarks in order to move towards algorithms that are orthogonal to regularized data.

1.2 Outline

Chapter 2 overviews related works. Section 2.1 presents algorithms developed for Domain Generalization, Section 2.2 focuses on approaches for the Unsupervised Domain Adaptation setting and its variations. The two following sections provide background context for our self-supervised based solutions: Section 2.3 covers self-supervision and its significance for training on unlabeled data, while Section 2.4 briefly describes multi-task learning, a paradigm we use to join self-supervision with adaptation and generalization tasks.

Chapter 3 presents two Domain Generalization specific approaches: D-SAM (Section 3.1.3), a multi-branch architecture separating domain-specific and domain-agnostic modules explicitly, and a study on the effect of data augmentation for DG, showing how refined image pre-processing enables a model trained with simple ERM to reach state-of-the-art performances (Section 3.2.3).

Chapter 4 focuses on our proposed self-supervised solutions for both Domain Generalization and Domain Adaptation. The first two sections present Jigen, a multi-task self-supervised approach for DG and DA (Section 4.1.3), and its extension to Partial Domain Adaptation (Section 4.2.4). Section 4.3.3 describes OSHOT, an approach for adapting model on one image in object detection tasks.

Finally, Chapter 5 wraps up our findings and outlines proposals for future work.

1.3 Publications

This is a list of the author's publications to Computer Vision conferences

- D'Innocente A, Carlucci FM, Colosi M, Caputo B. Bridging between computer and robot vision through data augmentation: a case study on object recognition. In International Conference on Computer Vision Systems 2017 Jul 10 (pp. 384-393). Springer, Cham.
- D'Innocente A, Caputo B. Domain generalization with domain-specific aggregation modules. In German Conference on Pattern Recognition 2018 Oct 9 (pp. 187-198). Springer, Cham.
- Carlucci FM, D'Innocente A, Bucci S, Caputo B, Tommasi T. Domain generalization by solving jigsaw puzzles. In Proceedings of the IEEE Conference on Computer Vision and Pattern Recognition 2019 (pp. 2229-2238).
- Bucci S, D'Innocente A, Tommasi T. Tackling partial domain adaptation with self-supervision. In International Conference on Image Analysis and Processing 2019 Sep 9 (pp. 70-81). Springer, Cham.
- D'Innocente A, Borlino FC, Bucci S, Caputo B, Tommasi T. One-Shot Un-supervised Cross-Domain Detection. arXiv preprint arXiv:2005.11610. 2020 May 23.

Chapter 2

Related Works

The dataset bias problem is well known in the computer vision community [105, 121]. Convolutional Neural Networks rely on substantial amount of labeled data for learning meaningful representations [30], yet even large scale image datasets cannot capture all of the variety and complexity of the visual world [105, 121] and, as a result, algorithms struggle if the distribution shifts after deployment.

Several algorithms have been developed to cope with domain shift, mainly in two different settings: Domain Generalization (DG) and Domain Adaptation (DA).

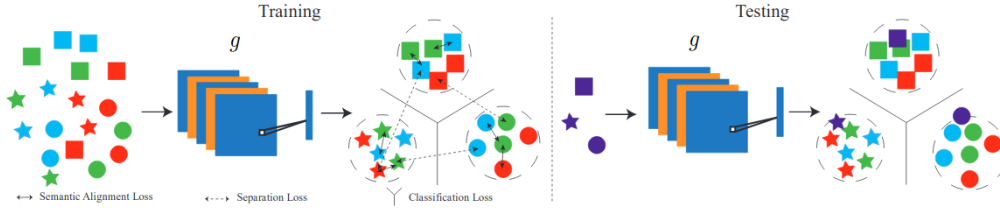


Figure 2.1. Feature-level domain generalization approach of [94]. At training time, the semantic alignment loss minimizes the distance between samples from different domains but the same class label and the separation loss maximizes the distance between samples from different domains and class labels. At test time, the embedding function embeds samples from unseen distributions to the domain invariant space and the prediction function classifies them (right). In this figure, different colors represent different domain distributions and different shapes represent different classes. [94]

2.1 Domain Generalization

True risk can be approximated by empirical risk, provided that we have enough data and that all samples are drawn from the same distribution (domain). However, when the test domain has not been seen at training time, performances are bound to drop substantially.

To overcome these limitations computer vision has studied the Domain Generalization (DG) problem [64], where, given multiple training sources, the algorithm has to learn how to generalize to unseen distributions. More formally, we assume to have n source domains $(D_1 \dots D_n)$, where D_i is the i^{th} source domain containing N_i data-label pairs $(x_i^j, y_i^j)_{j=1}^{N_i}$. Our goal is to learn a function $f : x \rightarrow y$ that generalizes well to any novel testing domain D_T not seen during training. The problem is studied under the assumption that all domains share the same feature space and label space.

Single-Source Domain Generalization, also known as Out-Of-Distribution Generalization, is an extension of DG in which only $n = 1$ source distribution is available during training. Since it can be difficult to separate style from semantics given only one observed distribution, it can be argued that the problem is ill-posed.

2.1.1 Literature Overview

Several strategies have been studied as solutions for the Domain Generalization problem DG.

Feature-level strategies focus on learning domain invariant data representations mainly by minimizing different domain shift measures. The metric learning approach of [94] exploits a Siamese architecture to learn an embedding subspace in which the semantics of the mapped domains are aligned while their visual style is maximally separated. Autoencoder based approaches have been used: MTAE [44] applies data-augmentation induced by deep autoencoders to transform the original image in the style of different related visual domains, [75] extends the traditional autoencoder framework with a Maximum-Mean-Discrepancy loss to align the distribution of different visual domains.

Model-level strategies, by leveraging the multi-source nature of DG, focus on architectural choices and/or optimization techniques to simulate out of distribution testing scenarios during training. Many studies leverage the meta-learning framework, MLDG [73] defines meta-training and meta-testing domains at each iteration, and increases the performance of the model on the meta-testing set with a second order optimization inspired by [40], MetaReg [3] defines a new regularization function which is learned through a learning-to-learn approach. [74] uses a multi-branch network and adopts an episodic training scheme to train the final feature extractor and classifier to be robust to unusual signals. [83] trains multiple source-specific predictors and, at test time, recombines these models based on the sample similarity to each source. Other works use low-rank network parameter decomposition [72, 31] with the goal of identifying and neglecting domain-specific signatures. [64] aims at neglecting domain specific signatures through a shallow method that exploits multi-task learning.

Finally, data-level employ data-augmentation techniques to synthesize new images. Several works in this direction employ variants of the Generative Adversarial Networks (GANs, [49]), [118, 125] learn how to properly perturb the source samples, even in the challenging case of DG from a single source. CROSSGRAD [117] adopts a Bayesian Network and a sampling step in which inputs are augmented through a domain-guided perturbation. [125] address the single-source DG problem through an adversarial data-augmentation scheme that systematically mimics a novel distribution by generating hard samples. In DDAIG [144], a domain transformation network is trained to map source data to unseen domains by optimizing an objective that preserves the label prediction but confuses the domain classifier. The combination of data and feature-level strategies has also shown further improvements in results [19].

The Deep-All algorithm is a standard ERM classifier that naively trains a deep model on the available source labeled data with backpropagation. Despite the existence of several solutions designed specifically for DG, it is not trivial to perform better than Deep-All [72, 74]. Recent work claims that, when properly regularized, the ERM algorithm is able to beat even the most performing DG algorithms [50].

2.2 Unsupervised Domain Adaptation

In the Unsupervised Domain Adaptation (UDA) setting, we are given N_s annotated samples from a source domain $D_s = (x_s^j, y_s^j)_{j=1}^{N_s}$, drawn from the distribution S , and N_T unlabeled samples of the target domain $D_T = (x_T^j)_{j=1}^{N_T}$ drawn from a different distribution T . The aim of UDA algorithms is to learn a function $f : x \rightarrow y$ that performs well on samples drawn from T . The setting can be either transductive (we want to deploy the model on D_T) or non-transductive (the model is going to be deployed on different data drawn from the distribution T).

UDA problems assume that all of the data shares the same feature and label space.

Multi-Source Domain Adaptation is a variation of the Unsupervised Domain Adaptation setting in which source data is collected from multiple source domains, so that we have our training set consisting of n source domains $(D_1 \dots D_n)$, where D_i is the i^{th} source domain containing N_i data-label pairs $(x_i^j, y_i^j)_{j=1}^{N_i}$. Solutions for multi-source UDA problems may leverage domain annotation [104] compared to the single-source setting, although in some instances the domain label of the sources may be unknown [85, 53, 17].

Partial Domain Adaptation (in this thesis the acronym PDA is used) is a recently introduced UDA scenario in which the label space of the target domain is strictly contained in that of the source domain $Y_T \subset Y_S$. Thus, besides dealing with the marginal shift in standard unsupervised domain adaptation, it is necessary to take care of the difference in the label space which makes the problem even more challenging. If this information is neglected and the matching between the whole source and target data is forced, any adaptive method may incur in a degenerate case producing worse performance than its plain non-adaptive version. Still the objective remains that of learning both class discriminative and domain invariant feature models.

Predictive Domain Adaptation is an intermediate setting between Domain Adaptation and Domain Generalization. In the predictive Domain Adaptation setting, we are given N_s annotated samples from a source domain $D_s = (x_s^j, y_s^j)_{j=1}^{N_s}$, drawn from the distribution S , and a auxiliary domains $(D_1 \dots D_a)$ where the i^{th} auxiliary domain contains N_i unlabeled samples $(x_i^j)_{j=1}^{N_i}$. The objective is to train a model on the source domain, while at the same time leveraging the meta-information in the auxiliary domains, in order to be able to generalize to any target distribution T not seen at training time.

2.2.1 Literature Overview

Single-Source and Multi-Source Unsupervised Domain Adaptation

Feature-level strategies have been long studied in Domain Adaptation. Compared to DG for which the target is unknown, given the availability of unlabeled target data during training in DA, it is possible to employ distance metrics and reduce the gap

between the source’s and target’s representations. [5] introduced the H-divergence metric between unlabeled data from two different distributions: given a domain \mathcal{X} with \mathcal{D} and \mathcal{D}' probability distributions over \mathcal{X} , let \mathcal{H} be a hypothesis class on \mathcal{X} and denote by $I(h)$ the set for which $h \in \mathcal{H}$ is the characteristic function; that is, $x \in I(h) \iff h(x) = 1$. The H-divergence between \mathcal{D} and \mathcal{D}' is

$$d_{\mathcal{H}}(\mathcal{D}, \mathcal{D}') = 2 \sup_{h \in \mathcal{H}} |Pr_{\mathcal{D}}[I(h)] - Pr_{\mathcal{D}'}[I(h)]| \quad (2.1)$$

It is furthermore proven in [5] that the H-divergence measure can, under some assumptions, bound the difference in error between the two distributions. Several works build upon the theoretical derivations of [5]. DAN [79] proposes a deep architecture with hidden representations embedded in a reproducing kernel Hilbert space where the means of different distributions are explicitly matched. DANN [42] uses a multi-task model with a domain discriminator that, through adversarial training, trains the backbone to extract similar representations for both the source and the target domain. This adversarial framework has become popular in the DA community and several works build on top of it with different flavors: ADDA [122] adds a GAN loss to DANN, [112] and [76] align the distributions of source and target by utilizing also the task-specific decision boundaries. Deep CORAL [119] learns a non-linear transformation to align correlations of layer activations in a deep neural network. Metric learning has also been successfully used in [94] by employing point-wise surrogates of distribution distances. Finally, [10] builds an autoencoder architecture with private and shared components, the model performs the main task in the source domain and the partitioned representation is also used to reconstruct images from both source and target.

Model-level strategies for UDA include the solution of [17], which introduces domain alignment layers in standard learning networks that, through batch-normalization and an entropy-loss regularization, align the statistics of source and target data. Those layers can also be used in multi-source DA to evaluate the relation between the sources and target and then perform source model weighting [82, 132].

Data-level techniques use data-augmentation to synthesize new images, and, as in the DG counterpart, many techniques use variants of Generative Adversarial Networks framework [49]. Particularly effective are the methods based style transfer algorithms such as CycleGAN [145]. Given two unlabeled distributions A and B , CycleGAN learns two mapping functions $F : x_A \rightarrow x_B$ and $G : x_B \rightarrow x_A$ by minimizing a cycle-consistency loss. SBADAGAN [110] and CyCADA [55] both integrate the CycleGAN approach in UDA settings by adding a semantic constraint through labels (for the source) and pseudo-labels (for the target) in order to generate target-like labeled images using source data. Furthermore, [19, 115] combine data-level and feature-level strategies for improved results.

Partial Domain Adaptation

The first work which considered this setting focused on localizing domain specific and generic image regions [1]. The attention maps produced by this initial procedure are less sensitive to the difference in class set with respect to the standard domain classification procedure and allow to guide the training of a robust source classification

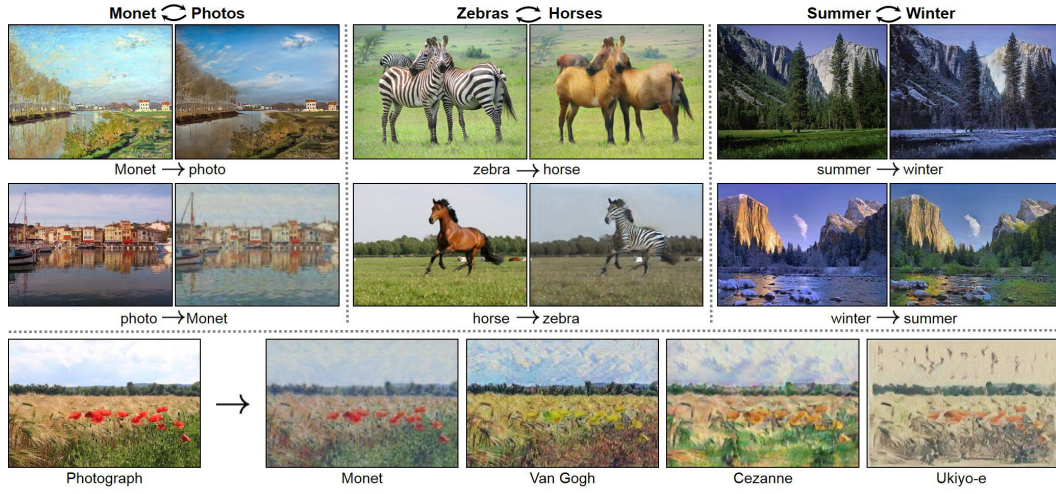


Figure 2.2. CycleGAN [145] performs unsupervised image-to-image translation with Generative networks and a cycle consistency loss. It is a style transfer technique, and it has been successfully used in Unsupervised Domain Adaptation to create target-like labeled images from source data due to the availability of the target set during training.

model. Although suitable for robotics applications, this solution is insufficient when each domain has spatially diffused characteristics. In those cases the more commonly used PDA technique consists in adding a re-weight source sample strategy to a standard domain adaptation learning process. Both the Selective Adversarial Network (SAN, [14]) and the Partial Adversarial Domain Adaptation (PADA, [15]) approaches build over the domain-adversarial neural network architecture [42] and exploit the source classification model predictions on the target samples to evaluate a statistics on the class distribution. The estimated contribution of each source class either weights the class-specific domain classifiers [14], or re-scales the respective classification loss and a single overall domain classifier [15]. A different solution is proposed in [139], where each domain has its own feature extractor and the source sample weight is obtained from the domain recognition model rather than from the source classifier. An alternative view on the PDA problem is presented in two recent preprints [89, 133]. The first work uses two separate deep classifiers to reduce the domain shift by enforcing a minimal inconsistency between their predictions on the target. Moreover the class-importance weight is formulated analogously to PADA, but averaging over the output of both the source classifiers. The second work does not attempt to aligning the whole domain distributions and focuses instead on matching the feature norm of source and target. This choice makes the proposed approach robust to negative transfer with good results in the PDA setting without any heuristic weighting mechanism.

Cross-Domain Object Detection

Many successful object detection approaches have been developed during the past several years, starting from the original sliding window methods based on handcrafted features, till the most recent deep-learning empowered solutions. Regardless of the specific implementation, the detector robustness across visual domain remains a

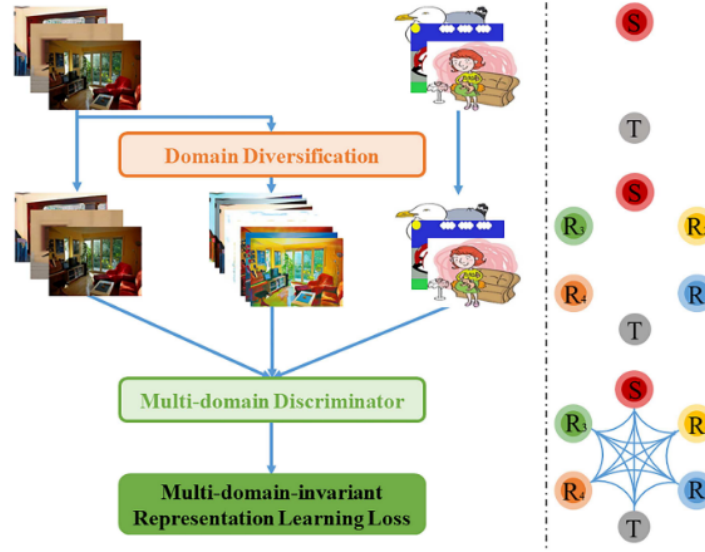


Figure 2.3. Cross-Domain paradigm proposed in [66]. In the diversification stage, multiple versions of the source domain are created through domain randomization via CycleGAN [145]. In the marching stage, representations distance of the source, target, and randomized domains is then minimized via adversarial learning. The framework exhibits competitive performance in cross-domain detection scenarios.

major issue.

Most of the Unsupervised Domain Adaptation literature has focused on object classification, while the task of cross-domain object detection has received relatively less attention. Only in the last two years adaptive detection methods have been developed considering three main components: (i) including multiple and increasingly more accurate feature alignment modules at different internal stages, (ii) adding a preliminary pixel-level adaptation and (iii) pseudo-labeling. The last one is also known as self-training and consists in using the output of the source model detector as coarse annotation on the target. The importance of considering both global and local domain adaptation, together with a consistency regularizer to bridge the two, was first highlighted in [23]. The Strong-Weak (SW) method of [113] improves over the previous one pointing out the need of a better balanced alignment with strong global and weak local adaptation and is further extended by [129] where the adaptive steps are multiplied at different depth in the network. By generating new source images that look like those of the target, the Domain-Transfer (DT, [59]) method was the first to adopt pixel adaptation for object detection and combine it with pseudo-labeling. More recently the Div-Match approach [66] re-elaborated the idea of domain randomization [120]: multiple CycleGAN [145] applications with different constraints produce three extra source variants with which the target can be aligned at different extent through an adversarial multi-domain discriminator. A weak self-training procedure (WST) to reduce false negatives is combined with adversarial background score regularization (BSR) in [65]. Finally, [63] followed the pseudo-labeling strategy including an approach to deal with noisy annotations.

Adaptive Learning on a Budget

There is a wide literature on learning from a limited amount of data, both for classification and detection. However, in case of domain shift, learning on a target budget becomes extremely challenging. Indeed, the standard assumption for adaptive learning is that a large amount of unsupervised target samples are available at training time so that a model can capture the domain style from them and close the gap with respect to the source. Only few attempts have been done to reduce the target cardinality. In [93] the considered setting is that of few-shot supervised domain adaptation: only a few target samples are available but they are fully labeled. In [6, 24] the focus is on one-shot unsupervised style transfer with a large source dataset and a single unsupervised target image. These works propose time-costly autoencoder-based methods to generate a version of the target image that maintains its content but visually resembles the source in its global appearance. Thus the goal is image generation with no discriminative purpose. A related setting is that of online domain adaptation where unsupervised target samples are initially scarce but accumulate in time [54, 128, 84]. In this case target samples belong to a continuous data stream with smooth domain changing, so the coherence among subsequent samples can be exploited for adaptation.

2.3 Self-Supervised Learning

The success of deep learning approaches for computer vision relies on the availability of large quantities of annotated data. Although data acquisition might not be a problem, data annotation could be costly. Self-supervision, a subset of unsupervised learning, is used to avoid paying the price of human annotation and learning features from images using only unlabeled data. Many self-supervised learning methods exist, but the vast majority of them consists on using a pretext task that exploits inherent data attributes to automatically generate surrogate labels: part of the existing knowledge about the images is manually removed (e.g. the color, the orientation, the patch order) and the task consists in recovering it. It has been shown that the first layers of a network trained in this way capture useful semantic knowledge [2]. The second step of the learning process consists in transferring the self-supervised learned model of those initial layers to a supervised downstream task (e.g. classification, detection), while the ending part of the network is newly trained. As the number of annotated samples of the downstream task gets lower, the advantage provided by the transferred model generally gets more evident [137, 2]. A literature survey on the most notable self-supervised learning methods for computer vision follows.

2.3.1 Literature Overview

The possible pretext tasks can be organized in three main groups. One group relies only on original visual cues and involves either the whole image with geometric transformations (e.g. translation, scaling, rotation [45, 36]), clustering [20], inpainting [103] and colorization [140], or considers image patches focusing on their equivariance (learning to count [100]) and relative position (solving jigsaw puzzles [98, 101]). A second group uses external sensory information either real or synthetic: this solution is often applied for multi-cue (visual-to-audio [102], RGB-to-depth [107]) and robotic data [60, 70]. Finally, the third group relies on video and on the regularities introduced by the temporal dimension [127, 116]. The most recent SSL research trends are mainly two. On one side there is the proposal of novel pretext tasks,

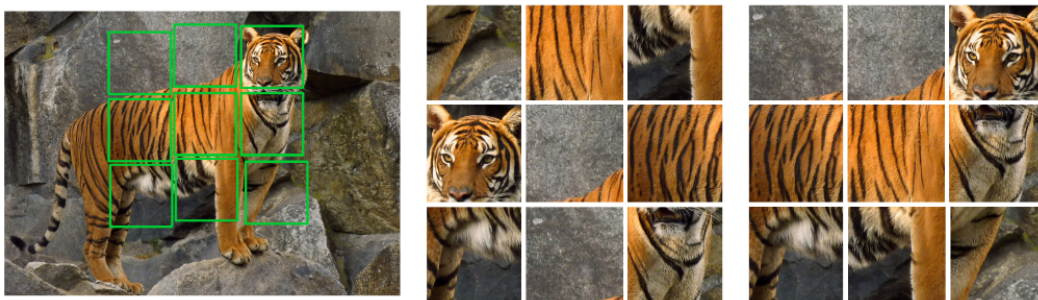


Figure 2.4. The self-supervised jigsaw puzzle solving task proposed in [99]. A subsection of the image is split in 9 tile from a 3x3 square grid. The tiles are then randomly re-arranged and the task is to retrieve the correct order. For simplicity, the problem is cast as classification by selecting only 1000 out of all the $9!$ possible permutations. Some data-augmentation is applied to the tiles so that the network cannot solve the task using low-level features, such as lines and color aberrations.

compared on the basis of their ability to initialize a downstream task with respect to using supervised models as in standard transfer learning [46, 61]. On the other side there are new approaches to combine several pretext tasks together in multi-task settings [35, 107].

2.4 Multi-Task Learning

Multi-task learning (MTL) is a learning paradigm in machine learning and its aim is to leverage useful information in multiple related tasks to help improve the generalization of all the tasks [142]. In deep learning, the idea of multi-task learning is that one task can teach the network to extract features which are useful, yet orthogonal, to different tasks. MTL improves generalization by leveraging the domain-specific information contained in the training signals of related tasks, this is referred to as the inductive bias [22]. Most works presented in this thesis exploit the multi-task learning paradigm by combining a main task (e.g. classification, object detection) with an auxiliary self-supervised task used to induce Domain Adaptation or Generalization for the primary objective.

2.4.1 Literature Overview

Hard and Soft parameter sharing

In deep learning, a common approach for MTL problems is hard parameter sharing, i.e. the sharing of a part of the model between different tasks [21, 67, 92, 34]. The first approach using hard parameter sharing [21] consists on having one shared backbone and multiple task-specific heads. Even though it has been shown this type of approach reduces overfitting [4], the amount of sharing is in essence an hyperparameter, and different levels of sharing work better for different tasks [90]. For these reasons, research has also explored soft parameter sharing, in which each task has his own dedicated model whose parameters are interconnected [90, 37, 135].

Multi-Task Networks

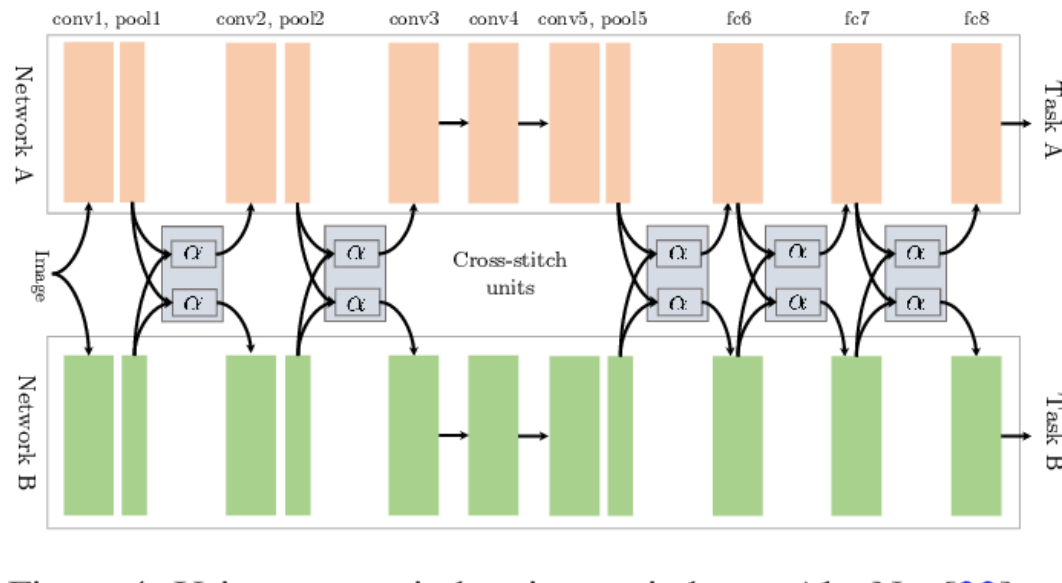


Figure 2.5. Cross-Stich Networks [90] with two tasks. The two models soft-share their parameters

In Ubernet [67], an algorithm is presented for containing the computational costs of training on 7 different tasks through skip connections, while also facing the realistic scenario of having unlabeled samples. [92] is the first work to formally introduce the primary-auxiliary multi-task paradigm, in which auxiliary task are used only to increase performances on the main task. It leverages residual blocks to collect auxiliary knowledge with a privileged information approach. Cross-Stich Networks [90] use soft parameter sharing: multiple networks are instantiated and each learns a different task. The parameters are then shared between layers through Cross-Stich units: linear combinations of layer outputs that learn how to better combine cross-task information. [109] improves over these Cross-Stich units by learning an optimal feature subspace for merging knowledge. [34] learn jointly four self-supervised tasks in a multi-task framework, and shows how this approach leads to better unsupervised feature learning, which is, in some instances, competitive with full supervision. Routing Networks [108] proposes a Reinforcement Learning approach for finding the optimal layer path for the feature extractor in a multi-task setting.

Task weighting in Multi-Task Learning

The Multi-Task Learning paradigm suffers from disruptive gradients: without optimal task weighting, the learned representations will not benefit from the inductive bias and the effects may be negative for all tasks involved [62]. This leads to resource consuming grid searches to find the optimal hyperparameters for the algorithm. [62] propose a novel loss for minimizing the homoscedastic uncertainty, thus obtaining an automatic task balancing effect which also adjusts the weights dynamically during training. Finally, [51] proposes a reinforcement learning strategy for prioritizing the most difficult tasks during the learning process by defining dynamic difficulty measures.

2.5 Datasets

The following section describes all the databases that were used to benchmark the algorithms presented in this thesis. All of these datasets are established testbeds widely used for Domain Generalization and Domain Adaptation research, with a focus on evaluating performances under different domain shifts scenarios.

2.5.1 Image Classification Datasets

PACS

The PACS database has been introduced in [72] as a testbed for Domain Generalization, and has quickly become a standard for evaluating DG algorithms in image classification. It consists of 9,991 images, of resolution 227×227 , taken from four different visual domains (Photo, Art paintings, Cartoon and Sketches), depicting seven categories. The established evaluation protocol consists of using three domains as source and the remaining domain as a target. PACS is a challenging benchmark, consisting of domains with very large distribution shifts. It has also been used for testing Domain Adaptation methods.

Office-Home

Much like PACS, Office-Home tests performances under large distribution shifts between source and target. It has been first used in [123] for evaluating Domain Adaptation algorithms. It provides images from four different domains: Artistic images, Clip art, Product images and Real-world images. Each domain depicts 65 object categories that can be found typically in office and home settings. High accuracy on the Office-Home dataset is difficult to obtain, besides the large distribution shifts, it deals with changes in scale, resolution and orientation of objects. The original experimental protocol involved a Domain Adaptation setting with one domain as



Figure 2.6. The PACS dataset consists of images captured from different visual domains: Photos, Art paintings, Cartoons and Sketches.

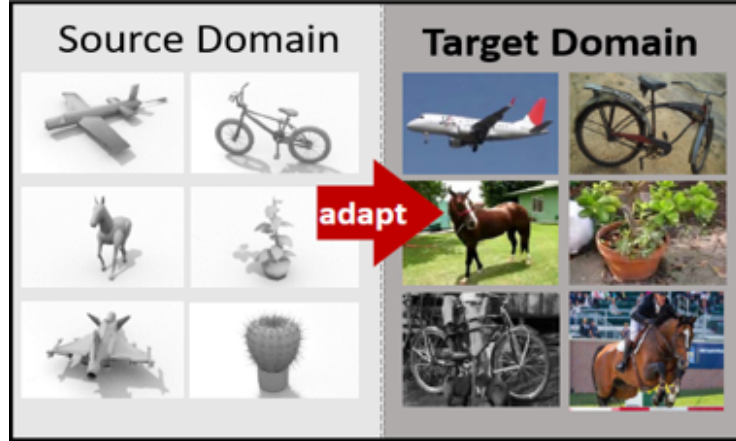


Figure 2.7. The 2017 Visual Domain Adaptation challenge dataset. It consists two distribution: a synthetic database and real images. Algorithms are trained on the synthetic to real transfer.

source and a different domain as target. In our works we repurposed Office-Home as a Domain Generalization benchmark by using three domains as source and the remaining domain as target, and it has subsequently been adopted as a standard benchmark from the DG community.

VLCS

VLCS [121] is built upon 4 different datasets: PASCAL VOC 2007, Labelme, Caltech and SUN and contains 5 object categories. Differently from other popular Domain Generalization testbeds, all the domains are composed of real world photos with the shift mainly due to camera type, illumination conditions, point of view, etc. Moreover, while Caltech is composed by object-centered images, the other three domains contain scene images containing objects at different scales. We use this dataset for Domain Generalization experiments, and follow the standard protocol of [44], using three domains as source and one as target, and dividing each domain into a training set (70%) and a test set (30%) by random selection from the overall dataset.

Office-31

Historically, Office-31 [111] has been widely used in Domain Adaptation. It contains 4652 images of 31 object categories common in office environment. Samples are drawn from three annotated distributions: Amazon (A), Webcam (W) and DSLR (D). The established Unsupervised Domain Adaptation setting considers one domain as a source and a different domain as a target. In our works, we use the Office-31 datasets for benchmarking Partial Domain Adaptation algorithms.

VisDA2017

VisDA2017 is the dataset used in the Visual Domain Adaptation challenge



Figure 2.8. Side-by-side comparison of MNIST samples (even columns) and SVHN samples (odd columns). The domain shift is large, and these two datasets are often used jointly as benchmark for Domain Adaptation and Domain Generalization methods.

(classification track). It has two domains, synthetic 2D object renderings and real images with a total of 208000 images organized in 12 categories. It is often used in the synthetic to real Domain Adaptation shift, in our experiments we used it for benchmarking Partial Domain Adaptation under the same distribution shift. With respect to most DA benchmarks, VisDA allows to investigate approaches on a very large scale sample size scenario.

CompCars

The Comprehensive Cars (CompCars) [134] is a large scale dataset. We used this dataset for Predictive Domain Adaptation experiments, by following the experimental protocol described in [86], we selected a subset of 24151 images with 4 categories (MPV, SUV, sedan and hatchback) which are type of cars produced between 2009 and 2014 and taken under 5 different viewpoints (front, front-side, side, rear, rear-side). Each view point and each manufacturing year define a separate domain, leading of a total of 30 domains. In the PDA setting, we select one domain as source and a different domain as target, and the images in the remaining 28 domains are used as auxiliary unlabeled data. Considering all possible pairs, we have a total of 870 experiments.

Digits Datasets

Digits dataset are all fairly similar, consisting of ten classes corresponding to the digits and low intra-domain variability. Digits recognition is considered a solved problem in computer vision, (the record accuracy of MNIST [69] is 99.82%), however they are still used for evaluating cross-domain methods due to domain shifts occurring under different acquisitions. In this thesis, we use three of these datasets for evaluating single-source Domain Generalization performances.

MNIST [69] contains 60000 samples for training and 10000 samples for testing. The digits are handwritten and all images are 28x28 one-channel black-or-white centered crops.

MNIST-M [42] is obtained from MNIST by substituting the black background with a random patch from RGB photos.

SVHN [96] stands for Street View House Numbers and it is a MNIST-like digits dataset obtained by house numbers from Google Street View images. It has 32x32 RGB samples, 73257 are used for training and 26032. Images are centered around the significant digit, as many of them contain different numbers at the sides.

2.5.2 Object Detection Datasets

Pascal-VOC

Pascal-VOC [38] is the standard real-world image dataset for object detection benchmarks. VOC2007 and VOC2012 both contain bounding boxes annotations of 20 common categories. VOC2007 has 5011 images in the train-val split and 4952 images in the test split, while VOC2012 contains 11540 images in the train-val split. In a Domain Adaptation setting, Pascal-VOC is often used as a source domain.

Artistic Media Datasets

Clipart1k, Comic2k and Watercolor2k [59] are referred to as the Artistic Media Datasets (AMD). These are three object detection databases designed for benchmarking Domain Adaptation methods when the source domain is Pascal-VOC. Clipart1k shares its 20 categories with Pascal-VOC: it has 500 images in the training set and 500 images in the test set. Comic2k and Watercolor2k both have the same 6 classes (a subset of the 20 classes of Pascal-VOC), and 1000-1000 images in the training-test splits each.

Cityscapes

Cityscapes [25] is an urban street scene dataset with pixel level annotations of 8 categories. It has 2975 and 500 images respectively in the training and validation splits. For usage in object detection, we use the pixel annotations along with instance masks to generate bounding boxes of objects, as in [23]. The Cityscapes dataset is used for evaluating cross-domain detection methods as a source or target dataset.

Foggy Cityscapes

Foggy Cityscapes [114] is obtained by adding different levels of synthetic fog to Cityscapes images. It is used as a target dataset for Domain Adaptation with Cityscapes as its source. We follow established protocols and only consider images with the highest amount of artificial fog, thus training-validation splits have 2975-500 images respectively.

KITTI

KITTI [43] is a dataset of images depicting several driving urban scenarios. It is used in Domain Adaptation in conjunction with Cityscapes as a source or target domain and in this setting only the boxes with "car" label are considered. By



Figure 2.9. The cityscapes dataset contains pixel level annotations of urban driving scenes. This dataset is often repurposed for object detection by computing bounding boxes of objects using semantic tags and instance masks [23].

following [23], we use the full 7481 images for both training (when used as source) and evaluation (when used as target).

Chapter 3

Domain Generalization-specific approaches

3.1 DSAM: a model based approach to Domain Generalization

Visual recognition systems are meant to work in the real world. For this to happen, they must work robustly in any visual domain, and not only on the data used during training. To this end, research on domain adaptation has proposed over the last years several solutions to reduce the covariate shift among the source and target data distributions. Within this context, a very realistic scenario deals with domain generalization, i.e. the ability to build visual recognition algorithms able to work robustly several visual domains, without having access to any information about target data statistic. This paper contributes to this research thread, proposing a deep architecture that maintains separated the information about the available source domains data while at the same time leveraging over generic perceptual information. We achieve this by introducing domain-specific aggregation modules that through an aggregation layer strategy are able to merge generic and specific information in an effective manner. Experiments on two different benchmark databases show the power of our approach, reaching the new state of the art in domain generalization.

As artificial intelligence, fueled by machine and deep learning, is entering more and more into our everyday lives, there is a growing need for visual recognition algorithms able to leave the controlled lab settings and work robustly in the wild. This problem has long been investigated in the community under the name of Domain Adaptation (DA): considering the underlying statistics generating the data used during training (source domain), and those expected at test time (target domain), DA assumes that the robustness issues are due to a covariate shift among the source and target distributions, and it attempts to align such distributions so to increase the recognition performances on the target domain. Since its definition [111], the vast majority of works has focused on the scenario where one single source is available at training time, and one specific target source is taken into consideration at test time, with or without any labeled data. Although useful, this setup is somewhat limited: given the large abundance of visual data produced daily worldwide and uploaded on the Web, it is very reasonable to assume that several source domains might be available at training time. Moreover, the assumption to have access to data representative of the underlying statistic of the target domain, regardless of annotation, is not always realistic. Rather than equipping a seeing machine with a DA algorithm able to solve the domain gap for a specific single target, one would hope to have methods able to solve the problem for any target domain. This last scenario, much closer to realistic settings, goes under the name of Domain Generalization (DG, [72]), and is the focus of our work.

Current approaches to DG tend to follow two alternative routes: the first tries to use all source data together in order to learn a joint, general representation for the categories of interest strong enough to work on any target domain [73]. The second instead opts for keeping separated the information coming from each source domain, trying to estimate at test time the similarity between the target domain represented by the incoming data and the known sources, and use only the classifier branch trained on that specific source for classification [83]. Our approach sits across these two philosophies, attempting to get the best of both worlds. Starting from a generic

convnet, pre-trained on a general knowledge database like ImageNet [30], we build a new multi-branch architecture with as many branches as the source domains available at training time. Each branch leverages over the general knowledge contained into the pre-trained convnet through a deep layer aggregation strategy inspired by [136], that we call Domain-Specific Aggregation Modules (D-SAM). The resulting architecture is trained so that all three branches contribute to the classification stage through an aggregation strategy. The resulting convnet can be used in an end-to-end fashion, or its learned representations can be used as features in a linear SVM. We tested both options on two different architectures and two different domain generalization databases, benchmarking against all recent approaches to the problem. Results show that our D-SAM architecture, in all cases, consistently achieve the state of the art.

3.1.1 Domain Specific Aggregation Modules

In this section we describe our aggregation strategy for DG. We will assume to have S source domains and T target domains, denoting with N_i the cardinality of the i_{th} source domain, for which we have $\{x_j^i, y_j^i\}_{j=1}^{N_i}$ labeled samples. Source and target domains share the same classification task; however, unlike DA, the target distribution is unknown and the algorithm is expected to generalize to new domains without ever having access to target data, and hence without any possibility to estimate the underlying statistic for the target domain.

The most basic approach, Deep All, consists of ignoring the domain membership of the images available from all training sources, and training a generic algorithm on the combined source samples. Despite its simplicity, Deep All outperforms many engineered methods in domain generalization, as shown in [72]. The domain specific aggregation modules we propose can be seen as a way to augment the generalization abilities of given CNN architectures by maintaining a generic core, while at the same time explicitly modeling the single domain specific features separately, in a whole coherent structure.

Our architecture consists of a main branch Θ and a collection of domain specific aggregation modules $\Lambda = \{\lambda_1 \dots \lambda_n\}$, each specialized on a single source domain. The main branch Θ is the backbone of our model, and it can be in principle any pre-trained off-the shelf convnet. Aggregation modules, which we design inspired by an iterative aggregation protocol described in [136], receive inputs from Θ and learn to combine features at different levels to produce classification outputs. At training time, each domain-specific aggregation module learns to specialize on a single source domain. In the validation phase, we use a variation of a leave-one-domain-out strategy: we average predictions of each module but, for each i_{th} source domain, we exclude the corresponding domain-specific module λ_i from the evaluation. We test the model in both an end-to-end fashion and by running a linear classifier on the extracted features. In the rest of the section we describe into detail the various components of our approach (section Section 3.1.1.1-Section 3.1.1.2) and the training protocol (section Section 3.1.1.3).

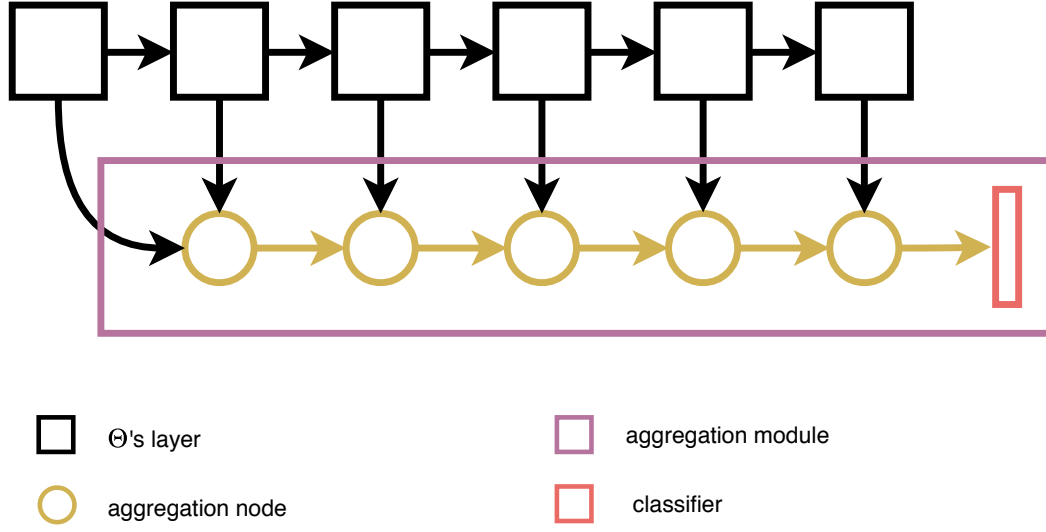


Figure 3.1. Architecture of an aggregation module (purple) augmenting a CNN model. Aggregation nodes (yellow) iteratively process input from Θ 's layers and propagate them to the classifier.

3.1.1.1 Aggregation Module

Deep Layer Aggregation [136] is a feature fusion strategy designed to augment a fully convolutional architecture with a parallel, layered structure whose task is to better process and propagate features from the original network to the classifier. Aggregation nodes, the main building block of the augmenting structure, learn to combine convolutional outputs from multiple layers with a compression technique, which in [136] is implemented with 1×1 convolutions followed by batch normalization and nonlinearity. The arrangement of connections between aggregation nodes and the augmented network's original layers yields an architecture more capable of extracting the full spectrum of spatial and semantical informations from the original model [136].

Inspired by the aggregations of [136], we implement aggregation modules as parallel feature processing branches pluggable in any CNN architecture. Our aggregation consists of a stacked sequence of aggregation nodes N , with each node iteratively combining outputs from Θ and from the previous node, as shown in Figure Figure 3.1. The nodes we use are implemented as 1×1 convolutions followed by nonlinearity. Our aggregation module visually resembles the Iterative Deep Aggregation (IDA) strategy described in [136], but the two are different. IDA is an aggregation pattern for merging different scales, and is implemented on top of a hierarchical structure. Our aggregation module is a pluggable augmentation which merges features from various layers sequentially. Compared to [136], our structure can be merged with any existing pre-trained model without disrupting the original features' propagation. We also extend its usage to non-fully convolutional models by viewing 2-dimensional outputs of fully connected nodes as 4-dimensional ($N \times C \times H \times W$) tensors whose H and W dimension are collapsed. As we designed these modules having in mind the DG problem and their usage for domain specific learning, we

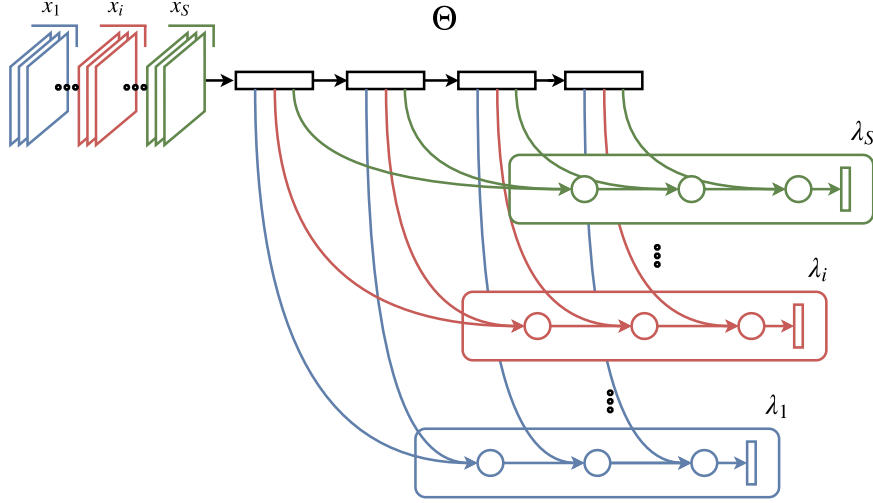


Figure 3.2. Simplified architecture with 3 aggregation nodes per aggregation module. The main branch Θ shares features with S specialized modules. At training time, the i_{th} aggregation module only processes outputs relative to the i_{th} domain.

call them Domain-Specific Aggregation Modules (D-SAM).

3.1.1.2 D-SAM Architecture for Domain Generalization

The modular nature of our D-SAMs allows the stacking of multiple augmentations on the same backbone network. Given a DG setting in which we have S source domains, we choose a pre-trained model Θ and augment it with S aggregation modules, each of which implements its own classifier while learning to specialize on an individual domain. The overall architecture is shown in Figure Figure 3.2.

Our intention is to model the domain specific part and the domain generic part within the architecture. While aggregation modules are domain specific, we may see Θ as the domain generic part that, via backpropagation, learns to yield general features which aggregation modules specialize upon. Although not explicitly trained to do so, our feature evaluations suggest that thanks to our training procedure, the backbone Θ implicitly learns more domain generic representations compared to the corresponding backbone model trained without aggregations.

3.1.1.3 Training and Testing

We train our model so that the backbone Θ processes all the input images, while each aggregation module learns to specialize on a single domain. To accomplish this, at each iteration we feed to the network S equal sized mini-batches grouped by domain. Given an input mini-batch x_i from the i_{th} source domain, the corresponding output of our function, as also shown graphically in Figure Figure 3.2, is:

$$f(x_i) = \lambda_i(\Theta(x_i)). \quad (3.1)$$

We optimize our model by minimizing the cross entropy loss function $L_C =$

$\sum_c y_{x_j^i, c} \log(p_{x_j^i, c})$, which for a training iteration we formalize as:

$$L(\Theta, \Lambda) = \sum_{i=1}^S L_C((\lambda_i \circ \Theta)(x_i)). \quad (3.2)$$

We validate our model by combining probabilities of the outputs of aggregation modules. One problem of the DG setting is that performance on the validation set is not very informative, since accuracy on source domains doesn't give much indication of the generalization ability. We partially mitigate this problem in our algorithm by calculating probabilities for validation as:

$$p_{x_j^v} = \sigma\left(\sum_{i=1, i \neq v}^S \lambda_i(\Theta(x_j^v))\right), \quad (3.3)$$

where σ is the softmax function. Given an input image belonging to the k source domain, all aggregation modules besides λ_k participate in the evaluation. With our validation we keep the model whose aggregation modules are general enough to distinguish between unseen distributions, while still training the main branch on all input data.

We test our model both in an end to end fashion and as a feature extractor. For end-to-end classification we calculate probabilities for the label as:

$$p_{x_j^t} = \sigma\left(\sum_{i=1}^S \lambda_i(\Theta(x_j^t))\right), \quad (3.4)$$

When testing our algorithm as a feature extractor, we evaluate Θ 's and Λ 's features by running an SVM Linear Classifier on the DG task.

3.1.2 Experiments

In this section we report experiments assessing the effectiveness of our DSAM-based architecture in the DG scenario, using two different backbone architectures (a ResNet-18 [52] and an AlexNet [68]), on two different databases. We first report the model setup (section Section 3.1.2.1), and then we proceed to report the training protocol adopted (section Section 3.1.2.2). Section Section 3.1.2.3 reports and comments upon the experimental results obtained.

3.1.2.1 Model setup

Aggregation Nodes

We implemented the aggregation nodes as 1x1 convolutional filters followed by nonlinearity. Compared to [136], we did not use batch normalization in the aggregations, since we empirically found it detrimental for our difficult DG targets. Whenever the inputs of a node have different scales, we downsampled with the same strategy used in the backbone model. For ResNet-18 experiments, we further regularized the convolutional inputs of our aggregations with dropout.

Aggregation of Fully Connected Layers

We observe that a fully connected layer’s output can be seen as a 4-dimensional (N, C, H, W) tensor with collapsed height and width dimensions, as each unit’s output is a function of the entire input image. A 1×1 convolutional layer whose input is such a tensor coincides with a fully connected layer whose input is a 2-dimensional (N, C) tensor, so for simplicity we implemented those aggregations with fully connected layers instead of convolutions.

Model Initialization

We experimented with two different backbone models: AlexNet and ResNet-18, both of which are pre-trained on the ImageNet 1000 object categories [30]. We initialized our aggregation modules Λ with random uniform initialization. We connected the aggregation nodes with the output of the AlexNet’s layers when using AlexNet as backbone, or with the exit of each residual block when using ResNet-18.

3.1.2.2 Training setup

We finetuned our models on $S = 3$ source domains and tested on the remaining target. We splitted our training sets in 90% train and 10% validation, and used the best performing model on the validation set for the final test, following the validation strategy described in Section Section 3.1.1. For preprocessing, we used random zooming with rescaling, horizontal flipping, brightness/contrast/saturation/hue perturbations and normalization using ImageNet’s statistics. We used a batch size of 96 (32 images per source domain) and trained using SGD with momentum set at 0.9 and initial learning rate at 0.01 and 0.007 for ResNet’s and AlexNet’s experiments respectively. We considered an epoch as the minimum number of steps necessary to iterate over the largest source domain and we trained our models for 30 epochs, scaling the learning rate by a factor of 0.2 every 10 epochs. We used the same setup to train our ResNet-18 Deep All baselines. We repeated each experiment 5 times, averaging the results.

3.1.2.3 Results

We run a first set of experiments with the D-SAMs using an AlexNet as backbone, to compare our results with those reported in the literature by previous works, as AlexNet has been so far the convnet of choice in DG. Results are reported in table Table 3.1. We see that our approach outperforms previous work by a sizable margin, showing the value of our architecture. Particularly, we underline that D-SAMs obtain remarkable performances on the challenging setting where the ‘Sketch’ domain acts as target.

We then run a second set of experiments, using both the PACS and Office-Home dataset, using as backbone architecture a ResNet-18. The goal of this set of experiments is on one side to showcase how our approach can be easily used with different Θ networks, on the other side to perform an ablation study with respect to the possibility to use D-SAMs not only in an end-to-end classification framework, but also to learn feature representations, suitable for domain generalization. To this

Table 3.1. PACS end-to-end results using D-SAMs coupled with the AlexNet architecture.

	Deep [72]	All	TF [72]	MLDG [73]	SSN [83]	D-SAMs
art painting	64.91		62.86	66.23	64.10	63.87
cartoon	64.28		66.97	66.88	66.80	70.70
photo	86.67		89.50	88.00	90.20	85.55
sketch	53.08		57.51	58.96	60.10	64.66
avg	67.24		69.21	70.01	70.30	71.20

Table 3.2. PACS results with ResNet-18 using features (top-rows) and end-to-end accuracy (bottom rows).

		art paint- ing	cartoon	sketch	photo	Avg
Deep (feat.)	All	77.06	77.81	74.09	93.28	80.56
Θ (feat.)		79.57	76.94	75.47	94.16	81.54
Λ (feat.)		79.48	77.13	75.30	94.30	81.55
$\Theta + \Lambda$ (feat.)		79.44	77.22	75.33	94.19	81.54
Deep All		77.84	75.89	69.27	95.19	79.55
D-SAMs		77.33	72.43	77.83	95.30	80.72

end, we report results on both databases using the end-to-end approach tested in the AlexNet experiments, plus results obtained using the feature representations learned by Θ , Λ and the combination of the two. Specifically, we extract and l_2 normalize features from the last pooling layer of each component. We integrate features of Λ 's modules with concatenation, and train the SVM classifier leaving the hyperparameter C at the default value. Our results in table Table 3.2 and Table 3.3 show that the SVM classifier trained on the l_2 normalized features always outperforms the corresponding end-to-end models, and that Θ 's and Λ 's features have similar performance, with Θ 's features outperforming the corresponding Deep All features while requiring no computational overhead for inference.

Table 3.3. OfficeHome results with ResNet-18 using features (top rows) and end-to-end accuracy (bottom rows).

		Art	Clipart	Product	Real- World	Avg
Deep (feat.)	All	52.66	48.35	71.37	71.47	60.96
Θ (feat.)		54.55	49.37	71.38	72.17	61.87
Λ (feat.)		54.53	49.04	71.57	71.90	61.76
$\Theta + \Lambda$ (feat.)		54.54	49.05	71.58	72.03	61.80
Deep All		55.59	42.42	70.34	70.86	59.81
D-SAMs		58.03	44.37	69.22	71.45	60.77

3.1.3 Conclusions

We presented a Domain Generalization architecture inspired by recent work on deep layer aggregation. We developed a convnet that, starting from a pre-trained model carrying generic perceptual knowledge, aggregates layers iteratively for as many branches as the available source domains data at training time. The model can be used in an end-to-end fashion, or its convolutional layers can be used as features in a linear SVM. Both approaches, tested with two popular pre-trained architectures on two benchmark databases, achieved state of the art. Future work in this direction should further study deep layer aggregation strategies within the context of domain generalization, as well as scalability with respect to the number of sources.

3.2 Rethinking Domain Generalization Baselines

Despite being very powerful in standard learning settings, deep learning models can be extremely brittle when deployed in scenarios different from those on which they were trained. Domain generalization methods investigate this problem and data augmentation strategies have shown to be helpful tools to increase data variability, supporting model robustness across domains. In our work we focus on style transfer data augmentation and we present how it can be implemented with a simple and inexpensive strategy to improve generalization. Moreover, we analyze the behavior of current state of the art domain generalization methods when integrated with this augmentation solution: our thorough experimental evaluation shows that their original effect almost always disappears with respect to the augmented baseline. This issue opens new scenarios for domain generalization research, highlighting the need of novel methods properly able to take advantage of the introduced data variability to further push domain generalization research.

The real world offers such a large diversity that the standard machine learning assumption of collecting train and test data under the same conditions, thus from the same domain/distribution, is broadly violated. Domain adaptation and domain generalization methods tackle this problem under different points of view. In the first case, unlabeled test data are considered available at training time, allowing the learning model to peek into the characteristics of the target set and adapt to it [27]. Domain generalization is a more challenging task because target data are fed to the system only during deployment [8, 95]. In this last setting it is crucial to train robust model, possibly exploiting multiple available sources. Towards this goal, most of the existing domain generalization strategies try to incorporate the observed data invariances, capturing them at feature [75] or model (meta-learning [74] and self-supervision [130]) level, in the hypothesis that analogous invariances hold for future test domains. An alternative solution consists in extending the source domains by synthesizing new images. This is usually done by learning generative models with the specific constraint of preserving the object content but varying the global image appearance, with the aim of better spanning the data space and include a larger variability in the training set. Thanks to the developments in generative learning, it is becoming more and more evident that their integration into domain generalization approaches is effective [144]. However their performance tends to grow together with the complexity of the learning model which may involve one or multiple generator modules that are notoriously difficult to train. We also noticed a particular trend in the most recent domain generalization research. Several papers discuss the merit of the proposed data augmentation solutions in comparison with feature and model-based generalization techniques [144, 143]. However, newly introduced feature and model-based approaches avoid benchmarks against data augmentation strategies considering them unfair competitors due to the extended training set [126, 58]. We believe that the field needs some clarification and we dedicate our work on this topic. Specifically our main contributions are:

- **A simple and effective style transfer data augmentation approach for domain generalization.** We show how the method AdaIN [57], that is able to

perform style transfer in real time, can be re-purposed for data augmentation, combining semantic and texture information of the available source data (see Figure 3.3). The extended training set allows to get top target results, outperforming existing state of the art approaches.

- **We designed tailored strategies to integrate for the first time style transfer data augmentation with the current state of the art approaches.** The obtained results indicate that the original advantage of those methods almost always disappears when compared with the data augmented baseline.

The scenario described by this analysis clearly suggests the need of rethinking domain generalization baselines. On one side simple data augmentation strategies should be envisaged to increase source data variability compatible with orthogonal feature and model generalization approaches. On the other, new cross-source adaptive strategies should be designed to build over images generated by style transfer approaches.

3.2.1 Source augmentation by style transfer

We focus on the multi-source domain generalization setting where $S = \{S_1, \dots, S_n\}$ denotes the n available data sources with the respective $\{x_i^s, y_i^s\}_{i=1}^{N_s} \in S$ samples, where y_i specifies the object classification label of its x_i image. The main goal is to generalize to an unknown target database $\{x_i^t, y_i^t\}_{i=1}^{N_t} \in T$, where T shares with S the same set of categories, while each source and the target are drawn from different marginal distributions. As indicated by the chosen notation, we disregard the specific domain annotation of each source sample, meaning that we do not need to know the exact source origin of each image.

We indicate with $C(x^s, \theta_c)$ a basic deep learning classifier parametrized by θ_c and trained on the source data by minimizing the standard cross-entropy loss $\mathcal{L}(C(x^s, \theta_c), y^s)$. To increase data variability we study how to augment each sample x^s by keeping its semantic content and changing the image style, borrowing it from the other available source data. The stylized sample \tilde{x}^s obtained from x^s inherits its label y^s and enriches the training set, possibly making the model learned by optimizing $\mathcal{L}(C(\tilde{x}^s, \theta_c), y^s)$ more robust to domain shifts. Thus, our analysis will consider a two step process, where a deep model A parametrized by θ_a is first learned on the source data to perform style transfer $x^s \rightarrow \tilde{x}^s = A(x^s, \theta_a)$, and then it is used to perform data augmentation at runtime while learning to classify the image object content.

3.2.1.1 Training the Style Transfer Model

To implement A we use AdaIN [57], a simple and effective encoder-decoder-based approach that allows style transfer in real time. The encoder E extracts representative features f_c, f_s respectively from the content and the style image, the first are then re-normalized to have the same channel-wise mean and standard deviation of the second as follows:

$$f_{cs} = \sigma(f_s) \left(\frac{f_c - \mu(f_c)}{\sigma(f_c)} \right) + \mu(f_s) . \quad (3.5)$$

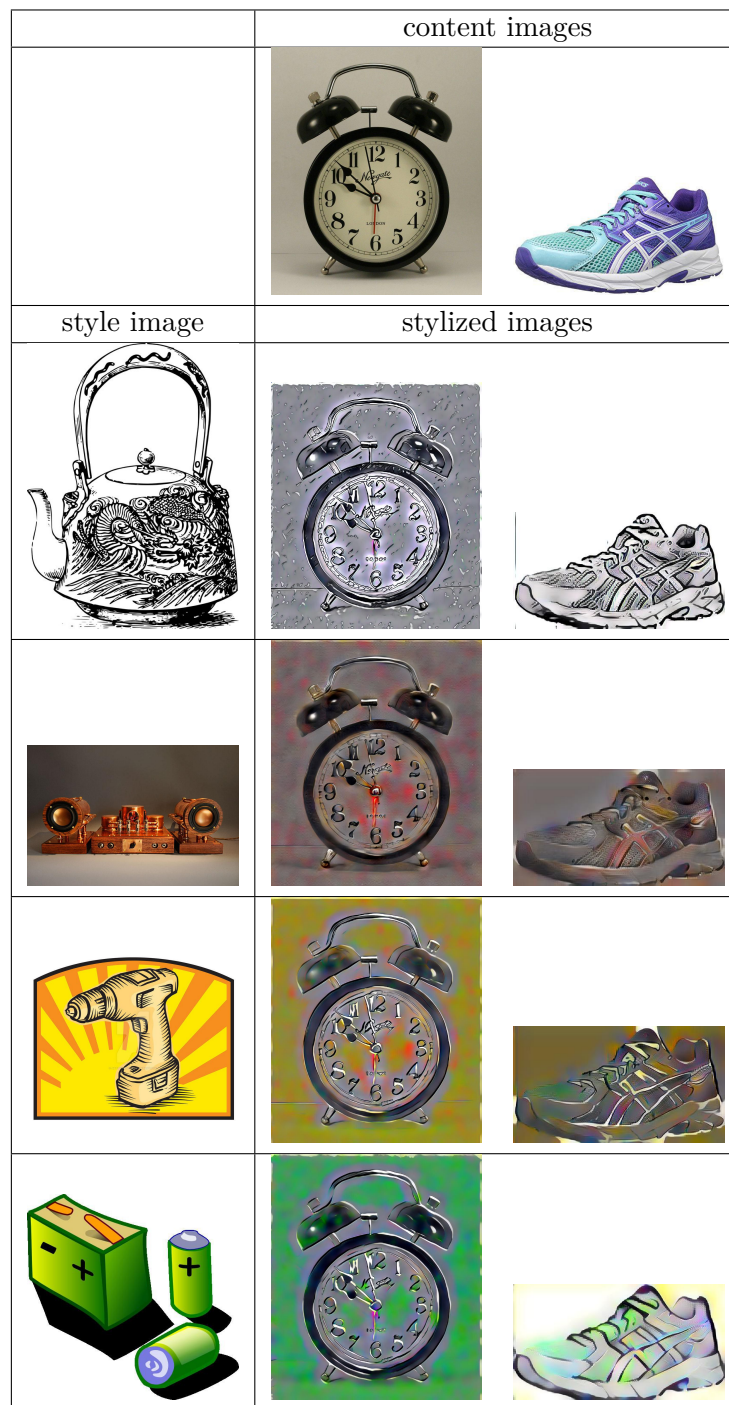


Figure 3.3. Source augmentation by style transfer allows to generate a large amount of different variations from each image, borrowing the style from any other image and by keeping the original semantic content. All the images are taken from OfficeHome dataset and the style transfer is performed using AdaIN.

Finally, the obtained feature f_{cs} is mapped back to the image space through the decoder D minimizing two losses:

$$\mathcal{L}_A = \mathcal{L}_c + \lambda \mathcal{L}_s . \quad (3.6)$$

Both the losses measure the distance between the features re-extracted through the encoder $E(D(f_{cs}))$ from the stylized output image, and f_{cs} . Specifically \mathcal{L}_c focuses on the content information considering the whole final feature output, while \mathcal{L}_s focuses on the style information, measuring the difference of mean and standard deviation of the Relu output of several encoder layers.

The method has two main hyperparameters $\theta_a = \{\lambda, \alpha\}$. The first controls the degree of the style transfer during training by adjusting the importance of the style loss and is generally kept fixed at $\lambda = 10$. The second allows a content-style trade-off at test time by interpolating between the feature maps that are fed to the decoder with $f_{cs\alpha} = D((1 - \alpha)f_c + \alpha f_{cs})$. When $\alpha = 0$ the network tries to reconstruct the content image, while when $\alpha = 1$ it produces the most stylized image.

3.2.1.2 Style Transfer as Data Augmentation

As already mentioned above, we disregard the source domain labels, thus when training our object classifier C the data batches contain samples extracted from all the source domains. Each sample in a batch has the role of content image and any of the remaining instances in the same batch can be selected randomly to work as style provider. In this scenario stylization can happen both from images of the same source domain (e.g. two photos) or from images of different domains (e.g. a photo and a painting). To regulate this process we use a stochastic approach with the transformed image \tilde{x}^s replacing its original version x^s with probability p .

We highlight that the described procedure for the application of AdaIN differs from what appeared in previous works. Indeed, both the original approach [57] and its use for data augmentation in [143], exploit the style transfer model trained on MS-COCO [77] as content images and paintings mostly collected from WikiArt [97] as style images. In our study we do not allow extra datasets besides those directly involved in the domain generalization task as source domains.

3.2.2 Experiments

We designed our experimental analysis with the aim of running a thorough evaluation of the impact of style transfer data augmentation on domain generalization. Besides observing how this data augmentation can improve the standard learning baseline model, and how it compares with the most recent state of the art DG methods, we are also interested in the effectiveness of their combination. In the following we provide details on the chosen data testbeds and sota models, describing how the data augmentation strategy is integrated in each approach.

3.2.2.1 Experimental Setting

We test our method on PACS, VLCS and OfficeHome benchmarks.

We apply the same experimental protocol of [18]: the predefined full training data is randomly partitioned in train and validation sets with a 90-10 ratio. The

training is performed on the train splits of the 3 source domains while the validation splits are used for model selection. At the end the model is tested on the predefined test split of the left out domain. This split has been defined randomly selecting 30% of images of the overall dataset.

All our results are obtained by performing an average over 3 runs. In the case of both OfficeHome and VLCS the random 90-10 train-val split was repeated for each run.

3.2.2.2 Comparison methods

We want to show that *source augmentation by style transfer* does not only allow to obtain performances higher than previous more complex methods, but more importantly that current state of the art methods, designed and built on a baseline that does not take into account the source augmentation by style transfer, loose their effectiveness when applied on this new stronger baseline. For this reason we have chosen a number of current state of the art approaches and integrated the source augmentation style transfer into them. We performed our choice considering methods that employ different approaches to deal with the Domain Generalization setting. For each of these methods we carefully designed the integration of the source augmentation by style transfer in order to not undermine their specific strategies. For our study we consider as main Baseline a classification model learned on all the source data and naïvely applied on the target. We indicate with Original the standard data augmentation with horizontal flipping and random cropping, while we use Stylized to specify the cases where we add style transfer data augmentation. The behavior of four among the most recent DG methods is evaluated under both these augmentation settings. We dedicate a particular attention to the integration of the style transfer data augmentation strategy with each of the considered approaches. The goal is getting the most out of them without undermining their nature. In particular, considering that the style transfer leads to domain mixing, it is important to not integrate it in procedures that need a separation among source domains.

DG-MMLD [88]

This approach exploits clustering and domain adversarial feature alignment. Since it does not need the source domain labels, the integration of the proposed style transfer data augmentation is straightforward: styles of random images are applied to each content images (inside a batch) with probability p , exactly as done for the Baseline.

Epi-FCR [74]

Epi-FCR is a meta-learning method which splits the network in two modules, each one is trained by pairing it with a partner that is badly tuned for the domain considered in the current learning episode. The modules are the feature extractor and the classifier which alternatively cover the two roles of learning part and bad reference. After this phase, a final model is learned by integrating the trained modules together with a random classifier used as regularizer. In the first stage, knowing the source domain labels is crucial to choose and set the two network

Table 3.4. PACS classification accuracy (%). We used AdaIN with $\alpha = 1.0$ and $p = 0.75$ for AlexNet-based experiments and AdaIN with $\alpha = 1.0$ and $p = 0.90$ for those based on ResNet18.

AlexNet						
		Painting	Cartoon	Sketch	Photo	Average
Original	Baseline	66.83	70.85	59.75	89.78	71.80
	Rotation	65.66	71.89	62.15	89.88	72.39
	DG-MMLD	69.27	72.83	66.44	88.98	74.38
	Epi-FCR	64.70	72.30	65.00	86.10	72.03
	DDAIG*	62.77	67.06	58.90	86.82	68.89
Stylized	Baseline	71.96	72.47	76.47	88.34	77.31
	Rotation	71.74	73.39	75.98	89.22	77.59
	DG-MMLD	70.50	70.84	75.39	88.43	76.29
	Epi-FCR	65.19	69.54	71.97	83.43	72.53
	DDAIG	69.35	71.10	70.99	87.70	74.79
Mixup	pixel-level	66.03	68.00	51.18	88.90	68.53
	feature-level	67.04	69.10	55.40	88.88	70.11
ResNet18						
Original	Baseline	77.28	73.89	67.01	95.83	78.50
	Rotation	78.16	76.64	72.20	95.57	80.64
	DG-MMLD	81.28	77.16	72.29	96.06	81.83
	Epi-FCR	82.10	77.00	73.00	93.90	81.50
	DDAIG*	79.41	74.81	69.29	95.22	79.68
Stylized	Baseline	82.73	77.97	81.61	94.95	84.32
	Rotation	79.51	79.93	82.01	93.55	83.75
	DG-MMLD	80.85	77.10	77.69	95.11	82.69
	Epi-FCR	80.68	78.87	76.57	92.50	82.15
	DDAIG	81.02	78.75	79.67	95.07	83.63
Mixup	pixel-level	78.09	71.08	66.58	93.85	77.40
	feature-level	81.20	76.41	69.67	96.31	80.90

modules, thus mixing the domains with style transfer augmentation could degrade its performance. In the ending stage instead, all the source data are considered together: we applied here the style data augmentation.

DDAIG [144]

This is a data augmentation strategy based on a transformation network which is trained so that every synthesized sample keeps the same label of the original image, but fools a domain classifier. In the learning procedure the transformation module, the label classifier and the domain classifier are iteratively updated. In particular the label classifier is trained on all the source data, both original and synthetic: we further extended this set with style transfer augmented data.

Rotation [130]

It has been shown that self-supervised knowledge supports domain generalization when combined with supervised learning in a multi-task model. In particular we focused on rotation recognition, where the orientation angle of each image should be recognized among $\{0^\circ, 90^\circ, 180^\circ, 270^\circ\}$. The model minimizes a combination of the supervised and self-supervised loss with linear weight σ generally kept lower than 1 to let the supervised model guide the learning process. In this case the domain labels are not used during training, so the application of the source augmentation by style transfer is straightforward.

Mixup [138]

An approach related to data augmentation, originally defined to improve generalization in standard in-domain learning, is Mixup: it interpolates samples and their labels, regularizing a neural network to favor a simple linear behavior between training examples. Its hyper-parameter $\gamma \in \{0, \infty\}$ controls the strength of interpolation between data pairs, recovering the Baseline for $\gamma = 0$. In our study we consider Mixup as further reference, and in particular we tested data mixing both at pixel and at feature level [131].

3.2.2.3 Training Setup

Our style transfer model A is trained on source data before training the classification model C . As already mentioned, A is implemented by AdaIN [57] and is therefore based on a VGG backbone. It is trained for 20 epochs with a learning rate equal to $5e-5$. The hyperparameters α and p used in each experiment are specified in the caption of the respective result tables and in depth analysis on the sensitivity of the method to them is presented in Section Section 3.2.2.5.

For the classification model C we use AlexNet and ResNet18 backbones. Specifically, Baseline, Rotation and Mixup are trained using SGD with 0.9 momentum for $30k$ iterations. We set the batch size to 32 images per source domain: since in all the testbed there are three source domains each data batch contains 96 images. The learning rate and the weigh decay are respectively fixed to 0.001 and 0.0001. Regarding the hyperparameters of the individual algorithms, we empirically set the

Table 3.5. OfficeHome classification accuracy (%). We used AdaIN with parameters $\alpha = 1.0$ and $p = 0.1$.

		ResNet18				
		Art	Clipart	Product	Real World	Average
Original	Baseline	57.14	46.96	73.50	75.72	63.33
	Rotation	55.94	47.26	72.38	74.84	62.61
	DG-MMLD*	58.08	49.32	72.91	74.69	63.75
	Epi-FCR*	53.34	49.66	68.56	70.14	60.43
	DDAIG*	57.79	48.32	73.28	74.99	63.59
Stylized	Baseline	58.71	52.33	72.95	75.00	64.75
	Rotation	57.24	52.15	72.33	73.66	63.85
	DG-MMLD	59.24	49.30	73.56	75.85	64.49
	Epi-FCR	52.97	50.14	67.03	70.66	60.20
	DDAIG	58.21	50.26	73.81	74.99	64.32
Mixup	feature-level	58.33	39.76	70.96	72.07	60.28

Rotation auxiliary weight to $\sigma = 0.5$ and for Mixup $\gamma = 0.4$.

We implement Rotation by adding a rotation recognition branch to our Baseline. For DG-MMLD, Epi-FCR and DDAIG, we use the code provided by the authors integrating different datasets/backbones where needed. The training setup for these experiments is the one defined in their papers for both the Original and Stylized version. We report the previously published results whenever possible. In the following we will indicate with a star (*) the results we obtained by running the authors' code.

3.2.2.4 Results analysis

Table Table 3.4 shows results on PACS benchmark with both AlexNet and ResNet18 backbones. We get two main outcomes. (1) There is an evident improvement of more than 5 percentage points in the Baseline performance when using the stylized augmented source data with respect to the original case. Looking at the results for the different domains we can see that improvement is higher for Art Painting, Cartoon and Sketch, than in Photo. (2) All the considered state of the art DG methods benefit from the source augmentation. Indeed in absolute terms their performance grows, but at the same time they loose in effectiveness as they cannot outperform the Baseline any more.

Table Table 3.5 shows results on OfficeHome dataset with ResNet18 backbone. Even if in this case the improvement produced by the source augmentation by style transfer is more limited, the results confirm what we have already observed for PACS. The Stylized Baseline obtains the best accuracy outperforming the competitor state of the art methods, even when those are improved using the same source augmentation.

Table Table 3.6 reports results on VLCS benchmark with AlexNet backbone. This dataset is particularly challenging and shows a fundamental limit of tackling DG through style transfer data augmentation. Since the domain shift is not originally due to style differences in this testbed, source augmentation by style transfer does

Table 3.6. VLCS classification accuracy (%). We used AdaIN with parameters are $\alpha = 1.0$ and $p = 0.75$.

		AlexNet				
		CALTECH	LABELME	PASCAL	SUN	Average
Original	Baseline	94.89	59.14	71.31	64.64	72.49
	Rotation	94.50	61.27	68.94	63.28	72.00
	DG-MMLD*	96.94	59.10	68.48	62.06	71.64
	Epi-FCR*	91.43	61.36	63.44	60.07	69.07
	DDAIG*	95.75	60.18	65.48	60.78	70.55
Stylized	Baseline	96.86	60.77	68.18	63.42	72.31
	Rotation	96.86	60.77	68.18	63.42	72.31
	DG-MMLD	97.49	61.02	64.23	62.37	71.28
	Epi-FCR	92.69	58.18	62.59	57.87	67.83
	DDAIG	97.48	60.48	65.19	62.57	71.43
Mixup	feature-level	94.73	62.15	69.82	62.98	72.42

not support generalization.

As a final remark, we focus on Mixup. The results over all the considered datasets show that it is not able to generalize across domains and it might perform even worse than the Original Baseline. Between the two considered pixel and feature variants, only the second shows some advantage on PACS, so we focused on it in the other tests. Still, its results remain lower than those obtained by the DG methods both with and without style based data augmentation.

3.2.2.5 Analysis of AdaIN hyperparameters

In Figures Figure 3.4 and Figure 3.5 we see how the PACS AlexNet results change when varying either α or p by keeping the other fixed. With a low value of α the style transfer is too weak to produce an effective appearance change of the source sample and introduce extra variability. In general the best results are obtained using $\alpha = 1$ regardless of the specific value of p .

For what concerns the value of p we can see that, if α is high enough, even a small p allows to obtain good performance with the best results obtained with $p = 0.5$ or $p = 0.75$.

3.2.2.6 Style transfer from external data vs source data

The described procedure for the application of AdaIN differs from what appeared in previous works. Indeed, both the original approach [57] and its use for data augmentation in [143], exploit the style transfer model trained on MS-COCO [77] as content images, and paintings mostly collected from WikiArt [97] as style images. In our study we did not allow extra datasets besides those directly involved in the domain generalization task as source domains. The reason is twofold: first, we want to keep the method as simple as possible, without the need of relying on external data; second, to perform a fair benchmark with the competitors DG methods all of them should have access to the same source information.

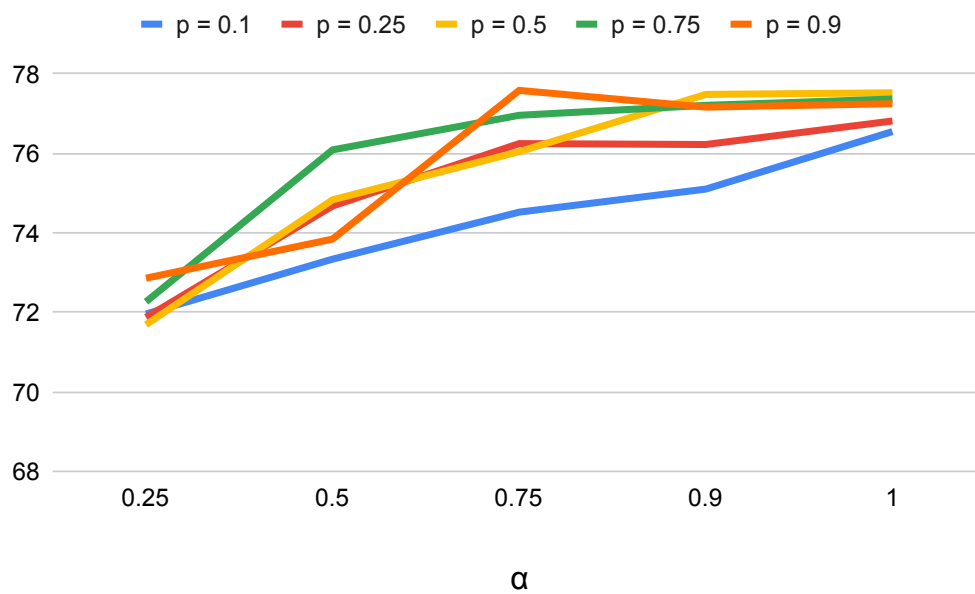


Figure 3.4. Average accuracy on PACS AlexNet with different values of p when varying α .

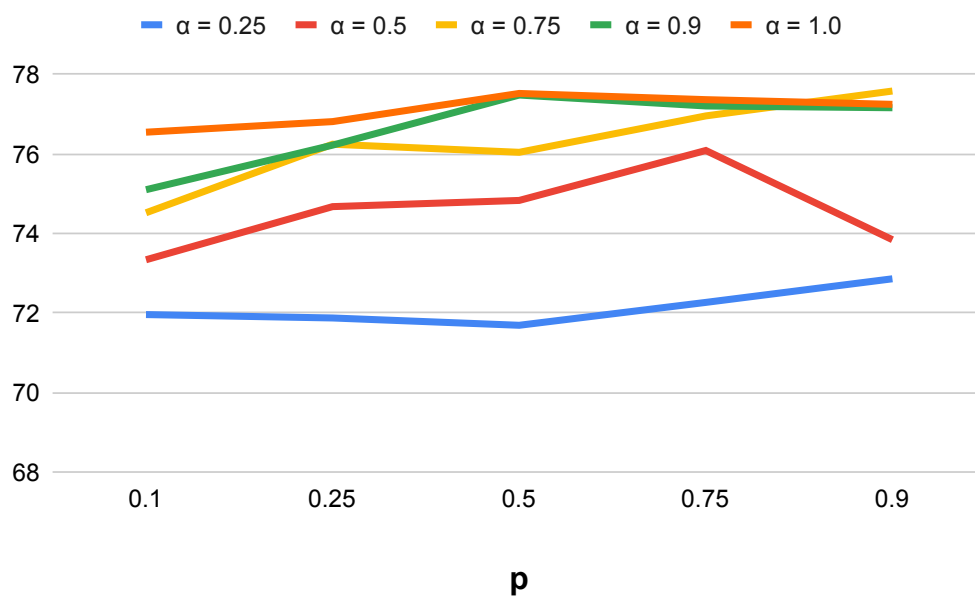


Figure 3.5. Average accuracy on PACS AlexNet with different values of α when varying p .



Figure 3.6. Example of application of style transfer using AdaIN. The first image comes from the PACS Photo domain and is used as content while the second comes from PACS Art Painting domain and is used as style image. On top right there is the translation performed using AdaIN trained on MS-COCO and WikiArt images. In the second row we see the translations performed using our AdaIN models trained on source data only, respectively when the Art Paintings, Cartoon, Sketch and Photo domains are used as target.

Table 3.7. Comparison of AdaIN training strategies

	Art Painting	Cartoon	Sketch	Photo	Average
Stylized Baseline	71.96	72.47	76.47	88.34	77.31 ± 1.1
MSCOCO-WikiArt Baseline	73.00	73.78	76.37	89.04	78.05 ± 0.9

Still, the interested reader may wonder what would be the effect of using the original AdaIN model trained on MSCOCO and WikiArt. Figure Figure 3.6 shows one example obtained in this way. Specifically we consider a dog image drawn from the PACS Photo domain and we analyse the images obtained by borrowing the style form the Art Painting guitar image. We compare the stylized sample produced with the MSCOCO-WikiArt AdaIN model against the outcomes of the four AdaIN variants trained on the source with every one of the four domains used as target.

As can be observed, the obtained results in terms of image quality are not so different and, as already indicated by the results discussed above, they are good enough to introduce variability in the source. We also run a quantitative analysis: in Table Table 3.7 we compare the performance of the our Stylized Baseline on PACS AlexNet with the analogous Baseline trained using the augmented data produced with the AdaIN MSCOCO-WikiArt pretrained model. The last one shows a slightly better accuracy which is though not significant if we consider the related standard deviation.

3.2.3 Conclusions

Among the current state of the art domain generalization methods some are based on data augmentation and use complex generative approaches, while other propose source feature adaptation and meta-learning strategies. Despite being orthogonal among each other, no previous work tried to integrate them. We investigated here a simple and effective style transfer data augmentation strategy for domain generalization and we showed how it overcomes its competitors. Moreover we designed proper combination of this approach with the most relevant existing DG approaches. Our experimental analysis indicates that the performance of the considered methods improves over the respective versions not including the style data augmentation, but surprisingly the methods lose their original effectiveness, not showing any improvement over the new data augmented baseline.

As other concurrent technical reports [50], our work suggests the need of a shading new light on domain generalization problems and calls for novel strategies able to take advantage of the data variability introduced by cross-domain style transfer.

Chapter 4

Self-Supervised approaches for Domain Generalization and Domain Adaptation

4.1 Domain Generalization by solving jigsaw puzzles

Human adaptability relies crucially on the ability to learn and merge knowledge both from supervised and unsupervised learning: the parents point out few important concepts, but then the children fill in the gaps on their own. This is particularly effective, because supervised learning can never be exhaustive and thus learning autonomously allows to discover invariances and regularities that help to generalize. In this paper we propose to apply a similar approach to the task of object recognition across domains: our model learns the semantic labels in a supervised fashion, and broadens its understanding of the data by learning from self-supervised signals how to solve a jigsaw puzzle on the same images. This secondary task helps the network to learn the concepts of spatial correlation while acting as a regularizer for the classification task. Multiple experiments on the PACS, VLCS, Office-Home and digits datasets confirm our intuition and show that this simple method outperforms previous domain generalization and adaptation solutions. An ablation study further illustrates the inner workings of our approach.

In the current gold rush towards artificial intelligent systems it is becoming more and more evident that there is little intelligence without the ability to transfer knowledge and generalize across tasks, domains and categories [27]. A large portion of computer vision research is dedicated to supervised methods that show remarkable results with convolutional neural networks in well defined settings, but still struggle when attempting these types of generalizations. Focusing on the ability to generalize across domains, the community has attacked this issue so far mainly by regularizing supervised learning processes with techniques that search for intermediate semantic spaces able to capture basic data knowledge regardless of the specific appearance of input images. Proposed methods range from decoupling image style from the shared object content [10], to pulling data of different domains together and imposing adversarial conditions [75, 76], up to generating new samples to better cover the space spanned by any future target [118, 125].

With the analogous aim of getting general purpose feature embeddings, an alternative research direction has been recently pursued in the area of unsupervised learning. The main techniques are based on the definition of tasks useful to learn visual invariances and regularities by exploiting self-supervisory signals as the spatial co-location of patches [98, 26, 101], counting primitives [100], image coloring [140], and video frame ordering [91, 127]. The large availability of variable unsupervised data, as well as their very nature which makes them free from the labeling bias issue [121], suggests that the unsupervised tasks may also capture knowledge independent from specific domain style. Despite their large potential, the existing unsupervised approaches often come with tailored architectures that need dedicated finetuning strategies to re-engineer the acquired knowledge and make it usable as input for a standard supervised training process [101]. Moreover, this knowledge is generally applied on real-world photos and has not been challenged before across large domain gaps with images of other nature like paintings or sketches.

This clear separation between learning intrinsic regularities from images and robust classification across domains is in contrast with the visual learning strategies of biological systems, and in particular of the human visual system. Indeed, numerous

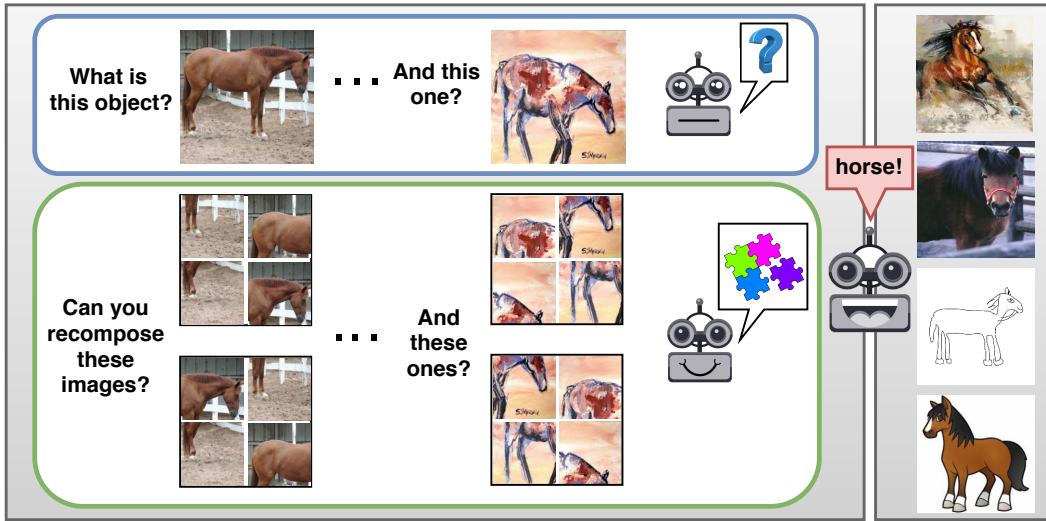


Figure 4.1. Recognizing objects across visual domains is a challenging task that requires high generalization abilities. Other tasks, based on intrinsic self-supervisory image signals, allow to capture natural invariances and regularities that can help to bridge across large style gaps. With JiGen we learn jointly to classify objects and solve jigsaw puzzles, showing that this supports generalization to new domains.

studies highlight that infants and toddlers learn both to categorize objects and about regularities at the same time [7]. For instance, popular toys for infants teach to recognize different categories by fitting them into shape sorters; jigsaw puzzles of animals or vehicles to encourage learning of object parts’ spatial relations are equally widespread among 12-18 months old. This type of joint learning is certainly a key ingredient in the ability of humans to reach sophisticated visual generalization abilities at an early age [39].

Inspired by this, we propose the first end-to-end architecture that learns simultaneously how to generalize across domains and about spatial co-location of image parts (Figure Figure 4.1, Figure 4.2). In this work we focus on the unsupervised task of recovering an original image from its shuffled parts, also known as solving jigsaw puzzles. We show how this popular game can be re-purposed as a side objective to be optimized jointly with object classification over different source domains and improve generalization with a simple multi-task process. We name our Jigsaw puzzle based Generalization method JiGen. Differently from previous approaches that deal with separate image patches and recombine their features towards the end of the learning process [98, 26, 101, 26], we move the patch re-assembly at the image level and we formalize the jigsaw task as a classification problem over recomposed images with the same dimension of the original one. In this way object recognition and patch reordering can share the same network backbone and we can seamlessly leverage over any convolutional learning structure as well as several pretrained models without the need of specific architectural changes.

We demonstrate that JiGen allows to better capture the shared knowledge among multiple sources and acts as a regularization tool for a single source. In the case unlabeled samples of the target data are available at training time, running the unsupervised jigsaw task on them contributes to the feature adaptation process

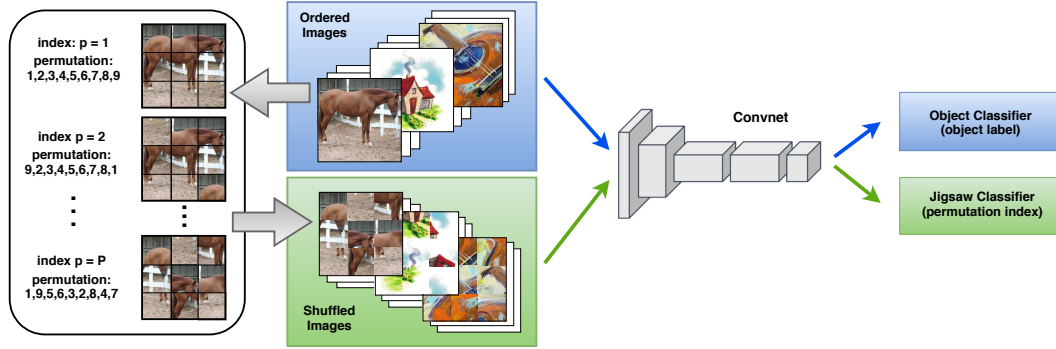


Figure 4.2. Illustration of the proposed method JiGen. We start from images of multiple domains and use a 3×3 grid to decompose them in 9 patches which are then randomly shuffled and used to form images of the same dimension of the original ones. By using the maximal Hamming distance algorithm in [98] we define a set of P patch permutations and assign an index to each of them. Both the original ordered and the shuffled images are fed to a convolutional network that is optimized to satisfy two objectives: object classification on the ordered images and jigsaw classification, meaning permutation index recognition, on the shuffled images.

and shows competing results with respect to state of the art unsupervised domain adaptation methods.

4.1.1 The JiGen approach

Starting from the samples of multiple source domains, we wish to learn a model that can perform well on any new target data population covering the same set of categories. Let us assume to observe S domains, with the i -th domain containing N_i labeled instances $\{(x_j^i, y_j^i)\}_{j=1}^{N_i}$, where x_j^i indicates the j -th image and $y_j^i \in \{1, \dots, C\}$ is its class label. The first basic objective of JiGen is to minimize the loss $\mathcal{L}_c(h(x|\theta_f, \theta_c), y)$ that measures the error between the true label y and the label predicted by the deep model function h , parametrized by θ_f and θ_c . These parameters define the feature embedding space and the final classifier, respectively for the convolutional and fully connected parts of the network. Together with this objective, we ask the network to satisfy a second condition related to solving jigsaw puzzles. We start by decomposing the source images using a regular $n \times n$ grid of patches, which are then shuffled and re-assigned to one of the n^2 grid positions. Out of the $n^2!$ possible permutations we select a set of P elements by following the Hamming distance based algorithm in [98], and we assign an index to each entry. In this way we define a second classification task on K_i labeled instances $\{(z_k^i, p_k^i)\}_{k=1}^{K_i}$, where z_k^i indicates the recomposed samples and $p_k^i \in \{1, \dots, P\}$ the related permutation index, for which we need to minimize the jigsaw loss $\mathcal{L}_p(h(z|\theta_f, \theta_p), p)$. Here the deep model function h has the same structure used for object classification and shares with that the parameters θ_f . The final fully connected layer dedicated to permutation recognition is parametrized by θ_p . Overall we train the network to

obtain the optimal model through

$$\underset{\theta_f, \theta_c, \theta_p}{\operatorname{argmin}} \sum_{i=1}^S \sum_{j=1}^{N_i} \mathcal{L}_c(h(x_j^i | \theta_f, \theta_c), y_j^i) + \sum_{k=1}^{K_i} \alpha \mathcal{L}_p(h(z_k^i | \theta_f, \theta_p), p_k^i) \quad (4.1)$$

where both \mathcal{L}_c and \mathcal{L}_p are standard cross-entropy losses. We underline that the jigsaw loss is also calculated on the ordered images. Indeed, the correct patch sorting corresponds to one of the possible permutations and we always include it in the considered subset P . On the other way round, the classification loss is not influenced by the shuffled images, since this would make object recognition tougher. At test time we use only the object classifier to predict on the new target images.

4.1.1.1 Extension to Unsupervised Domain Adaptation

Thanks to the unsupervised nature of the jigsaw puzzle task, we can always extend JiGen to the unlabeled samples of target domain when available at training time. This allows us to exploit the jigsaw task for unsupervised domain adaptation. In this setting, for the target ordered images we minimize the classifier prediction uncertainty through the empirical entropy loss $\mathcal{L}_E(x^t) = \sum_{y \in \mathcal{Y}} h(x^t | \theta_f, \theta_c) \log\{h(x^t | \theta_f, \theta_c)\}$, while for the shuffled target images we keep optimizing the jigsaw loss $\mathcal{L}_p(h(z^t | \theta_f, \theta_p), p^t)$.

4.1.1.2 Implementation Details

Overall JiGen¹ has two parameters related to how we define the jigsaw task, and three related to the learning process. The first two are respectively the grid size $n \times n$ used to define the image patches and the cardinality of the patch permutation subset P . As we will detail in the following section, JiGen is robust to these values and for all our experiments we kept them fixed, using 3×3 patch grids and $P = 30$. The remaining parameters are the weights α of the jigsaw loss, and γ assigned to the entropy loss when included in the optimization process for unsupervised domain adaptation. The final third parameter regulates the data input process: the shuffled images enter the network together with the original ordered ones, hence each image batch contains both of them. We define a data bias parameter β to specify their relative ratio. For instance $\beta = 0.6$ means that for each batch, 60% of the images are ordered, while the remaining 40% are shuffled. These last three parameters were chosen by cross validation on a 10% subset of the source images for each experimental setting.

We designed the JiGen network making it able to leverage over many possible convolutional deep architectures. Indeed it is sufficient to remove the existing last fully connected layer of a network and substitute it with the new object and jigsaw classification layers. JiGen is trained with SGD solver, 30 epochs, batch size 128, learning rate set to 0.001 and stepped down to 0.0001 after 80% of the training epochs. We used a simple data augmentation protocol by randomly cropping the images to

¹Code available at <https://github.com/fmcarlucci/JigenDG>

Table 4.1. Domain Generalization results on PACS. The results of JiGen are average over three repetitions of each run. The top part of the table is dedicated to a comparison with previous methods that use the jigsaw task as a pretext to learn transferable features using a context-free siamese-enned network (CFN). The central and bottom part of the table show the comparison of JiGen with several domain generalization methods when using respectively Alexnet and Resnet-18 architectures. Each column title indicates the name of the domain used as target. We use the bold font to highlight the best results of the generalization methods, while we underline a result when it is higher than all the others despite produced by the naïve Deep All baseline.

	PACS	art_paint.	cartoon	sketches	photo	Avg.
CFN - Alexnet						
	J-CFN-Finetune	47.23	62.18	58.03	70.18	59.41
	J-CFN-Finetune++	51.14	58.83	54.85	73.44	59.57
	C-CFN-Deep All	59.69	59.88	45.66	85.42	62.66
	C-CFN-JiGen	60.68	60.55	55.66	82.68	64.89
Alexnet						
[72]	Deep All	63.30	63.13	54.07	87.70	67.05
	TF	62.86	66.97	57.51	89.50	69.21
[76]	Deep All	57.55	67.04	58.52	77.98	65.27
	DeepC	62.30	69.58	64.45	80.72	69.26
	CIDDG	62.70	69.73	64.45	78.65	68.88
[73]	Deep All	64.91	64.28	53.08	86.67	67.24
	MLDG	66.23	66.88	58.96	88.00	70.01
[32]	Deep All	64.44	72.07	58.07	87.50	70.52
	D-SAM	63.87	70.70	64.66	85.55	71.20
	Deep All	66.68	69.41	60.02	<u>89.98</u>	71.52
	JiGen	67.63	71.71	65.18	89.00	73.38
Resnet-18						
[32]	Deep All	77.87	<u>75.89</u>	69.27	95.19	79.55
	D-SAM	77.33	72.43	77.83	95.30	80.72
	Deep All	77.85	74.86	67.74	95.73	79.05
	JiGen	79.42	75.25	71.35	96.03	80.51

retain between 80 – 100% and randomly applied horizontal flipping. Following [101] we randomly (10% probability) convert an image tile to grayscale.

4.1.2 Experiments

4.1.2.1 Patch-Based Convolutional Models for Jigsaw Puzzles

We start our experimental analysis by evaluating the application of existing jigsaw related patch-based convolutional architectures and models to the domain generalization task. We considered two recent works that proposed a jigsaw puzzle solver for 9

shuffled patches from images decomposed by a regular 3×3 grid. Both [98] and [101] use a Context-Free Network (CFN) with 9 siamese branches that extract features separately from each image patch and then recombine them before entering the final classification layer. Specifically, each CFN branch is an Alexnet up to the first fully connected layer (*fc6*) and all the branches share their weights. Finally, the branches' outputs are concatenated and given as input to the following fully connected layer (*fc7*). The jigsaw puzzle task is formalized as a classification problem on a subset of patch permutations and, once the network is trained on a shuffled version of Imagenet [30], the learned weights can be used to initialize the *conv* layers of a standard Alexnet while the rest of the network is trained from scratch for a new target task. Indeed, according to the original works, the learned representation is able to capture semantically relevant content from the images regardless of the object labels. We followed the instructions in [98] and started from the pretrained Jigsaw CFN (J-CFN) model provided by the authors to run finetuning on the PACS dataset with all the source domain samples aggregated together. In the top part of Table 4.1 we indicate with J-CFN-Finetune the results of this experiment using the jigsaw model proposed in [98], while with J-CFN-Finetune++ the results from the advanced model proposed in [101]. In both cases the average classification accuracy on the domains is lower than what can be obtained with a standard Alexnet model pre-trained for object classification on Imagenet and finetuned on all the source data aggregated together. We indicate this baseline approach with Deep All and we can use as reference the corresponding values in the following central part of Table 4.1. We can conclude that, despite its power as an unsupervised pretext task, completely disregarding the object labels when solving jigsaw puzzles induces a loss of semantic information that may still be crucial for generalization across multiple domains.

To demonstrate the potentialities of the CFN architecture, the authors of [98] used it also to train a supervised object Classification model on Imagenet (C-CFN) and demonstrated that it can produce results analogous to the standard Alexnet. With the aim of further testing this network to understand if and how much its peculiar siamese-ennet structure can be useful to distill shared knowledge across domains, we considered it as the main convolutional backbone for JiGen. Starting from the C-CFN model provided by the authors, we run the obtained C-CFN-JiGen on PACS data, as well as its plain object classification version with the jigsaw loss disabled ($\alpha = 0$) that we indicate as C-CFN-Deep All. From the obtained recognition accuracy we can state that combining the jigsaw puzzle with the classification task provides an average improvement in performance, which is the first result to confirm our intuition. However, C-CFN-Deep All is still lower than the reference results obtained with standard Alexnet.

For all the following experiments we consider the convolutional architecture of JiGen built with the same main structure of Alexnet or Resnet, using always the image as a whole (ordered or shuffled) instead of relying on separate patch-based network branches.

Table 4.2. Domain Generalization results on VLCS. The results of JiGen are average over three repetitions of each run. Each column title indicates the name of the domain used as target. We use the bold font for the best generalization result, while we underline the highest result when produced by the naïve Deep All baseline.

	VLCS	Caltech	Labelme	Pascal	Sun	Avg.
Alexnet						
[76]	Deep All	85.73	61.28	62.71	59.33	67.26
	DeepC	87.47	62.60	63.97	61.51	68.89
	CIDDG	88.83	63.06	64.38	62.10	69.59
[94]	Deep All	86.10	55.60	59.10	54.60	63.85
	CCSA	92.30	62.10	67.10	59.10	70.15
[31]	Deep All	86.67	58.20	59.10	57.86	65.46
	SLRC	92.76	62.34	65.25	63.54	70.97
[72]	Deep All	93.40	62.11	68.41	64.16	72.02
	TF	93.63	63.49	69.99	61.32	72.11
[75]	MMD-AAE	94.40	62.60	67.70	64.40	72.28
[32]	Deep All	94.95	57.45	66.06	65.87	71.08
	D-SAM	91.75	56.95	58.59	60.84	67.03
	Deep All	<u>96.93</u>	59.18	<u>71.96</u>	62.57	72.66
	JiGen	96.93	60.90	70.62	64.30	73.19

4.1.2.2 Multi-Source Domain Generalization

We compare the performance of JiGen against several recent domain generalization methods. TF is the low-rank parametrized network that was presented together with the dataset PACS in [72]. CIDDG is the conditional invariant deep domain generalization method presented in [76] that trains for image classification with two adversarial constraints: one that maximizes the overall domain confusion following [42] and a second one that does the same per-class. In the DeepC variant, only this second condition is enabled. MLDG [73] is a meta-learning approach that simulates train/test domain shift during training and exploit them to optimize the learning model. CCSA [94] learns an embedding subspace where mapped visual domains are semantically aligned and yet maximally separated. MMD-AAE [75] is a deep method based on adversarial autoencoders that learns an invariant feature representation by aligning the data distributions to an arbitrary prior through the Maximum Mean Discrepancy (MMD). SLRC [31] is based on a single domain invariant network and multiple domain specific ones and it applies a low rank constraint among them. D-SAM [32] is a method based on the use of domain-specific aggregation modules combined to improve model generalization: it provides the current sota results on PACS and Office-Home. For each of these methods, the Deep All baseline indicates the performance of the corresponding network when all the introduced domain adaptive conditions are disabled.

The central and bottom parts of Table Table 4.1 show the results of JiGen on

Table 4.3. Domain Generalization results on Office-Home. The results of JiGen are average over three repetitions of each run. Each column title indicates the name of the domain used as target.

	Office-Home	Art	Clipart	Product	Real-World	Avg.
	Resnet-18					
[32]	Deep All	55.59	42.42	70.34	70.86	59.81
	D-SAM	58.03	44.37	69.22	71.45	60.77
	Deep All	52.15	45.86	70.86	73.15	60.51
	JiGen	53.04	47.51	71.47	72.79	61.20

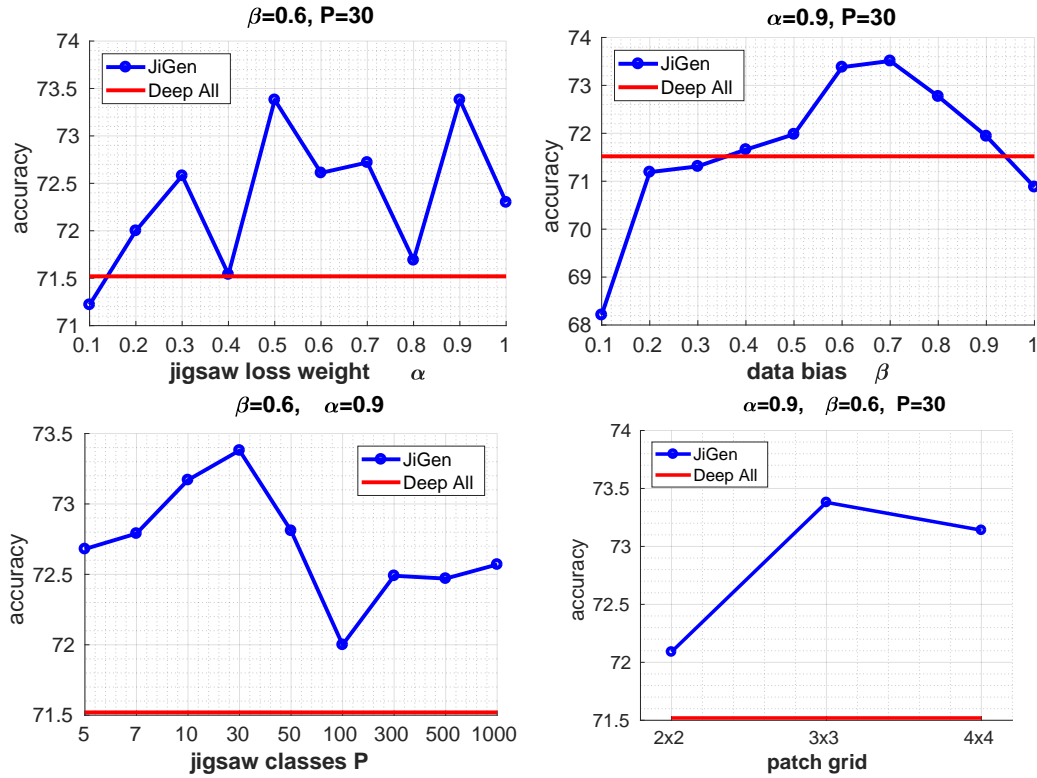


Figure 4.3. Ablation results on the Alexnet-PACS DG setting. The reported accuracy is the global average over all the target domains of the setting, obtained by averaging over three repetitions of each run. The red line represents our Deep All average from Table 4.1.

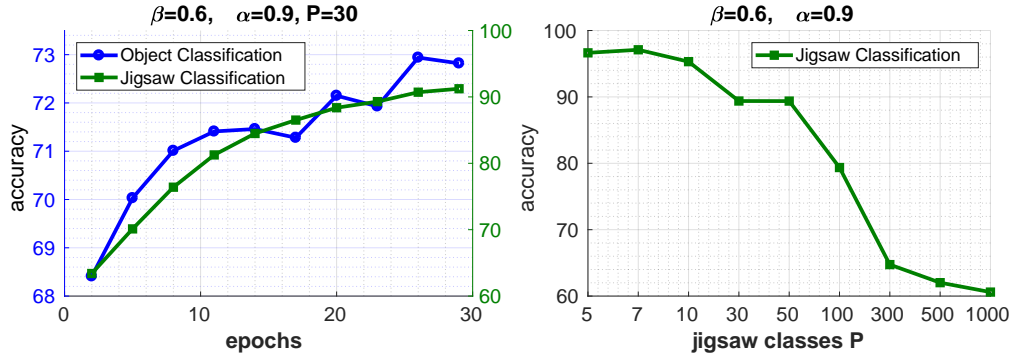


Figure 4.4. Analysis of the behaviour of the jigsaw classifier on the Alexnet-PACS DG setting. For the plot on the left the color of the axes refer to each of the matching curve in the graph.

the dataset PACS when using as backbone architecture Alexnet and Resnet-18². On average JiGen produces the best result when using Alexnet and it is just slightly worse than the D-SAM reference for Resnet-18. Note however, that in this last case, JiGen outperforms D-SAM in three out of four target cases and the average advantage of D-SAM originate only from its result on sketches. On average, JiGen outperforms also the competing methods on the VLCS and on the Office-Home datasets (see respectively Table Table 4.2 and Table 4.3). In particular we remark that VLCS is a tough setting where the most recent works have only presented small gain in accuracy with respect to the corresponding Deep All baseline (e.g. TF). Since [32] did not present the results of D-SAM on the VLCS dataset, we used the code provided by the authors³ to run these experiments. The obtained results show that, although generally able to close large domain gaps across images of different styles as in PACS and Office-Home, when dealing with domains all coming from real-world images, the use of aggregative modules tend to overfit, not supporting generalization.

4.1.2.3 Ablation

Here we evaluate the robustness of JiGen showing its behaviour when the hyperparameter values are systematically changed on the Alexnet-PACS domain generalization setting. First of all, we focus on the case with fixed number of jigsaw classes $P = 30$, ordered/shuffled data bias $\beta = 0.6$, as well as patch grid 3×3 and varying the jigsaw loss weight α in $\{0.1, 1\}$. We show the obtained global average classification accuracy on the first plot on the left of Figure Figure 4.3. We notice that only for the very low value $\alpha = 0.1$ the obtained accuracy is just slightly lower than the Deep All baseline, while overall we observe an advantage regardless of the specific chosen α . From the second plot in Figure Figure 4.3, it appears that the data bias β has a more significant impact on the result than α . Indeed, $\beta < 0.5$ implies that the amount of shuffled images fed to the network is higher than the respective amount

²With Resnet18, to put JiGen on equal footing with D-SAM we follow the same data augmentation protocol in [32] and enabled color jittering.

³https://github.com/VeloDC/D-SAM_public

of ordered ones. In those cases object classification assumes almost a secondary role with respect to the jigsaw reordering task, which implies a classification accuracy equal or lower than the Deep All baseline. On the other way round, for $\beta \geq 0.5$ the performance increases and gets to its maximum to then decrease again. This behaviour is logically related to the fact that $\beta = 1$ implies that we are considering only ordered images: the jigsaw loss encourages the network to correctly recognize always the same permutation class, which may increase the risk of overfitting. The third plot in Figure Figure 4.3 shows the change in performance when the number of jigsaw classes P varies between 5 and 1000. We started from a low number, with the same order of magnitude of the number of object classes in PACS, and we grew till 1000 which is the number used for the experiments in [98]. We observe an overall variation of 1.5 percentage point in the accuracy, but it always remains higher than the Deep All baseline. Finally, although for all our experiments we used images decomposed in 9 patches from a 3×3 grid, we also ran a further test to check the accuracy when changing the grid size and consequently the patch number. Even in this case, the range of variation is limited when passing from a 2×2 to a 4×4 grid, confirming the conclusions of robustness already obtained for this parameter in [98] and [26]. Moreover all the results are better than the Deep All reference.

In all our experiments we are using the jigsaw puzzle as a side task to help generalization, but it is also interesting to check if the jigsaw classifier is producing meaningful results. We show its recognition accuracy when testing it on the same images used to evaluate the object classifier but with shuffled patches. In Figure Figure 4.4, the first plot on the left shows the accuracy over the learning epochs for the object and jigsaw classifiers indicating that both grows simultaneously (on different scales). The plot on the right of the same figure shows the jigsaw recognition accuracy when changing the number of jigsaw classes P : of course the performance decreases when the task becomes more difficult, but overall the obtained results indicate that the jigsaw model is always effective in reordering the shuffled image patches.

To further evaluate how JiGen is using the jigsaw puzzle task to learn spatial correlations, we consider the results per class produced when using the challenging sketches domain of PACS as target and comparing the obtained accuracy against J-CFN-Finetune++ and Deep All. The confusion matrices in Figure Figure 4.5, indicate that for four out of seven categories, J-CFN-Finetune++ that leverages over the jigsaw model trained to relocate patch features, is actually doing a good job, better than Deep All. With JiGen we improve over Deep All for the same categories by exploiting the knowledge from solving jigsaw puzzles at image level and we keep the advantage of Deep All for the remaining categories.

4.1.2.4 Single Source Domain Generalization

The generalization ability of a model is intrinsically related to the way in which it was trained so it depends both on the used data and on its own learning structure. To understand the potentialities of JiGen we decided to limit the variability in the training data by considering experiments with a single source domain, so that we can better focus on the regularization effect provided by the jigsaw task in the learning process.

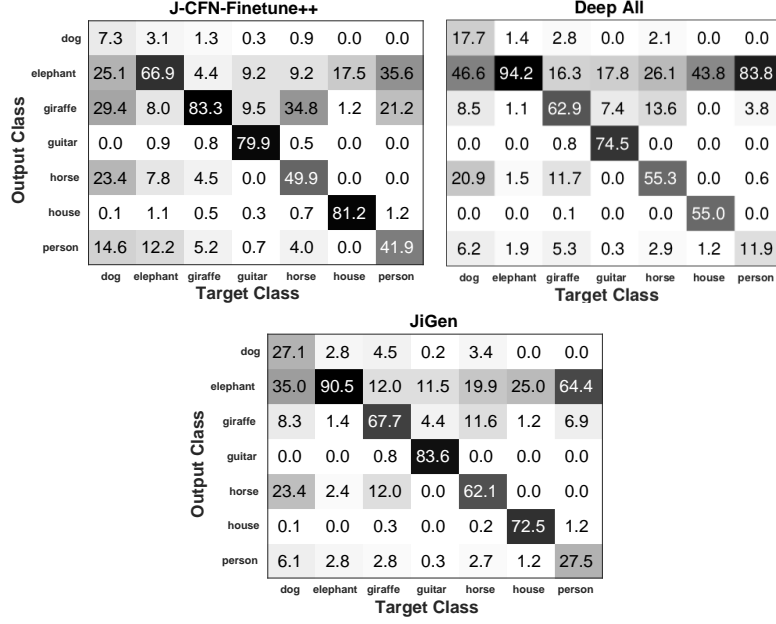


Figure 4.5. Confusion matrices on Alexnet-PACS DG setting, when sketches is used as target domain.

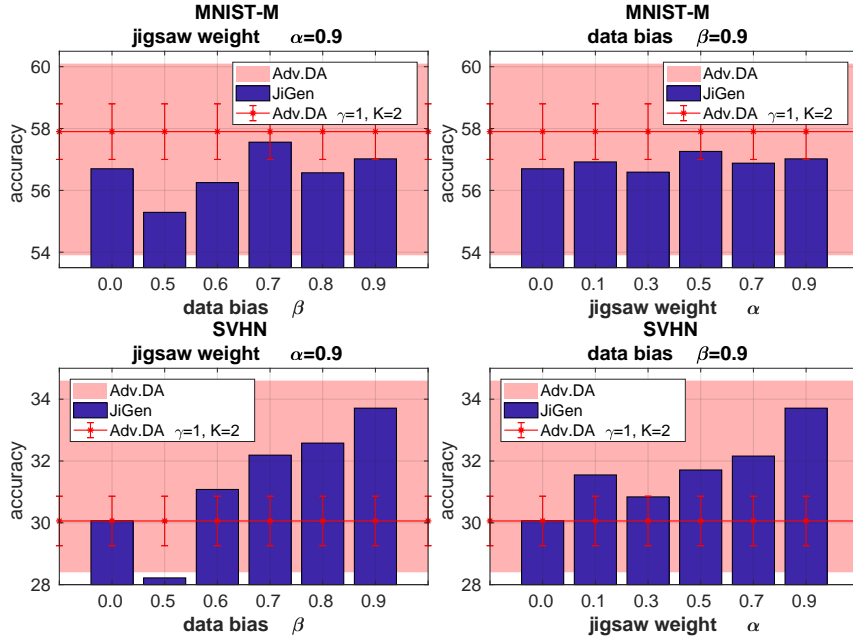


Figure 4.6. Single Source Domain Generalization experiments. We analyze the performance of JiGen in comparison with the method Adv.DA [125]. The shaded background area covers the overall range of results of Adv.DA obtained when changing the hyper-parameters of the method. The reference result of Adv.DA ($\gamma = 1$, $K = 2$) together with its standard deviation is indicated here by the horizontal red line. The blue histogram bars show the performance of JiGen when changing the jigsaw weight α and data bias β .

Table 4.4. Multi-source Domain Adaptation results on PACS obtained as average over three repetitions for each run. Besides considering the same jigsaw loss weight for source and target samples $\alpha^s = \alpha^t$, we also tuned just the target jigsaw loss weight while keeping $\alpha^s = 0.7$ showing that we can get even higher results.

	PACS-DA	art_paint.	cartoon	sketches	photo	Avg.
	Resnet-18					
[85]	Deep All	74.70	72.40	60.10	92.90	75.03
	Dial	87.30	85.50	66.80	97.00	84.15
	DDiscovery	87.70	86.90	69.60	97.00	85.30
	Deep All	77.85	74.86	67.74	95.73	79.05
	JiGen $\alpha^s=\alpha^t=0.7$	84.88	81.07	79.05	97.96	85.74
	JiGen $\alpha^t=0.1$	85.58	82.18	78.61	98.26	86.15
	JiGen $\alpha^t=0.3$	85.08	81.28	81.50	97.96	86.46
	JiGen $\alpha^t=0.5$	85.73	82.58	78.34	98.10	86.19
	JiGen $\alpha^t=0.9$	85.32	80.56	79.93	97.63	85.86

For these experiments we compare against the generalization method based on adversarial data augmentation (Adv.DA) recently presented in [125]. This work proposes an iterative procedure that perturbs the data to make them hard to recognize under the current model and then combine them with the original samples while solving the classification task. We reproduced the experimental setting used in [125] and adopt a similar result display style with bar plots for experiments on the MNIST-M and SVHN target datasets when training on MNIST. In Figure 4.6 we show the performance of JiGen when varying the data bias β and the jigsaw weight α . With the red background shadow we indicate the overall range covered by Adv.DA results when changing its parameters⁴, while the horizontal line is the reference Adv.DA results around which the authors of [125] ran their parameter ablation analysis. The figure indicates that, although Adv.DA can reach high peak values, it is also very sensitive to the chosen hyperparameters. On the other hand, JiGen is much more stable and it is always better than the lower accuracy value of Adv.DA with a single exception for SVHN and data bias 0.5, but we know from the ablation analysis, that this corresponds to a limit case for the proper combination of object and jigsaw classification. Moreover, JiGen gets close to Adv.DA reference results for MNIST-M and significantly outperform it for SVHN.

4.1.2.5 Unsupervised Domain Adaptation

When unlabeled target samples are available at training time we can let the jigsaw puzzle task involve these data. Indeed patch reordering does not need image labels and running the jigsaw optimization process on both source and target data may positively influence the source classification model for adaptation. To verify this intuition we considered again the PACS dataset and used it in the same

⁴The whole set of results is provided as supplementary material of [125].

unsupervised domain adaptation setting of [85]. This previous work proposed a method to first discover the existence of multiple latent domains in the source data and then differently adapt their knowledge to the target depending on their respective similarity. It has been shown that this domain discovery (DDiscovery) technique outperforms other powerful adaptive approaches as Dial [16] when the source actually includes multiple domains. Both these methods exploit the minimization of the entropy loss as an extra domain alignment condition: in this way the source model when predicting on the target samples is encouraged to assign maximum prediction probability to a single label rather than distributing it over multiple class options. For a fair comparison we also turned on the entropy loss for JiGen with weight $\gamma = 0.1$. Moreover, we considered two cases for the jigsaw loss: either keeping the weight α already used for the PACS-Resnet-18 DG experiments for both the source and target data ($\alpha = \alpha^s = \alpha^t = 0.7$), or treating the domain separately with a dedicated lower weight for the jigsaw target loss ($\alpha^s = 0.7$, $\alpha^t = [0.1, 0.3, 0.5, 0.7]$). The results for this setting are summarized in Table Table 4.4. The obtained accuracy indicates that JiGen outperforms the competing methods on average and in particular the difficult task of recognizing images of sketches is the one that better shows its advantage. Furthermore, the advantage remains true regardless of the specific choice of the target jigsaw loss weight.

4.1.3 Conclusions

In this paper we showed for the first time that generalization across domains can be achieved effectively by learning to classify and learning intrinsic invariances in images at the same time. We focused on learning spatial co-location of image parts, and proposed a simple yet powerful framework that can accommodate a wide spectrum of pre-trained convolutional architectures. Our method JiGen can be seamlessly used for domain adaptation and generalization scenarios, always with great effectiveness as shown by the experimental results.

We see this paper as opening the door to a new research thread in domain adaptation and generalization. While here we focused on a specific type of invariance, several other regularities could be learned possibly leading to an even stronger benefit. Also, the simplicity of our approach calls for testing its effectiveness in applications different from object categorization, like semantic segmentation and person re-identification, where the domain shift effect strongly impact the deployment of methods in the wild.

4.2 Tackling PDA with self-supervision

Domain adaptation approaches have shown promising results in reducing the marginal distribution difference among visual domains. They allow to train reliable models that work over datasets of different nature (photos, paintings etc.), but they still struggle when the domains do not share an identical label space. In the partial domain adaptation setting, where the target covers only a subset of the source classes, it is challenging to reduce the domain gap without incurring in negative transfer. Many solutions just keep the standard domain adaptation techniques by adding heuristic sample weighting strategies. In this work we show how the self-supervisory signal obtained from the spatial co-location of patches can be used to define a side task that supports adaptation regardless of the exact label sharing condition across domains. We build over a recent work that introduced a jigsaw puzzle task for domain generalization: we describe how to reformulate this approach for partial domain adaptation and we show how it boosts existing adaptive solutions when combined with them. The obtained experimental results on three datasets supports the effectiveness of our approach.

Today the most popular synonym of Artificial Intelligence is Deep Learning: new convolutional neural network architectures constantly hit the headlines by improving the state of the art for a wide variety of machine learning problems and applications with impressive results. The large availability of annotated data, as well as the assumption of training and testing on the same domain and label set, are important ingredients of this success. However this closed set condition is not realistic and the learned models cannot be said fully intelligent. Indeed, when trying to summarize several definitions of intelligence from dictionaries, psychologists and computer scientists of the last fifty years, it turns out that all of them highlight as fundamental the ability to adapt and achieve goals in a wide range of environments and conditions [71]. Domain Adaptation (DA) and Domain Generalization (DG) methods are trying to go over this issue and allow the application of deep learning models in the wild. Many DA and DG approaches have been developed for the object classification task to reduce the domain gap across samples obtained from different acquisition systems, different illumination conditions and visual styles, but most of them keep a strong control on the class set, supposing that the trained model will be deployed exactly on the same categories observed during training. When part of the source classes are missing at test time, those models show a drop in performance which indicates the effect of negative transfer in this Partial Domain Adaptation (PDA) setting. The culprit must be searched in the need of solving two challenging tasks at the same time: one that exploits all the available source labeled data to train a reliable classification model in the source domain and another that estimates and minimizes the marginal distribution difference between source and target, but disregards the potential presence of a conditional distribution shift. Very recently it has been shown that this second task may be substituted with self-supervised objectives which are agnostic with respect to the domain identity of each sample. In particular, [18] exploits image patch shuffling and reordering as a side task over multiple sources: it leverages the intrinsic regularity of the spatial co-location of patches and generalizes to new domains. This information appears

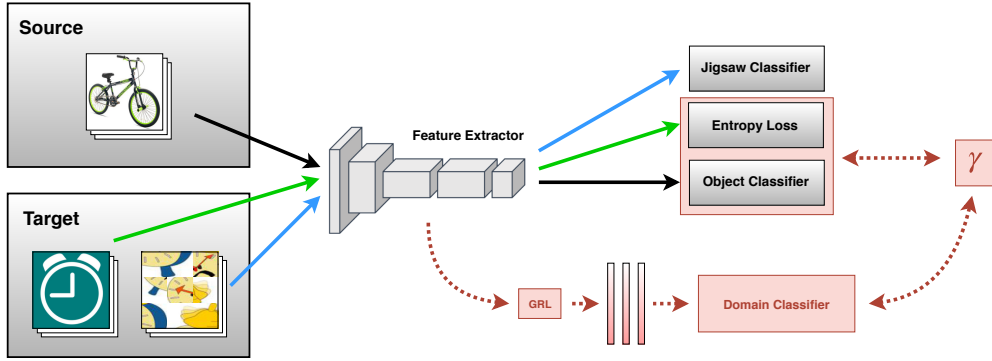


Figure 4.7. Schematic representation of our SSPDA approach. All the parts in gray describe the main blocks of the network with the solid line arrows indicating the contribution of each group of training samples to the corresponding final tasks and related optimization objectives according to the assigned blue/green/black colors. The blocks in red illustrate the domain adversarial classifier with the gradient reversal layer (GRL) and source sample weighting procedure (weight γ) that can be added to SSPDA

also independent from the specific class label of each image, which makes it an interesting reference knowledge also when the class set of source and target are only partially overlapping. We dedicate this work to investigate how the jigsaw puzzle task of [18] performs in the PDA setting and how it can be reformulated to reduce the number of needed learning parameters. The results on three different datasets indicate that our approach outperforms several competitors whose adaptive solutions include specific strategies to down-weight the samples belonging to classes supposedly absent from the target. We also discuss how such a re-scaling process can be combined with the jigsaw puzzle obtaining further gains in performance.

4.2.1 Solving jigsaw puzzles for Partial Domain Adaptation

4.2.1.1 Problem Setting

Let us introduce the technical terminology for the PDA scenario. We have n^s annotated samples from a source domain $\mathcal{D}_s = \{(\mathbf{x}_i^s, \mathbf{y}_i^s)\}_{i=1}^{n^s}$, drawn from the distribution S , and n^t unlabeled examples of the target domain $\mathcal{D}_t = \{\mathbf{x}_j^t\}_{j=1}^{n^t}$ drawn from a different distribution T . The label space of the target domain is contained in that of the source domain $\mathcal{Y}_t \subseteq \mathcal{Y}_s$. Thus, besides dealing with the marginal shift $S \neq T$ as in standard unsupervised domain adaptation, it is necessary to take care of the difference in the label space which makes the problem even more challenging. If this information is neglected and the matching between the whole source and target data is forced, any adaptive method may incur in a degenerate case producing worse performance than its plain non-adaptive version. Still the objective remains that of learning both class discriminative and domain invariant feature models which can be formulated as a multi-task learning problem [22]. Instead of just focusing on the explicit reduction of the feature domain discrepancy, one could consider some inherent characteristics shared by any visual domain regardless of the assigned label and derive a learning problem to solve together with the main classification task. By leveraging the inductive bias of related objectives, multi-task learning regularizes

the overall model and improves generalization having as an implicit consequence the reduction of the domain bias. This reasoning is at the basis of the recent work [18], which proposed to use jigsaw puzzle as a side task for closed set domain adaptation and generalization: the model named JiGen is described in details in the next subsection.

4.2.1.2 Jigsaw Puzzle Closed Set Adaptation

Starting from the n^s labeled and n^t unlabeled images, the method in [18] decomposes them according to an 3×3 grid obtaining 9 squared patches from every sample, which are then moved from their original location and re-positioned randomly to form a shuffled version \mathbf{z} of the original image \mathbf{x} . Out of all the $9!$ possibilities, a set of $p = 1, \dots, P$ permutations are chosen on the basis of their maximal reciprocal Hamming distance [98] and used to define a jigsaw puzzle classification task which consists in recognizing the index p of the permutation used to scramble a certain sample. All the original $\{(\mathbf{x}_i^s, \mathbf{y}_i^s)\}_{i=1}^{n^s}$, $\{\mathbf{x}_j^t\}_{j=1}^{n^t}$ as well as the shuffled versions of the images $\{(\mathbf{z}_k^s, \mathbf{p}_k^s)\}_{k=1}^{K^s}$, $\{(\mathbf{z}_k^t, \mathbf{p}_k^t)\}_{k=1}^{K^t}$ are given as input to a multi-task deep network where the convolutional feature extraction backbone is indicated by G_f and is parametrized by θ_f , while the classifier G_c of the object labels and G_p of the permutation indices, are parametrized respectively by θ_c and θ_p . The source samples are involved both in the object classification and in the jigsaw puzzle classification task, while the unlabeled target samples deal only with the puzzle task. To further exploit the available target data, the uncertainty of the estimated prediction $\hat{\mathbf{y}}^t = G_c(G_f(\mathbf{x}^t))$ is evaluated through the entropy $H = -\sum_{l=1}^{|\mathcal{Y}_s|} \hat{y}_l^t \log \hat{y}_l^t$ and minimized to enforce the decision boundary to pass through low-density areas.

Overall the end-to-end JiGen multi-task network is trained by optimizing the following objective

$$\begin{aligned} \arg \min_{\theta_f, \theta_c, \theta_p} & \frac{1}{n^s} \sum_{i=1}^{n^s} \mathcal{L}_c(G_c(G_f(\mathbf{x}_i^s), y_i^s)) + \alpha_s \frac{1}{K^s} \sum_{k=1}^{K^s} \mathcal{L}_p(G_p(G_f(\mathbf{z}_k^s), \mathbf{p}_k^s)) + \\ & \eta \frac{1}{n^t} \sum_{j=1}^{n^t} H(G_c(G_f(\mathbf{x}_j^t))) + \alpha_t \frac{1}{K^t} \sum_{k=1}^{K^t} \mathcal{L}_p(G_p(G_f(\mathbf{z}_k^t), \mathbf{p}_k^t)), \end{aligned} \quad (4.2)$$

where \mathcal{L}_c and \mathcal{L}_p are cross entropy losses for both the object and puzzle classifiers. In the closed set scenario, the experimental evaluation of [18] showed that tuning two different hyperparameters α_s and α_t respectively for the source and target puzzle classification loss is beneficial with respect to just using a single value $\alpha = \alpha_s = \alpha_t$, while it is enough to assign a small value to η ($\sim 10^{-1}$).

4.2.1.3 Jigsaw Puzzle for Partial Domain Adaptation

We investigate here if the approach in [18] can be extended to the PDA setting and how to improve it to deal with the specific characteristics of the considered scenario. The two \mathcal{L}_p terms in (Equation (4.2)) provide a domain shift reduction effect on the learned feature representation, however their co-presence seem redundant: indeed the features are already chosen to minimize the source classification loss and the self-supervised jigsaw puzzle task on the target back-propagates its effect directly on

the learned features inducing a cross-domain adjustment. By following this logic, we decided to drop the source jigsaw puzzle term, which corresponds to setting $\alpha_s = 0$. This choice has a double positive effect: on one side it allows to reduce the number of hyper-parameters in the learning process leaving space for the introduction of other complementary learning conditions, on the other we let the self-supervised module focus only on the samples from the target without involving the extra classes of the source. In the following we indicate this approach as SSPDA: Self-Supervised Partial Domain Adaptation. A schematic illustration of the method is presented in Figure Figure 4.7.

4.2.2 Combining Self-Supervision with other PDA Strategies

To further enforce the focus on the shared classes, SSPDA can be extended to integrate a weighting mechanism analogous to that presented in [15]. The source classification output on the target data are accumulated as follow $\gamma = \frac{1}{n^t} \sum_{j=1}^{n^t} \hat{\mathbf{y}}_j^t$ and normalized $\gamma \leftarrow \gamma / \max(\gamma)$, obtaining a $|\mathcal{Y}_t|$ -dimensional vector that quantifies the contribution of each source class. Moreover, we can easily integrate a domain discriminator G_d with a gradient reversal layers as in [42], and adversarially maximize the related binary cross-entropy to increase the domain confusion, taking also into consideration the defined class weighting procedure for the source samples. In more formal terms, the final objective of our multi-task problem is

$$\begin{aligned} \arg \min_{\theta_f, \theta_c, \theta_p} \max_{\theta_d} & \frac{1}{n^s} \sum_{i=1}^{n^s} \gamma_y \left(\mathcal{L}_c(G_c(G_f(\mathbf{x}_i^s), y_i^s)) + \lambda \log(G_d(G_f(\mathbf{x}_i^s))) \right) + \\ & \frac{1}{n^t} \sum_{j=1}^{n^t} \gamma_y \left(\eta H(G_c(G_f(\mathbf{x}_j^t))) + \lambda \log(1 - G_d(G_f(\mathbf{x}_j^t))) \right) + \\ & \alpha_t \frac{1}{K^t} \sum_{k=1}^{K^t} \mathcal{L}_p(G_p(G_f(\mathbf{z}_k^t), p_k^t)) , \end{aligned} \quad (4.3)$$

where λ is a hyper-parameter that adjusts the importance of the introduced domain discriminator. We adopted the same scheduling of [42] to update the value of λ , so that the importance of the domain discriminator increases with the training epochs, from 0 at the first epoch to λ -max at the last epoch, avoiding the noisy signal at the early stages of the learning procedure. When $\lambda = 0$ and $\gamma_y = 1/|\mathcal{Y}_s|$ we fall back to SSPDA. Note that here the entropy term H is also weighted with a per-class score γ based on the predicted target class.

4.2.3 Experiments

4.2.3.1 Implementation Details

We implemented all our deep methods in PyTorch. Specifically the main backbone of our SSPDA network is a ResNet-50 pre-trained on ImageNet and corresponds to the feature extractor defined as G_f , while the specific object and puzzle classifiers G_c, G_p are implemented each by an ending fully connected layer. The domain classifier G_d is introduced by adding three fully connected layers after the last pooling layer of

the main backbone, and using a sigmoid function for the last activation as in [42]. By training the network end-to-end we fine-tune all the feature layers, while G_c, G_p and G_d are learned from scratch. We train the model with backpropagation using SGD with momentum set at 0.9, weight decay 0.0005 and initial learning rate 0.0005. We use a batch size of 64 (32 source samples + 32 target samples) and, following [18], we shuffle the tiles of each input image with probability $1 - \beta$, with $\beta = 0.7$. Shuffled samples are only used for the auxiliary jigsaw task, therefore only unshuffled (original) samples are passed to G_d and G_c for domain and label predictions. The entropy weight η and jigsaw task weight α_t are set respectively to 0.2 and 1. Our data augmentation protocol is the same of [18].

Model Selection

As standard practice, we used 10% of the source training domain to define a validation set on which the model is evaluated after each epoch e . The obtained accuracy A_e is dynamically averaged with the value obtained at the previous epoch with $A_e \leftarrow wA_{e-1} + (1 - w)A_e$. The final model to apply on the target is chosen as the one producing the top accuracy over all the epochs $e = 1, \dots, E$. We noticed that this procedure leads to a more reliable selection of the best trained model, preventing to choose one that might have overfitted on the validation set. For all our experiments we kept $w = 0.6$. We underline that this smoothing procedure was applied uniformly on all our experiments. Moreover the hyper-parameters of our model are the same for all the domain pairs within each dataset and also across all the datasets. In other words we did not select a tailored set of parameters for each sub-task of a certain dataset which could lead to further performance gains, a procedure used in previous works [15, 14].

4.2.3.2 Results of SSPDA

Here we present and discuss the obtained classification accuracy results on the three considered datasets: Office-31 in Table Table 4.5, Office-Home in Table Table 4.6 and VisDA in Table Table 4.7. Each table is organized in three horizontal blocks: the first one shows the results obtained with standard DA methods, the second block illustrates the performance with algorithms designed to deal with PDA and the third one includes the scores of JiGen and SSPDA. Only Table Table 4.5 has an extra fourth block that we will discuss in details in the following section.

Both JiGen and SSPDA exceed all plain DA methods and present accuracy value comparable to those of the PDA methods. In particular SSPDA is always better than PADA [15] on average, and for both Office-Home and VisDA it also outperforms all the other competing PDA methods with the only exception of IAFN [133]. We highlight that this approach uses a competitive version of ResNet-50 as backbone, with extra bottleneck fully connected layers which add about 2 million parameters to the standard version of ResNet-50 that we adopted.

4.2.3.3 Results of SSPDA combined with other PDA strategies

To analyze the combination of SSPDA with the standard PDA source re-weighting technique and the adversarial domain classifier, we extended the experiments on

Table 4.5. Classification accuracy in the PDA setting defined on the Office-31 dataset with all the 31 classes used for each source domain, and a fixed set of 10 classes used for each target domain. The results are obtained using 10 random crop predictions on each target image and are averaged over three repetitions of each run.

	Office-31						Avg.
	A→W	D→W	W→D	A→D	D→A	W→A	
Resnet-50	75.37	94.13	98.84	79.19	81.28	85.49	85.73
DAN[79]	59.32	73.90	90.45	61.78	74.95	67.64	71.34
DANN[42]	75.56	96.27	98.73	81.53	82.78	86.12	86.50
ADDA[122]	75.67	95.38	99.85	83.41	83.62	84.25	87.03
RTN[80]	78.98	93.22	85.35	77.07	89.25	89.46	85.56
IWAN [139]	89.15	99.32	99.36	90.45	95.62	94.26	94.69
SAN [14]	93.90	99.32	99.36	94.27	94.15	88.73	94.96
PADA[15]	86.54	99.32	100	82.17	92.69	95.41	92.69
TWIN [89]	86.00	99.30	100	86.80	94.70	94.50	93.60
JiGen [18]	92.88	92.43	98.94	89.6	84.06	92.94	91.81
SSPDA	91.52	92.88	98.94	90.87	90.61	94.36	93.20
SSPDA- γ	99.32	94.69	99.36	96.39	86.36	94.22	95.06
SSPDA-PADA	99.66	94.46	99.57	97.67	87.33	94.26	95.49

Table 4.6. Classification accuracy in the PDA setting defined on the Office-Home dataset with all the 65 classes used for each source domain, and a fixed set of 25 classes used for each target domain. The results are obtained by averaging over three repetitions of each run.

	Office-Home												Avg.
	Ar→Cl	Ar→Pr	Ar→Rw	Cl→Ar	Cl→Pr	Cl→Rw	Pr→Ar	Pr→Cl	Pr→Rw	Rw→Ar	Rw→Cl	Rw→Pr	
Resnet-50	38.57	60.78	75.21	39.94	48.12	52.90	49.68	30.91	70.79	65.38	41.79	70.42	53.71
DAN[79]	44.36	61.79	74.49	41.78	45.21	54.11	46.92	38.14	68.42	64.37	45.37	68.85	54.48
DANN[42]	44.89	54.06	68.97	36.27	34.34	45.22	44.08	38.03	68.69	52.98	34.68	46.50	47.39
RTN[80]	49.37	64.33	76.19	47.56	51.74	57.67	50.38	41.45	75.53	70.17	51.82	74.78	59.25
IWAN [139]	53.94	54.45	78.12	61.31	47.95	63.32	54.17	52.02	81.28	76.46	56.75	82.90	63.56
SAN [14]	44.42	68.68	74.60	67.49	64.99	77.80	59.78	44.72	80.07	72.18	50.21	78.66	65.30
PADA[15]	51.95	67.00	78.74	52.16	53.78	59.03	52.61	43.22	78.79	73.73	56.60	77.09	62.06
HAFN[133]	53.35	72.66	80.84	64.16	65.34	71.07	66.08	51.64	78.26	72.45	55.28	79.02	67.51
IAFN[133]	58.93	76.25	81.42	70.43	72.97	77.78	72.36	55.34	80.40	75.81	60.42	79.92	71.83
JiGen [18]	53.19	65.45	81.30	68.84	58.95	74.34	69.94	50.95	85.38	75.60	60.02	81.96	68.83
SSPDA	52.02	63.64	77.95	65.66	59.31	73.48	70.49	51.54	84.89	76.25	60.74	80.86	68.07

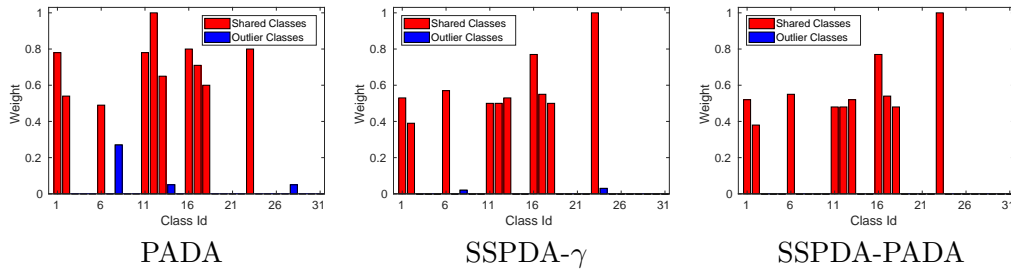


Figure 4.8. Histogram showing the elements of the γ vector, corresponding to the class weight learned by PADA, SSPDA- γ and SSPDA-PADA for the A→W experiment.

the Office-31 dataset. The bottom part of Table Table 4.5 reports the obtained results when we add the estimate of the target class statistics through the weight γ (SSPDA- γ) and when also the domain classifier is included in the network as in [15]

Table 4.7. Classification accuracy in the PDA setting defined on VisDA2017 dataset with all the 12 classes used for each source domain, and a fixed set of 6 classes used for each target domain. The results are obtained using 10 random crop predictions on each target image and are averaged over three repetitions of each run.

VisDA2017	
	Syn. \rightarrow Real
Resnet-50	45.26
DAN[79]	47.60
DANN[42]	51.01
RTN[80]	50.04
PADA[15]	53.53
HAFN[133]	65.06
IAFN[133]	67.65
JiGen [18]	68.33
SSPDA	68.89

(SSPDA-PADA). In the first case, estimating the target statistics helps the network to focus only on the shared categories, with an average accuracy improvement of two percentage points over the plain SSPDA. Moreover, since the technique to evaluate γ is the same used in [15], we can state that the advantage comes from a better alignment of the domain features, thus from the introduction of the self-supervised jigsaw task. Indeed, by comparing the γ values on the $A \rightarrow W$ domain shift we observe that SSPDA- γ is more precise in identifying the missing classes of the target (see Figure Figure 4.8). In the second case, since the produced features are already well aligned across domains, we fixed λ -max to 0.1 and observed a further small average improvement, with the largest advantage when the A domain is used as source. From the last bar plot on the right of Figure Figure 4.8 we also observe a further improvement in the identification of the missing target classes.

4.2.4 Conclusions

In this paper we discussed how the self-supervised jigsaw puzzle task can be used for domain adaptation in the challenging partial setting with some of the source classes missing in the target. Since the high-level knowledge captured by the spatial co-location of patches is unsupervised with respect to the image object content, this task can be applied on the unlabeled target samples and help to close the domain gap without suffering from negative transfer. Moreover we showed that the proposed solution can be seamlessly integrated with other existing partial domain adaptation methods and it contributes to a reliable identification of the categories absent in the target with a consequent further improvement in the recognition results. In the future we plan to further explore the jigsaw puzzle task also in the open-set scenario where the target contains new unknown classes with respect to the source.

4.3 One-Shot unsupervised cross-domain detection

Despite impressive progress in object detection over the last years, it is still an open challenge to reliably detect objects across visual domains. All current approaches access a sizable amount of target data at training time. This is a heavy assumption, as often it is not possible to anticipate the domain where a detector will be used, nor to access it in advance for data acquisition. Consider for instance the task of monitoring image feeds from social media: as every image is uploaded by a different user it belongs to a different target domain that is impossible to foresee during training. Our work addresses this setting, presenting an object detection algorithm able to perform unsupervised adaptation across domains by using only one target sample, seen at test time. We introduce a multi-task architecture that one-shot adapts to any incoming sample by iteratively solving a self-supervised task on it. We further enhance this auxiliary adaptation with cross-task pseudo-labeling. A thorough benchmark analysis against the most recent cross-domain detection methods and a detailed ablation study show the advantage of our approach.

Social media feed us every day with an unprecedented amount of visual data. Images are uploaded by various actors, from corporations to political parties, institutions, entrepreneurs and private citizens, with roughly 10^2M unique images shared everyday on Twitter, Facebook and Instagram. For the sake of freedom of expression, control over their content is limited, and their vast majority is uploaded without any textual description of their content. Their sheer magnitude makes it imperative to use algorithms to monitor and make sense of them, finding the right balance between protecting the privacy of citizens and their right of expression, and tracking fake news (often associated with malicious intentions) while fighting illegal and hate content. This in most cases boils down to the ability to automatically associate as many tags as possible to images, which in turns means determining which objects are present in a scene.

Object detection has been largely investigated since the infancy of computer vision [124, 29] and continues to attract a large attention in the current deep learning era [48, 28, 141, 78]. Most of the algorithms assume that training and test data come from the same visual domain [48, 47, 106]. Recently, some authors have started to investigate the more challenging yet realistic scenario where the detector is trained on data from a visual source domain, and deployed at test time in a different target domain [79, 81, 119, 122]. This setting is usually referred to as cross-domain detection and heavily relies on concepts and results from the domain adaptation literature [79, 41, 49]. Specifically, it inherits the standard transductive logic, according to which unsupervised target data is available at training time together with annotated source data, and can be used to adapt across domains. This approach is not suitable, neither effective, for monitoring social media feeds. Consider for instance the scenario depicted in Figure Figure 4.9, where there is an incoming stream of images from various social media and the detector is asked to look for instances of the class bicycle. The images come continuously, but they are produced by different users that share them on different social platforms. Hence, even though they might contain the same object, each of them has been acquired by a different person, in a different context, under different viewpoints and illuminations.

In other words, each image comes from a different visual domain, distinct from the visual domain where the detector has been trained. This poses two key challenges to current cross-domain detectors: (1) to adapt to the target data, these algorithms need first to gather feeds, and only after enough target data has been collected they can learn to adapt and start performing on the incoming images; (2) even if the algorithms have learned to adapt on target images from the feed up to time t , there is no guarantee that the images that will arrive from time $t + 1$ will come from the same target domain.

This is the scenario we address. We focus on cross-domain detection when only one target sample is available for adaptation, without any form of supervision. We propose an object detection method able to adapt from one target image, hence suitable for the social media scenario described above. Specifically, we build a multi-task deep architecture that adapts across domains by leveraging over a pretext task. This auxiliary knowledge is further guided by a cross-task pseudo-labeling that injects the locality specific of object detection into self-supervised learning. The result is an architecture able to perform unsupervised adaptive object detection from a single image. Extensive experiments show the power of our method compared to previous state-of-the-art approaches. To summarize, the contributions of our paper are as follows:

- (1) we introduce the One-Shot Unsupervised Cross-Domain Detection setting, a cross-domain detection scenario where the target domain changes from sample to sample, hence adaptation can be learned only from one image. This scenario is especially relevant for monitoring social media image feeds. We are not aware of previous works addressing it.
- (2) We propose OSHOT, the first cross-domain object detector able to perform one-shot unsupervised adaptation. Our approach leverages over self-supervised one-shot learning guided by a cross-task pseudo-labeling procedure, embedded into a multi-task architecture. A thorough ablation study showcases the importance of each component.
- (3) We present a new experimental setup for studying one-shot unsupervised cross-domain adaptation, designed on three existing databases plus a new test set collected from social media feed. We compare against recent algorithms in cross-domain adaptive detection [113, 66] and one-shot unsupervised learning [24], achieving the state-of-the-art.

We make the code of our project available at https://github.com/VeloDC/oshot_detection.

4.3.1 Method

Problem Setting

We introduce the one-shot unsupervised cross-domain detection scenario where our goal is to predict on a single image x^t , with t being any target domain not available at training time, starting from N annotated samples of the source domain $S = \{x_i^s, y_i^s\}_{i=1}^N$. Here the structured labels $y^s = (c, b)$ describe class identity c and

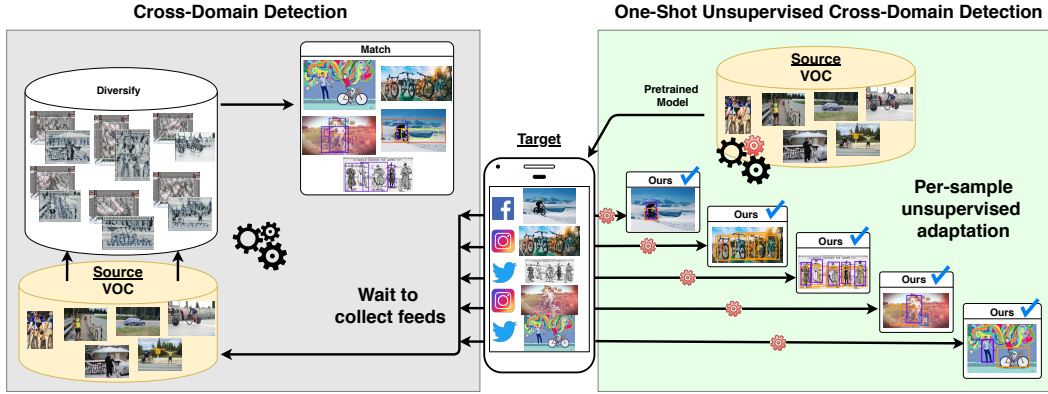


Figure 4.9. Each social media image comes from a different domain. Existing Cross-Domain Detection algorithms (e.g. [66] in the left gray box) struggle to adapt in this setting. OSHOT (right) is able to adapt across domains from one single target image, thanks to the combined use of self-supervision and pseudo-labeling

bounding box location b in each image x^s , and we aim to obtain y^t that precisely detects objects in x^t despite the domain shift.

OSHOT strategy

To pursue the described goal, our strategy is to train the parameters of a detection learning model such that it can be ready to get the maximal performance on a single unsupervised sample from a new domain after few gradient update steps on it. Since we have no ground truth on the target sample, we implement this strategy by learning a representation that exploits inherent data information as that captured by a self-supervised task, and then finetune it on the target sample (see Figure Figure 4.10). Thus, we design our OSHOT to include (1) an initial pretraining phase where we extend a standard deep detection model adding an image rotation classifier, and (2) a following adaptation stage where the network features are updated on the single target sample by further optimization of the rotation objective. Moreover, we exploit pseudo-labeling to focus the auxiliary task on the local object context. A clear advantage of this solution is that we decouple source training from target testing, with no need to access the source data while adapting on the target sample.

Preliminaries

We leverage on Faster R-CNN [106] as our base detection model. It is a two-stage detector with three main components: an initial block of convolutional layers, a region proposal network (RPN) and a region-of-interest (ROI) based classifier. The bottom layers transform any input image x into its convolutional feature map $G_f(x|\theta_f)$ where θ_f is used to parametrize the feature extraction model. The feature map is then used by RPN to generate candidate object proposals. Finally the ROI-wise classifier predicts the category label from the feature vector obtained using ROI-pooling. The training objective combines the loss of both RPN and ROI, each of them composed by two terms:

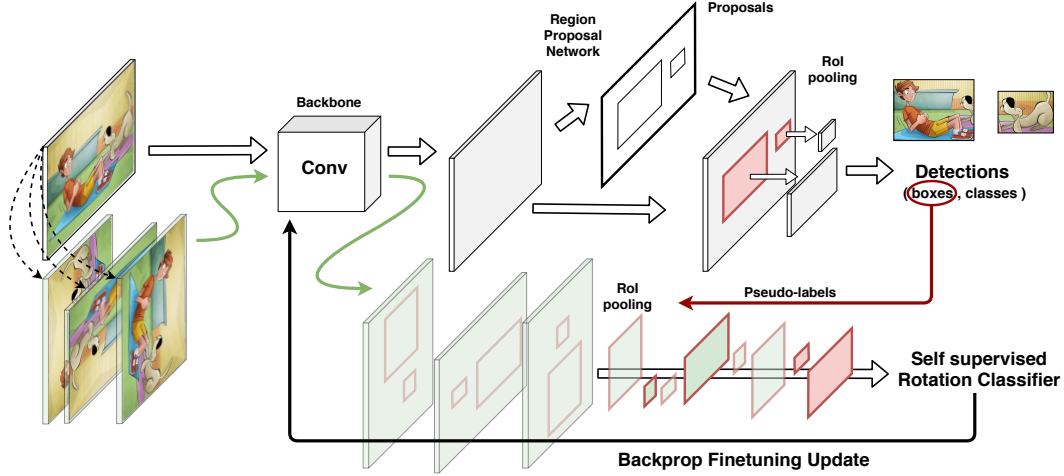


Figure 4.10. Visualization of the adaptive phase of OSHOT with cross-task pseudo-labeling. The target image passes through the network and produces detections. While the class information is not used, the identified boxes are exploited to select object regions from the feature maps of the rotated image. The obtained region-specific feature vectors are finally sent to the rotation classifier. A number of subsequent finetuning iterations allows to adapt the convolutional backbone to the domain represented by the test image

$$\mathcal{L}_d(G_d(G_f(x|\theta_f)|\theta_d), y) = (\mathcal{L}_{class}(c^*) + \mathcal{L}_{regr}(b))_{RPN} + (\mathcal{L}_{class}(c) + \mathcal{L}_{regr}(b))_{ROI} . \quad (4.4)$$

Here \mathcal{L}_{class} is a classification loss to evaluate the object recognition accuracy, while \mathcal{L}_{regr} is a regression loss on the box coordinates for better localization. To maintain a simple notation we summarize the role of ROI and RPN with the function $G_d(G_f(x|\theta_f)|\theta_d)$ parametrized by θ_d . Moreover, we use c^* to highlight that RPN deals with a binary classification task to separate foreground and background objects, while ROI deals with the multi-class objective needed to discriminate among c foreground object categories. As mentioned above, ROI and RPN are applied in sequence: they both elaborate on the feature maps produced by the convolutional block, and then influence each other in the final optimization of the multi-task (classification, regression) objective function.

OSHOT pretraining

As a first step, we extend Faster R-CNN to include image rotation recognition. Formally, to each source training image x^s we apply four geometric transformations $R(x, \alpha)$ where $\alpha = q \times 90^\circ$ indicates rotations with $q \in \{1, \dots, 4\}$. In this way we obtain a new set of samples $\{R(x)_j, q_j\}_{j=1}^M$ where we dropped the α without loss of generality. We indicate the auxiliary rotation classifier and its parameters respectively with G_r and θ_r and we train our network to optimize the following multi-task objective

$$\operatorname{argmin}_{\theta_f, \theta_d, \theta_r} \sum_{i=1}^N \mathcal{L}_d(G_d(G_f(x_i^s | \theta_f) | \theta_d), y_i^s) + \lambda \sum_{j=1}^M \mathcal{L}_r(G_r(G_f(R(x^s)_j | \theta_f) | \theta_r), q_j^s) , \quad (4.5)$$

where \mathcal{L}_r is the cross-entropy loss. When solving this problem, we can design G_r in two different ways. Indeed it can either be a Fully Connected layer that naïvely takes as input the feature map produced by the whole (rotated) image $G_r(\cdot | \theta_r) = \text{FC}_{\theta_r}(\cdot)$, or it can exploit the ground truth location of each object with a subselection of the features only from its bounding box in the original map $G_r(\cdot | \theta_r) = \text{FC}_{\theta_r}(\text{boxcrop}(\cdot))$. The *boxcrop* operation includes pooling to rescale the feature dimension before entering the final FC layer. In this last case the network is encouraged to focus only on the object orientation without introducing noisy information from the background and provides better results with respect to the whole image option as we will discuss in Section 4.3.2.4. In practical terms, both in the case of image and box rotations, we randomly pick one rotation angle per instance, rather than considering all four of them: this avoids any troublesome unbalance between rotated and non-rotated data when solving the multi-task optimization problem.

OSHOT adaptation

Given the single target image x^t , we finetune the backbone’s parameters θ_f by iteratively solving a self-supervised task on it. This allows to adapt the original feature representation both to the content and to the style of the new sample. Specifically, we start from the rotated versions $R(x^t)$ of the provided sample and optimize the rotation classifier through

$$\operatorname{argmin}_{\theta_f, \theta_r} \mathcal{L}_r(G_r(G_f(R(x^t) | \theta_f) | \theta_r), q^t) . \quad (4.6)$$

This process involves only G_f and G_r , while the RPN and ROI detection components described by G_d remain unchanged. In the following we use γ to indicate the number of gradient steps (i.e. iterations), with $\gamma = 0$ corresponding to the OSHOT pretraining phase. At the end of the finetuning process, the inner feature model is described by θ_f^* and the detection prediction on x^t is obtained by $y^{t*} = G_d(G_f(x^t | \theta_f^*) | \theta_d)$.

Cross-task pseudo-labeling

As in the pretraining phase, also in the adaptation stage we have two possible choices to design G_r : either considering the whole feature map $G_r(\cdot | \theta_r) = \text{FC}_{\theta_r}(\cdot)$, or focusing on the object locations $G_r(\cdot | \theta_r) = \text{FC}_{\theta_r}(\text{pseudoboxcrop}(\cdot))$. For both variants we include dropout to prevent overfitting on the single target sample. With *pseudoboxcrop* we mean a localized feature extraction operation analogous to that discussed for pretraining, but obtained through a particular form of cross-task self-training. Specifically, we follow the self-training strategy used in [65, 59] with a cross-task variant: instead of reusing the pseudo-labels produced by the source model

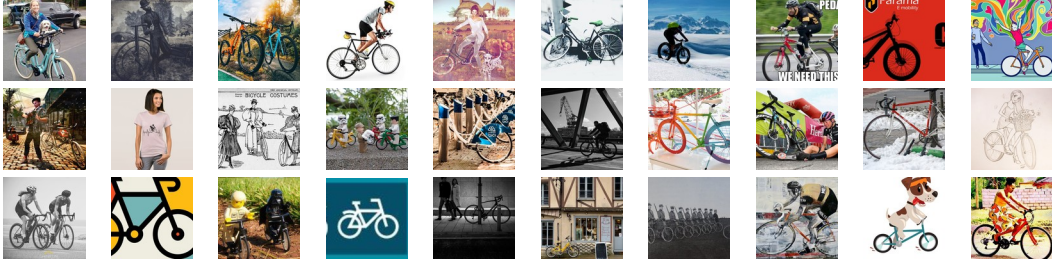


Figure 4.11. The Social Bikes concept-dataset. A random data acquisition from multiple users/feeds leads to a target distribution with several, uneven domain shifts

on the target to update the detector, we exploit them for the self-supervised rotation classifier. In this way we keep the advantage of the self-training initialization, largely reducing the risks of error propagation due to wrong class pseudo-labels.

More practically, we start from the (θ_f, θ_d) model parameters of the pretraining stage and we get the feature maps from all the rotated versions of the target sample $G_f(\{R(x^t), q\}|\theta_f)$, $q = 1, \dots, 4$. Only the feature map produced by the original image (i.e. $q = 4$) is provided as input to the RPN and ROI network components to get the predicted detection $y^t = (c, b) = G_d(G_f(x^t|\theta_f)|\theta_d)$. This pseudo-label is composed by the class label c and the bounding box location b . We discard the first and consider only the second to localize the region containing an object in all the four feature maps, also recalibrating the position to compensate for the orientation of each map. Once passed through this pseudoboxcrop operation, the obtained features are used to finetune the rotation classifier, updating the bottom convolutional network block.

4.3.2 Experiments

4.3.2.1 Datasets

Social Bikes

Social Bikes is our new concept-dataset containing 30 images of scenes with persons/bicycles collected from Twitter, Instagram and Facebook by searching for #bike tags. Square crops of the full dataset are presented in Figure Figure 4.11: images acquired randomly from social feeds show diverse style properties and cannot be grouped under a single shared domain.

4.3.2.2 Performance analysis

Experimental Setup

We evaluate OSHOT on several testbeds using the described datasets. In the following we will use an arrow $Source \rightarrow Target$ to indicate the experimental setting. Our base detector is Faster-RCNN [87] with a ResNet-50 [52] backbone pre-trained on ImageNet, RPN with 300 top proposals after non-maximum-supression, anchors

at three scales (128, 256, 512) and three aspect ratios (1:1, 1:2, 2:1). For all our experiments we set the IoU threshold at 0.5 for the mAP results, and report the average of three independent runs.

OSHOT pretraining. We always resize the image’s shorter size to 600 pixels and apply random horizontal flipping. Unless differently specified, we train the base network for 70k iterations using SGD with momentum set at 0.9, the initial learning rate is 0.001 and decays after 50k iterations. We use a batch size of 1, keep batch normalization layers fixed for both pretraining and adaptation phases and freeze the first 2 blocks of ResNet50. The weight of the auxiliary task is set to $\lambda = 0.05$.

OSHOT adaptation. We increase the weight of the auxiliary task to $\lambda = 0.2$ to speed up adaptation and keep all other training hyperparameters fixed. For each test instance, we finetune the initial model on the auxiliary task for 30 iterations before testing.

Benchmark methods. We compare OSHOT with the following algorithms. FRCNN: baseline Faster-RCNN with ResNet50 backbone, trained on the source domain and deployed on the target without further adaptation. DivMatch [66]: cross-domain detection algorithm that, by exploiting target data, creates multiple randomized domains via CycleGAN and aligns their representations using an adversarial loss. SW [113]: adaptive detection algorithm that aligns source and target features based on global context similarity. For both DivMatch and SW, we use a ResNet-50 backbone pretrained on ImageNet for fair comparison. Since all cross-domain algorithms need target data in advance and are not designed to work in our one-shot unsupervised setting, we provide them with the advantage of 10 target images accessible during training and randomly selected at each run. We collect average precision statistics during inference under the favorable assumption that the target domain will not shift after deployment.

Adapting to social feeds

When data is collected from multiple sources, the assumption that all target images originate from the same underlying distribution does not hold and standard cross-domain detection methods are penalized regardless of the number of seen target samples. We pretrain the source detector on Pascal VOC, and deploy it on Social Bikes. We consider only the bicycle and person annotations for this target, since all other instances of VOC classes are scarce.

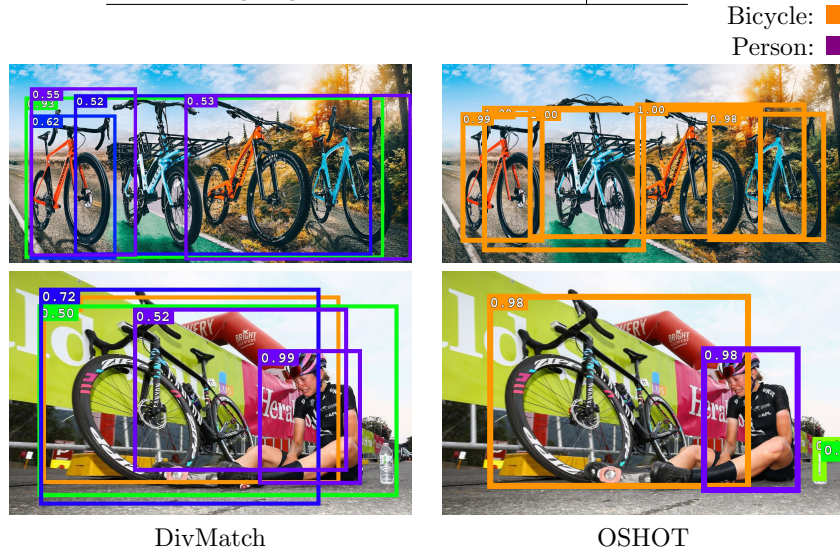
Results. We report results in Table Table 4.8. OSHOT outperforms all considered competitors, with a mAP score of 64.4. Despite granting them access to the full target, adaptive algorithms incur in negative transfer due to data scarcity and large variety of target styles.

Large distribution shifts

Artistic images are difficult benchmarks for cross-domain methods. Unpredictable perturbations in shape and color are challenging to detectors trained only on realistic

Table 4.8. (top) VOC \rightarrow Social Bikes mAP results; (bottom) visualization of DivMatch and OSHOT detections. The number associated with each bounding box indicates the model’s confidence in localization. Examples show how OSHOT detection is accurate, while most DivMatch boxes are false positives

<i>One-Shot Target</i>			
Method	person	bicycle	mAP
FRCNN	67.7	56.6	62.1
OSHOT ($\gamma = 0$)	72.1	52.8	62.4
OSHOT ($\gamma = 30$)	69.4	59.4	64.4
<i>Full Target</i>			
DivMatch [66]	63.7	51.7	57.7
SW [113]	63.2	44.3	53.7



images. We investigate this setting by training the source detector on Pascal VOC and deploying it on Clipart, Comic and Watercolor datasets.

Results. Table 4.9 summarizes results on the three adaptation splits. We can see how OSHOT with 30 finetuning iterations outperforms all competitors, with mAP gains ranging from 7.5 points on Clipart to 9.2 points on Watercolor. Cross-detection methods perform poorly in this setting, despite using 9 more samples in the adaptation phase compared to OSHOT that only uses the test sample. These results confirm that they are not designed to tackle data scarcity conditions and exhibit negligible improvements compared to the baseline.

Adverse weather

Some peculiar environmental conditions, such as fog, may be disregarded in source data acquisition, yet adaptation to these circumstances is crucial for real world applications. We assess the performance of OSHOT on Cityscapes \rightarrow FoggyCityscapes. We train our base detector on Cityscapes for 30k iterations without stepdown, as in [13]. We select the best performing model on the Cityscapes validation split and

Table 4.9. mAP results for VOC \rightarrow AMD

One-Shot Target																					
Method	aero	bike	bird	boat	bottle	bus	car	cat	chair	cow	table	dog	horse	mbike	person	plant	sheep	sofa	train	tv	mAP
FRCNN	18.5	43.3	20.4	13.3	21.0	47.8	29.0	16.9	28.8	12.5	19.5	17.1	23.8	40.6	34.9	34.7	9.1	18.3	40.2	38.0	26.4
<i>OSHOT</i> ($\gamma = 0$)	23.1	55.3	22.7	21.4	26.8	53.3	28.9	4.6	31.4	9.2	27.8	9.6	30.9	47.0	38.2	35.2	11.1	20.4	36.0	33.6	28.3
<i>OSHOT</i> ($\gamma = 10$)	25.4	61.6	23.8	21.1	31.3	55.1	31.6	5.3	34.0	10.1	28.8	7.3	33.1	59.9	44.2	38.8	15.9	19.1	39.5	33.9	31.0
<i>OSHOT</i> ($\gamma = 30$)	25.4	56.0	24.7	25.3	36.7	58.0	34.4	5.9	34.9	10.3	29.2	11.8	46.9	70.9	52.9	41.5	21.1	21.0	38.5	31.8	33.9

Ten-Shot Target																					
DivMatch [66]	19.5	57.2	17.0	23.8	14.4	25.4	29.4	2.7	35.0	8.4	22.9	14.2	30.0	55.6	50.8	30.2	1.9	12.3	37.8	37.2	26.3
SW [113]	21.5	39.9	21.7	20.5	32.7	34.1	25.1	8.5	33.2	10.9	15.2	3.4	32.2	56.9	46.5	35.4	14.7	15.2	29.2	32.0	26.4

(b) VOC \rightarrow Comic

(c) VOC \rightarrow Watercolor

One-Shot Target							
Method	bike	bird	car	cat	dog	person	mAP
FRCNN	25.2	10.0	21.1	14.1	11.0	27.1	18.1
<i>OSHOT</i> ($\gamma = 0$)	26.9	11.6	22.7	9.1	14.2	28.3	18.8
<i>OSHOT</i> ($\gamma = 10$)	35.5	11.7	25.1	9.1	15.8	34.5	22.0
<i>OSHOT</i> ($\gamma = 30$)	35.2	14.4	30.0	14.8	20.0	46.7	26.9

One-Shot Target							
Method	bike	bird	car	cat	dog	person	mAP
FRCNN	62.5	39.7	43.4	31.9	26.7	52.4	42.8
<i>OSHOT</i> ($\gamma = 0$)	70.2	46.7	45.5	31.2	27.2	55.7	46.1
<i>OSHOT</i> ($\gamma = 10$)	70.2	46.7	48.1	30.9	32.3	59.9	48.0
<i>OSHOT</i> ($\gamma = 30$)	77.1	44.7	52.4	37.3	37.0	63.3	52.0

Ten-Shot Target							
DivMatch [66]	64.6	44.1	44.6	34.1	24.9	60.0	45.4
SW [113]	66.3	41.1	41.1	30.5	20.5	52.3	42.0

Table 4.10. mAP results for Cityscapes \rightarrow FoggyCityscapes

<i>One-Shot Target</i>									
Method	person	rider	car	truck	bus	train	mcycle	bicycle	mAP
FRCNN	30.4	36.3	41.4	18.5	32.8	9.1	20.3	25.9	26.8
<i>OSHOT</i> ($\gamma = 0$)	31.8	42.0	42.6	20.1	31.6	10.6	24.8	30.7	29.3
<i>OSHOT</i> ($\gamma = 10$)	31.9	41.9	43.0	19.7	38.0	10.4	25.5	30.2	30.1
<i>OSHOT</i> ($\gamma = 30$)	32.1	46.1	43.1	20.4	39.8	15.9	27.1	32.4	31.9
<i>Ten-Shot Target</i>									
DivMatch [66]	27.6	38.1	42.9	17.1	27.6	14.3	14.6	32.8	26.9
SW [113]	25.5	30.8	40.4	21.1	26.1	34.5	6.1	13.4	24.7
<i>Full Target</i>									
DivMatch [66]	32.3	43.5	47.6	23.9	38.0	23.1	27.6	37.2	34.2
SW [113]	31.3	32.1	47.4	19.6	28.8	41.0	9.8	20.1	28.8

deploy it to FoggyCityscapes.

Results. Experimental evaluation in Table Table 4.10 shows that OSHOT outperforms all compared approaches. Without finetuning iterations, performance using the auxiliary rotation task increases compared to the baseline. Subsequent finetuning iterations on the target sample improve these results, and 30 iterations yield models able to outperform the second-best method by 5 mAP. Cross-domain algorithms used in this setting struggle to surpass the baseline (DivMatch) or suffer negative transfer (SW).

Cross-camera transfer

Dataset bias between training and testing is unavoidable in practical applications, as for urban scene scenarios collected in different cities and with different cameras. Subtle changes in illumination conditions and camera resolution might preclude a model trained on one realistic domain to optimally perform in another realistic

Table 4.11. mAP of car class in KITTI/Cityscapes detection experiments (top). Random samples from the Cityscapes dataset, showing low intra-domain variance (bottom)

<i>One-Shot Target</i>		
Method	KITTI \rightarrow Cityscapes	Cityscapes \rightarrow KITTI
FRCNN	26.5	75.1
OSHOT $\gamma = 0$	26.2	75.4
OSHOT $\gamma = 10$	33.2	75.3
OSHOT $\gamma = 30$	33.5	75.0
<i>Ten-Shot Target</i>		
DivMatch [66]	37.9	74.1
SW [113]	39.2	74.6



but different domain. We test adaptation between KITTI and Cityscapes in both directions. For cross-domain evaluation we consider only the label car as standard practice.

Results. In Table 4.11, OSHOT improves by 7 mAP points on KITTI \rightarrow Cityscapes compared to the FRCNN baseline. DivMatch and SW both show a gain in this split, with SW obtaining the highest mAP of 39.2 in the ten-shot setting. We argue that this is not surprising considering that, as shown in the visualization of Table 4.11, the Cityscapes images share all a uniform visual style. As a consequence, 10 target images may be enough for standard cross-domain detection methods. Despite visual style homogeneity, the diversity among car instances in Cityscapes is high enough for learning a good car detection model. This is highlighted by the results in Cityscapes \rightarrow KITTI task, for which adaptation performance for all methods is similar, and OSHOT with $\gamma = 0$ obtains the highest mAP of 75.4. The FRCNN baseline on KITTI scores a high mAP of 75.1: in this favorable condition detection doesn't benefit from adaptation.

Table 4.12. Comparison between baseline, one-shot style transfer and OSHOT in the one-shot unsupervised cross-domain detection setting

	FRCNN	BiOST [24]	OSHOT ($\gamma = 30$)
mAP on Clipart100	27.9	29.8	30.7
mAP on Social Bikes	62.1	51.1	64.4
Adaptation time (seconds per sample)	-	$\sim 2.4 * 10^4$	7.8

4.3.2.3 Comparison with One-Shot Style Transfer

Although not specifically designed for cross-domain detection, in principle it is possible to apply one-shot style transfer methods as an alternative solution for our setting. We use BiOST [24], the current state-of-the-art method for one-shot transfer, to modify the style of the target sample towards that of the source domain before performing inference. Due to the time-heavy requirements to perform BiOST on each test sample⁵, we test it on Social Bikes and on a random subset of 100 Clipart images that we name Clipart100. We compare performance and time requirements of OSHOT and BiOST on these two targets. Speed has been computed on an RTX2080Ti with full precision settings.

Results. Table Table 4.12 shows summary mAP results using BiOST and OSHOT. On Clipart100, the baseline FRCNN detector obtains 27.9 mAP. We can see how BiOST is effective in the adaptation from one-sample, gaining 1.9 points over the baseline, however it is outperformed by OSHOT, which obtains 30.7 mAP. On Social Bikes, while OSHOT still outperforms the baseline, BiOST incurs in negative transfer, indicating that it was not able to effectively modify the source’s style on the images we collected. Furthermore, BiOST is affected by two strong issues: (1) as already mentioned, it has an extremely high time complexity, with more than 6 hours needed to modify the style of a single source instance; (2) it works under the strict assumption of accessing at the same time the entire source training set and the target sample. Due to these weaknesses, and the fact that OSHOT still outperforms BiOST, we argue that existing one-shot translation methods are not suitable for one shot unsupervised cross-domain adaptation.

4.3.2.4 Ablation Study

Detection error analysis

Following [56], we provide detection error analysis for VOC \rightarrow Clipart setting in Figure Figure 4.12. We select the 1000 most confident detections, and assign error classes based on IoU with ground truth (IoUgt). Errors are categorized as: correct (IoUgt ≥ 0.5), mislocalized ($0.3 \leq \text{IoUgt} < 0.5$) and background (IoUgt < 0.3). Results show that, compared to the baseline FRCNN model, the regularization effect of adding a self-supervised task at training time ($\gamma = 0$) marginally increases

⁵To get the style update, BiOST trains of a double-variational autoencoder using the entire source besides the single target sample. As advised by the authors through personal communications, we trained the model for 5 epochs.

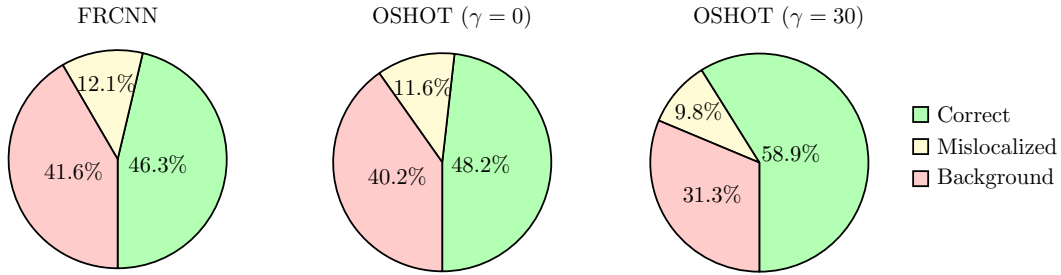


Figure 4.12. Detection error analysis on the most confident detections on Clipart

Table 4.13. Rotating image vs rotating objects via pseudo-labeling on OSHOT

	$G_r(image)$	$G_r(pseudoboxcrop)$
VOC \rightarrow Clipart	31.0	33.9
VOC \rightarrow Comic	21.0	26.9
VOC \rightarrow Watercolor	48.2	52.0
Cityscapes \rightarrow Foggy Cityscapes	27.7	31.9

the quality of detections. Instead subsequent finetuning iterations on the test sample substantially improve the number of correct detections, while also decreasing both false positives and mislocalization errors.

Cross-task pseudo-labeling ablation

As explained in Section 4.3.1 we have two options in the OSHOT adaptation phase: either considering the whole image, or focusing on pseudo-labeled bounding boxes obtained from the detector after the first OSHOT pretraining stage. For all the experiments presented above we focused on the second case. Indeed by solving the auxiliary task only on objects, we limit the use of background features which may mislead the network towards solutions of the rotation task not based on relevant semantic information (e.g.: finding fixed patterns in images, exploiting watermarks). We validate our choice by comparing it against using the rotation task on the entire image in both training and adaptation phases. Table 4.13 shows results for VOC \rightarrow AMD and Cityscapes \rightarrow Foggy Cityscapes using OSHOT. We observe that the choice of rotated regions is critical for the effectiveness of the algorithm. Solving the rotation task on objects using pseudo-annotations results in mAP improvements that range from 2.9 to 5.9 points, indicating that we learn better features for the main task.

Self-supervised iterations

We study the effects of adapting with up to $\gamma = 70$ iterations on VOC \rightarrow Clipart, Cityscapes \rightarrow FoggyCityscapes and KITTI \rightarrow Cityscapes. Results are shown in Figure 4.13. We observe a positive correlation between number of finetuning iterations and final mAP of the model in the earliest steps. This correlation is strong for the first 10 iterations and gets to a plateau after about 30 iterations: increasing γ beyond this point doesn't affect the final results.

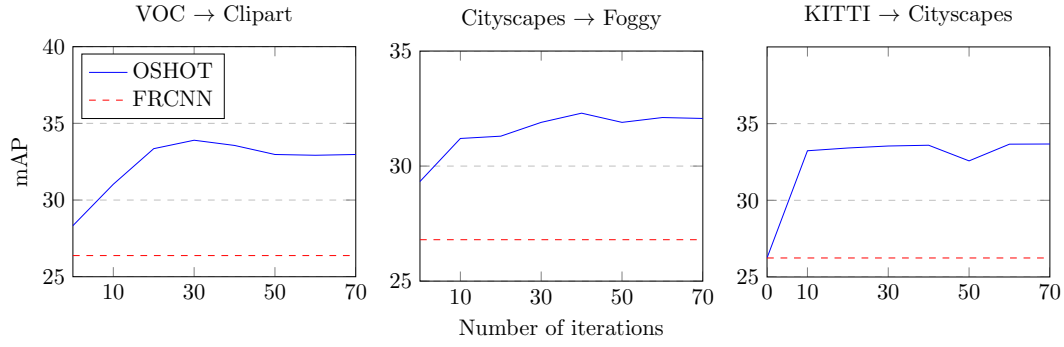


Figure 4.13. Performance of OSHOT at different self-supervised iterations

4.3.3 Conclusions

This paper introduced the one-shot unsupervised cross-domain detection scenario, which is extremely relevant for monitoring image feeds on social media, where algorithms are called to adapt to a new visual domain from one single image. We showed that existing cross-domain detection methods suffer in this setting, as they are all explicitly designed to adapt from far larger quantities of target data. We presented OSHOT, the first deep architecture able to reduce the domain gap between source and target distribution by leveraging over one single target image. Our approach is based on a multi-task structure that exploits self-supervision and cross-task self-labeling. Extensive quantitative experiments and a qualitative analysis clearly demonstrate its effectiveness.

Chapter 5

Conclusions and Future Work

5.1 Conclusions

Dataset bias is an ever-present problem in Computer Vision, as data acquisition and subsequent annotation is often performed in controlled settings, making the training distribution unlikely to correspond to the testing one. Hence, research in Domain Generalization and Domain Adaptation has flourished, with methods at *feature*, *model* and *data* levels.

We contributed to these research areas by presenting novel approaches for Domain Generalization and Domain Adaptation that are based on data aggregations and transformations.

In DSAM [32], we proposed a model-based algorithm for DG that achieves generalization by explicitly separating agnostic and specific components within the architecture. The approach has shown promising results, although it requires source-awareness during training in the form of domain labels for each image.

With self-supervised solutions, we overcome the need of source domain labels by aligning features with a proxy task. The auxiliary loss enhances model regularization for out-of-distribution generalization [18], while the pretext labels allow unsupervised learning on the unlabeled target set for Domain Adaptation [18] and Partial Domain Adaptation [11]. Furthermore, by having the source pre-text task shared with the test sample, we’ve designed an object detection model that can adapt on individual images on the fly by performing the auxiliary task on them [33]. These approaches, despite being relatively simple, have been shown to be competitive with more elaborate methods for generalization and adaptation [12]. They might, however, introduce many additional hyperparameters to balance auxiliary losses [11], a weakness that is shared with most Domain Adaptation literature. Another limitation lies in the choice of the best self-supervised task, specifically, the multi-task inductive bias is effective as much as the auxiliary task is semantically related with the primary task. This was most evident in OSHOT, when we used the entire image for self-supervised pre-training and adaptation. There, we could see how the model started to exploit visual cues unrelated to the detection task, such as the position of the ground. At the moment, the best thing we can do is manual searching of the better correlated task with expensive trainings.

We’ve also shown how non-naïve data-augmentation via style-transfer is a simple

and inexpensive strategy to improve generalization on new distributions [9]. Established Domain Generalization methods that leverage the multi-source nature of data fail to take advantage of the augmented sources and their original benefit disappears when compared with the baseline, highlighting the need for new algorithms that can properly incorporate data-augmentation.

5.2 Future Work

Future work could expand more on the use of transformations for Domain Adaptation. Specifically, the success of self-supervision on the unlabeled target depends on how semantically related the auxiliary task is with respect to the main task. This makes the choice of auxiliary task crucial, however, a brute-force search to find the best fitting task is expensive. One solution could do by leveraging a linear combination of tasks (task-ensemble) to approximate the semantics of the main problem. This method could be effective at improving performances on the main objective, but would still raise the computational cost for model training. A more refined approach could instead use meta-learning to align different losses for main and auxiliary objectives to improve Domain Adaptation and One-Shot Adaptation regardless of the chosen task.

Self-supervision could also be used to enhance model validation in Domain Adaptation. Hyperparameter optimization is an open problem in DA, as it is not possible to validate on the unlabeled target set. Despite this limitation, most methods in this literature tend to introduce multiple additional tasks/losses that need to be tuned. A self-supervised task that is semantically close to the main task could potentially overcome this limitation by acting as a proxy objective for validating any algorithm’s hyperparameters.

Future work will also focus on expanding the OSHOT method. One possible direction is to explore different tasks other than object detection, as the training and adaptation phases use a general multi-task paradigm that can be easily extended. In particular, tasks for which semantics of target images are abundant, such as semantic segmentation or aerial image understanding, are good candidates. Furthermore, meta-learning is a natural extension of OSHOT, as it allows to optimize a model to perform well on a given task when a different objective has been applied beforehand. In our case, we could train the detection task to better detect boxes on the target image when the model has been fine-tuned on the auxiliary task.

Finally, given the effectiveness and convenience of style-transfer based data-augmentation in Domain Generalization, future research should focus on integrating these transformations in generalization pipelines. Most DG approaches that expect well separated input distribution could be relaxed to allow for samples with mixed source styles.

Bibliography

- [1] G. Angeletti, B. Caputo, and T. Tommasi. Adaptive deep learning through visual domain localization. In *International Conference on Robotic Automation (ICRA)*, 2018.
- [2] Y. M. Asano, C. Rupprecht, and A. Vedaldi. A critical analysis of self-supervision, or what we can learn from a single image. In *ICLR*, 2020.
- [3] Y. Balaji, S. Sankaranarayanan, and R. Chellappa. Metareg: Towards domain generalization using meta-regularization. In *NeurIPS*, 2018.
- [4] J. Baxter. A bayesian/information theoretic model of learning to learn via multiple task sampling. *Machine Learning*, 28(1):7–39, Jul 1997. ISSN 1573-0565. doi: 10.1023/A:1007327622663. URL <https://doi.org/10.1023/A:1007327622663>.
- [5] S. Ben-David, J. Blitzer, K. Crammer, A. Kulesza, F. Pereira, and J. Vaughan. A theory of learning from different domains. *Machine Learning*, 79:151–175, 2010.
- [6] S. Benaim and L. Wolf. One-shot unsupervised cross domain translation. In *NeurIPS*. 2018.
- [7] J. Bisanz, G. L. Bisanz, and R. Kail, editors. *Learning in Children: Progress in Cognitive Development Research*. Springer-Verlag, 1983.
- [8] G. Blanchard, G. Lee, and C. Scott. Generalizing from several related classification tasks to a new unlabeled sample. In *NIPS*. 2011.
- [9] F. C. Borlino, A. D’Innocente, and T. Tommasi. Rethinking domain generalization baselines. *arXiv preprint arXiv:2101.09060*, 2021.
- [10] K. Bousmalis, G. Trigeorgis, N. Silberman, D. Krishnan, and D. Erhan. Domain Separation Networks. In *NeurIPS*, 2016.
- [11] S. Bucci, A. D’Innocente, and T. Tommasi. Tackling partial domain adaptation with self-supervision. In *ICIAP*, 2019.
- [12] S. Bucci, A. D’Innocente, Y. Liao, F. M. Carlucci, B. Caputo, and T. Tommasi. Self-supervised learning across domains. *IEEE Transactions on Pattern Analysis and Machine Intelligence*, 2021.

- [13] Q. Cai, Y. Pan, C.-W. Ngo, X. Tian, L. Duan, and T. Yao. Exploring object relation in mean teacher for cross-domain detection. In *CVPR*, 2019.
- [14] Z. Cao, M. Long, J. Wang, and M. I. Jordan. Partial transfer learning with selective adversarial networks. In *CVPR*, 2018.
- [15] Z. Cao, L. Ma, M. Long, and J. Wang. Partial adversarial domain adaptation. In *ECCV*, 2018.
- [16] F. M. Carlucci, L. Porzi, B. Caputo, E. Ricci, and S. R. Bulò. Just DIAL: domain alignment layers for unsupervised domain adaptation. In *ICIAP*, 2017.
- [17] F. M. Carlucci, L. Porzi, B. Caputo, E. Ricci, and S. Rota Bulò. Autodial: Automatic domain alignment layers. In *ICCV*, 2017.
- [18] F. M. Carlucci, A. D’Innocente, S. Bucci, B. Caputo, and T. Tommasi. Domain generalization by solving jigsaw puzzles. In *Proceedings of the IEEE Conference on Computer Vision and Pattern Recognition*, pages 2229–2238, 2019.
- [19] F. M. Carlucci, P. Russo, T. Tommasi, and B. Caputo. Hallucinating agnostic images to generalize across domains. In *ICCV-Workshop*, 2019.
- [20] M. Caron, P. Bojanowski, A. Joulin, and M. Douze. Deep clustering for unsupervised learning of visual features. In *ECCV*, 2018.
- [21] R. Caruana. Multitask learning: A knowledge-based source of inductive bias. In *Proceedings of the Tenth International Conference on Machine Learning*, pages 41–48. Morgan Kaufmann, 1993.
- [22] R. Caruana. Multitask learning. *Machine Learning*, 28(1):41–75, 1997.
- [23] Y. Chen, W. Li, C. Sakaridis, D. Dai, and L. Van Gool. Domain adaptive faster r-cnn for object detection in the wild. In *CVPR*, 2018.
- [24] T. Cohen and L. Wolf. Bidirectional one-shot unsupervised domain mapping. In *ICCV*, 2019.
- [25] M. Cordts, M. Omran, S. Ramos, T. Rehfeld, M. Enzweiler, R. Benenson, U. Franke, S. Roth, and B. Schiele. The cityscapes dataset for semantic urban scene understanding. In *Proc. of the IEEE Conference on Computer Vision and Pattern Recognition (CVPR)*, 2016.
- [26] R. S. Cruz, B. Fernando, A. Cherian, and S. Gould. Visual permutation learning. In *CVPR*, 2017.
- [27] G. Csurka, editor. *Domain Adaptation in Computer Vision Applications*. Advances in Computer Vision and Pattern Recognition. Springer, 2017.
- [28] J. Dai, Y. Li, K. He, and J. Sun. R-fcn: Object detection via region-based fully convolutional networks. In *NIPS*, 2016.
- [29] N. Dalal and B. Triggs. Histograms of oriented gradients for human detection. In *CVPR*, 2005.

- [30] J. Deng, W. Dong, R. Socher, L. jia Li, K. Li, and L. Fei-Fei. Imagenet: A large-scale hierarchical image database. In *CVPR*, 2009.
- [31] Z. Ding and Y. Fu. Deep domain generalization with structured low-rank constraint. *IEEE TIP*, 27:304–313, 2017.
- [32] A. D’Innocente and B. Caputo. Domain generalization with domain-specific aggregation modules. In *GCPR*, 2018.
- [33] A. D’Innocente, F. C. Borlino, S. Bucci, B. Caputo, and T. Tommasi. One-shot unsupervised cross-domain detection. *arXiv preprint arXiv:2005.11610*, 2020.
- [34] C. Doersch and A. Zisserman. Multi-task self-supervised visual learning. In *The IEEE International Conference on Computer Vision (ICCV)*, 2017.
- [35] C. Doersch and A. Zisserman. Multi-task self-supervised visual learning. In *ICCV*, 2017.
- [36] A. Dosovitskiy, J. T. Springenberg, M. Riedmiller, and T. Brox. Discriminative unsupervised feature learning with convolutional neural networks. In *NeurIPS*, 2014.
- [37] L. Duong, T. Cohn, S. Bird, and P. Cook. Low resource dependency parsing: Cross-lingual parameter sharing in a neural network parser. In *Proceedings of the 53rd Annual Meeting of the Association for Computational Linguistics and the 7th International Joint Conference on Natural Language Processing (Volume 2: Short Papers)*, volume 2, pages 845–850, 2015.
- [38] M. Everingham, L. Van Gool, C. K. Williams, J. Winn, and A. Zisserman. The pascal visual object classes (voc) challenge. *IJCV*, 88(2):303–338, 2010.
- [39] B. Ferguson, S. L. Franconeri, and S. R. Waxman. Very young infants learn abstract rules in the visual modality. *PLOS ONE*, 13(1):1–14, 01 2018. doi: 10.1371/journal.pone.0190185. URL <https://doi.org/10.1371/journal.pone.0190185>.
- [40] C. Finn, P. Abbeel, and S. Levine. Model-agnostic meta-learning for fast adaptation of deep networks. *arXiv preprint arXiv:1703.03400*, 2017.
- [41] Y. Ganin and V. Lempitsky. Unsupervised domain adaptation by backpropagation. In *ICML*, 2015.
- [42] Y. Ganin, E. Ustinova, H. Ajakan, P. Germain, H. Larochelle, F. Laviolette, M. Marchand, and V. Lempitsky. Domain-adversarial training of neural networks. *J. Mach. Learn. Res.*, 17(1):2096–2030, 2016.
- [43] A. Geiger, P. Lenz, C. Stiller, and R. Urtasun. Vision meets robotics: The kitti dataset. *The International Journal of Robotics Research*, 32(11):1231–1237, 2013.
- [44] M. Ghifary, W. B. Kleijn, M. Zhang, and D. Balduzzi. Domain generalization for object recognition with multi-task autoencoders. In *ICCV*, 2015.

- [45] S. Gidaris, P. Singh, and N. Komodakis. Unsupervised representation learning by predicting image rotations. In *ICLR*, 2018.
- [46] S. Gidaris, A. Bursuc, N. Komodakis, P. Pérez, and M. Cord. Learning representations by predicting bags of visual words. In *CVPR*, 2020.
- [47] R. Girshick. Fast r-cnn. In *ICCV*, 2015.
- [48] R. Girshick, J. Donahue, T. Darrell, and J. Malik. Rich feature hierarchies for accurate object detection and semantic segmentation. In *CVPR*, 2014.
- [49] I. Goodfellow, J. Pouget-Abadie, M. Mirza, B. Xu, D. Warde-Farley, S. Ozair, A. Courville, and Y. Bengio. Generative adversarial nets. In *NeurIPS*, 2014.
- [50] I. Gulrajani and D. Lopez-Paz. In search of lost domain generalization. *arXiv preprint arXiv:2007.01434*, 2020.
- [51] M. Guo, A. Haque, D.-A. Huang, S. Yeung, and L. Fei-Fei. Dynamic task prioritization for multitask learning. In *European Conference on Computer Vision*, pages 282–299. Springer, 2018.
- [52] K. He, X. Zhang, S. Ren, and J. Sun. Deep residual learning for image recognition. In *Conference on Computer Vision and Pattern Recognition (CVPR)*, 2016.
- [53] J. Hoffman, B. Kulis, T. Darrell, and K. Saenko. Discovering latent domains for multisource domain adaptation. In *ECCV*, 2012.
- [54] J. Hoffman, T. Darrell, and K. Saenko. Continuous manifold based adaptation for evolving visual domains. In *CVPR*, 2014.
- [55] J. Hoffman, E. Tzeng, T. Park, J.-Y. Zhu, P. Isola, K. Saenko, A. Efros, and T. Darrell. CyCADA: Cycle-consistent adversarial domain adaptation. In *ICML*, 2018.
- [56] D. Hoiem, Y. Chodpathumwan, and Q. Dai. Diagnosing error in object detectors. In *ECCV*, 2012.
- [57] X. Huang and S. Belongie. Arbitrary style transfer in real-time with adaptive instance normalization. In *ICCV*, 2017.
- [58] Z. Huang, H. Wang, E. P. Xing, and D. Huang. Self-challenging improves cross-domain generalization. In *ECCV*, 2020.
- [59] N. Inoue, R. Furuta, T. Yamasaki, and K. Aizawa. Cross-domain weakly-supervised object detection through progressive domain adaptation. In *CVPR*, 2018.
- [60] E. Jang, C. Devin, V. Vanhoucke, and S. Levine. Grasp2vec: Learning object representations from self-supervised grasping. In *CoRL*, 2018.
- [61] S. Jenni, H. Jin, and P. Favaro. Steering self-supervised feature learning beyond local pixel statistics. In *CVPR*, 2020.

- [62] A. Kendall, Y. Gal, and R. Cipolla. Multi-task learning using uncertainty to weigh losses for scene geometry and semantics. In *Conference on Computer Vision and Pattern Recognition (CVPR)*, 2018.
- [63] M. Khodabandeh, A. Vahdat, M. Ranjbar, and W. G. Macready. A robust learning approach to domain adaptive object detection. In *ICCV*, 2019.
- [64] A. Khosla, T. Zhou, T. Malisiewicz, A. Efros, and A. Torralba. Undoing the damage of dataset bias. In *ECCV*, 2012.
- [65] S. Kim, J. Choi, T. Kim, and C. Kim. Self-training and adversarial background regularization for unsupervised domain adaptive one-stage object detection. In *ICCV*, 2019.
- [66] T. Kim, M. Jeong, S. Kim, S. Choi, and C. Kim. Diversify and match: A domain adaptive representation learning paradigm for object detection. In *CVPR*, 2019.
- [67] I. Kokkinos. Ubertnet: Training a ‘universal’ convolutional neural network for low-, mid-, and high-level vision using diverse datasets and limited memory. In *Computer Vision and Pattern Recognition (CVPR)*, 2017.
- [68] A. Krizhevsky, I. Sutskever, and G. E. Hinton. Imagenet classification with deep convolutional neural networks. In *NeurIPS*, 2012.
- [69] Y. LeCun, L. Bottou, Y. Bengio, and P. Haffner. Gradient-based learning applied to document recognition. *IEEE*, 86(11):2278–2324, 1998.
- [70] M. A. Lee, Y. Zhu, K. Srinivasan, P. Shah, S. Savarese, L. Fei-Fei, A. Garg, and J. Bohg. Making sense of vision and touch: Self-supervised learning of multimodal representations for contact-rich tasks. In *ICRA*, 2019.
- [71] S. Legg and M. Hutter. A collection of definitions of intelligence. *Frontiers in Artificial Intelligence and Applications (FAIA)*, 157:17, 2007.
- [72] D. Li, Y. Yang, Y.-Z. Song, and T. M. Hospedales. Deeper, broader and artier domain generalization. In *ICCV*, 2017.
- [73] D. Li, Y. Yang, Y. Song, and T. M. Hospedales. Learning to generalize: Meta-learning for domain generalization. In *AAAI*, 2018.
- [74] D. Li, J. Zhang, Y. Yang, C. Liu, Y.-Z. Song, and T. M. Hospedales. Episodic training for domain generalization. In *ICCV*, 2019.
- [75] H. Li, S. Jialin Pan, S. Wang, and A. C. Kot. Domain generalization with adversarial feature learning. In *CVPR*, 2018.
- [76] Y. Li, X. Tian, M. Gong, Y. Liu, T. Liu, K. Zhang, and D. Tao. Deep domain generalization via conditional invariant adversarial networks. In *ECCV*, 2018.
- [77] T.-Y. Lin, M. Maire, S. Belongie, J. Hays, P. Perona, D. Ramanan, P. Dollár, and C. L. Zitnick. Microsoft coco: Common objects in context. In *ECCV*, 2014.

- [78] S. Liu, D. Huang, et al. Receptive field block net for accurate and fast object detection. In *Proceedings of the European Conference on Computer Vision (ECCV)*, pages 385–400, 2018.
- [79] M. Long, Y. Cao, J. Wang, and M. I. Jordan. Learning transferable features with deep adaptation networks. In *ICML*, 2015.
- [80] M. Long, H. Zhu, J. Wang, and M. I. Jordan. Unsupervised domain adaptation with residual transfer networks. In *NeurIPS*, 2016.
- [81] M. Long, H. Zhu, J. Wang, and M. I. Jordan. Deep transfer learning with joint adaptation networks. In *ICML*, 2017.
- [82] M. Mancini, S. R. Bulò, B. Caputo, and E. Ricci. Robust place categorization with deep domain generalization. *IEEE Robotics and Automation Letters (RA-L)*, 2018.
- [83] M. Mancini, S. R. Bulò, B. Caputo, and E. Ricci. Best sources forward: domain generalization through source-specific nets. *arXiv preprint arXiv:1806.05810*, 2018.
- [84] M. Mancini, H. Karaoguz, E. Ricci, P. Jensfelt, and B. Caputo. Kitting in the wild through online domain adaptation. In *IROS*, 2018.
- [85] M. Mancini, L. Porzi, S. Rota Bulò, B. Caputo, and E. Ricci. Boosting domain adaptation by discovering latent domains. In *CVPR*, 2018.
- [86] M. Mancini, S. Rota Bulò, B. Caputo, and E. Ricci. Adagraph: Unifying predictive and continuous domain adaptation through graphs. In *CVPR*, 2019.
- [87] F. Massa and R. Girshick. maskrcnn-benchmark: Fast, modular reference implementation of Instance Segmentation and Object Detection algorithms in PyTorch. <https://github.com/facebookresearch/maskrcnn-benchmark>, 2018. Accessed: 22/08/2019.
- [88] T. Matsuura and T. Harada. Domain generalization using a mixture of multiple latent domains. In *AAAI*, 2020.
- [89] T. Matsuura, K. Saito, and T. Harada. Twins: Two weighted inconsistency-reduced networks for partial domain adaptation. *arXiv:1812.07405*, 2018.
- [90] I. Misra, A. Shrivastava, A. Gupta, and M. Hebert. Cross-stitch networks for multi-task learning. In *Proceedings of the IEEE Conference on Computer Vision and Pattern Recognition*, pages 3994–4003, 2016.
- [91] I. Misra, C. L. Zitnick, and M. Hebert. Shuffle and Learn: Unsupervised Learning using Temporal Order Verification. In *ECCV*, 2016.
- [92] T. Mordan, N. Thome, G. Henaff, and M. Cord. Revisiting multi-task learning with rock: a deep residual auxiliary block for visual detection supplementary material.

- [93] S. Motiian, Q. Jones, S. Iranmanesh, and G. Doretto. Few-shot adversarial domain adaptation. In *NeurIPS*, 2017.
- [94] S. Motiian, M. Piccirilli, D. A. Adjeroh, and G. Doretto. Unified deep supervised domain adaptation and generalization. In *ICCV*, 2017.
- [95] K. Muandet, D. Balduzzi, and B. Schölkopf. Domain generalization via invariant feature representation. In *ICML*, 2013.
- [96] Y. Netzer, T. Wang, A. Coates, A. Bissacco, B. Wu, and A. Y. Ng. Reading digits in natural images with unsupervised feature learning. In *NIPS-Workshop*, 2011.
- [97] K. Nichol. Painter by numbers, WikiArt, 2016. URL <https://www.kaggle.com/c/painter-by-numbers>.
- [98] M. Noroozi and P. Favaro. Unsupervised learning of visual representations by solving jigsaw puzzles. In *ECCV*, 2016.
- [99] M. Noroozi and P. Favaro. Unsupervised learning of visual representations by solving jigsaw puzzles. In *European Conference on Computer Vision*, pages 69–84. Springer, 2016.
- [100] M. Noroozi, H. Pirsiavash, and P. Favaro. Representation learning by learning to count. In *ICCV*, 2017.
- [101] M. Noroozi, A. Vinjimoor, P. Favaro, and H. Pirsiavash. Boosting self-supervised learning via knowledge transfer. In *CVPR*, 2018.
- [102] A. Owens and A. A. Efros. Audio-visual scene analysis with self-supervised multisensory features. In *ECCV*, 2018.
- [103] D. Pathak, P. Krähenbühl, J. Donahue, T. Darrell, and A. Efros. Context encoders: Feature learning by inpainting. In *CVPR*, 2016.
- [104] X. Peng, Q. Bai, X. Xia, Z. Huang, K. Saenko, and B. Wang. Moment matching for multi-source domain adaptation. In *Proceedings of the IEEE International Conference on Computer Vision*, pages 1406–1415, 2019.
- [105] J. Ponce, M. Hebert, C. Schmid, and A. Zisserman. *Toward category-level object recognition*, volume 4170. Springer, 2007.
- [106] S. Ren, K. He, R. Girshick, and J. Sun. Faster r-cnn: Towards real-time object detection with region proposal networks. In *NIPS*, 2015.
- [107] Z. Ren and Y. J. Lee. Cross-domain self-supervised multi-task feature learning using synthetic imagery. In *CVPR*, 2018.
- [108] C. Rosenbaum, T. Klinger, and M. Riemer. Routing networks: Adaptive selection of non-linear functions for multi-task learning. *arXiv preprint arXiv:1711.01239*, 2017.

- [109] S. Ruder¹², J. Bingel, I. Augenstein, and A. Søgaard. Sluice networks: Learning what to share between loosely related tasks. *stat*, 1050:23, 2017.
- [110] P. Russo, F. M. Carlucci, T. Tommasi, and B. Caputo. From source to target and back: symmetric bi-directional adaptive gan. In *CVPR*, 2018.
- [111] K. Saenko, B. Kulis, M. Fritz, and T. Darrell. Adapting visual category models to new domains. In *ECCV*, 2010.
- [112] K. Saito, K. Watanabe, Y. Ushiku, and T. Harada. Maximum classifier discrepancy for unsupervised domain adaptation. *CVPR*, 2018.
- [113] K. Saito, Y. Ushiku, T. Harada, and K. Saenko. Strong-weak distribution alignment for adaptive object detection. In *CVPR*, 2019.
- [114] C. Sakaridis, D. Dai, and L. Van Gool. Semantic foggy scene understanding with synthetic data. *IJCV*, 126(9):973–992, 2018.
- [115] S. Sankaranarayanan, Y. Balaji, C. D. Castillo, and R. Chellappa. Generate to adapt: Aligning domains using generative adversarial networks. In *CVPR*, 2018.
- [116] P. Sermanet, C. Lynch, Y. Chebotar, J. Hsu, E. Jang, S. Schaal, and S. Levine. Time-contrastive networks: Self-supervised learning from video. In *ICRA*, 2018.
- [117] S. Shankar, V. Piratla, S. Chakrabarti, S. Chaudhuri, P. Jyothi, and S. Sarawagi. Generalizing across domains via cross-gradient training. *arXiv preprint arXiv:1804.10745*, 2018.
- [118] S. Shankar, V. Piratla, S. Chakrabarti, S. Chaudhuri, P. Jyothi, and S. Sarawagi. Generalizing across domains via cross-gradient training. In *ICLR*, 2018.
- [119] B. Sun and K. Saenko. Deep coral: Correlation alignment for deep domain adaptation. In *Workshop of the European Conference on Computer Vision (ECCV-Workshop)*, 2016.
- [120] J. Tobin, R. Fong, A. Ray, J. Schneider, W. Zaremba, and P. Abbeel. Domain randomization for transferring deep neural networks from simulation to the real world. In *International Conference on Intelligent Robots and Systems (IROS)*, 2017.
- [121] A. Torralba and A. A. Efros. Unbiased look at dataset bias. In *CVPR*, 2011.
- [122] E. Tzeng, J. Hoffman, T. Darrell, and K. Saenko. Adversarial discriminative domain adaptation. In *CVPR*, 2017.
- [123] H. Venkateswara, J. Eusebio, S. Chakraborty, and S. Panchanathan. Deep hashing network for unsupervised domain adaptation. In *CVPR*, 2017.
- [124] P. Viola and M. Jones. Rapid object detection using a boosted cascade of simple features. In *CVPR*, 2001.

- [125] R. Volpi, H. Namkoong, O. Sener, J. Duchi, V. Murino, and S. Savarese. Generalizing to unseen domains via adversarial data augmentation. In *NeurIPS*, 2018.
- [126] H. Wang, S. Ge, Z. Lipton, and E. P. Xing. Learning robust global representations by penalizing local predictive power. In *NeurIPS*, 2019.
- [127] X. Wang and A. Gupta. Unsupervised learning of visual representations using videos. In *ICCV*, 2015.
- [128] M. Wulfmeier, A. Bewley, and I. Posner. Incremental adversarial domain adaptation for continually changing environments. 2018.
- [129] R. Xie, F. Yu, J. Wang, Y. Wang, and L. Zhang. Multi-level domain adaptive learning for cross-domain detection. In *ICCV Workshops*, 2019.
- [130] J. Xu, L. Xiao, and A. M. López. Self-supervised domain adaptation for computer vision tasks. *IEEE Access*, 7:156694–156706, 2019.
- [131] M. Xu, J. Zhang, B. Ni, T. Li, C. Wang, Q. Tian, and W. Zhang. Adversarial domain adaptation with domain mixup. In *AAAI*, 2020.
- [132] R. Xu, Z. Chen, W. Zuo, J. Yan, and L. Lin. Deep cocktail network: Multi-source unsupervised domain adaptation with category shift. In *CVPR*, 2018.
- [133] R. Xu, G. Li, J. Yang, and L. Lin. Larger norm more transferable: An adaptive feature norm approach for unsupervised domain adaptation. In *ICCV*, 2019.
- [134] L. Yang, P. Luo, C. Change Loy, and X. Tang. A large-scale car dataset for fine-grained categorization and verification. In *CVPR*, 2015.
- [135] Y. Yang and T. M. Hospedales. Trace norm regularised deep multi-task learning. *arXiv preprint arXiv:1606.04038*, 2016.
- [136] F. Yu, D. Wang, E. Shelhamer, and T. Darrell. Deep layer aggregation. In *CVPR*, 2018.
- [137] X. Zhai, A. Oliver, A. Kolesnikov, and L. Beyer. S4l: Self-supervised semi-supervised learning. In *ICCV*, 2019.
- [138] H. Zhang, M. Cisse, Y. N. Dauphin, and D. Lopez-Paz. mixup: Beyond empirical risk minimization. In *ICLR*, 2018.
- [139] J. Zhang, Z. Ding, W. Li, and P. Ogunbona. Importance weighted adversarial nets for partial domain adaptation. In *CVPR*, 2018.
- [140] R. Zhang, P. Isola, and A. A. Efros. Colorful image colorization. In *European Conference on Computer Vision*, pages 649–666. Springer, 2016.
- [141] S. Zhang, L. Wen, X. Bian, Z. Lei, and S. Z. Li. Single-shot refinement neural network for object detection. In *Proceedings of the IEEE conference on computer vision and pattern recognition*, pages 4203–4212, 2018.

-
- [142] Y. Zhang and Q. Yang. A survey on multi-task learning. *CoRR*, abs/1707.08114, 2017. URL <http://arxiv.org/abs/1707.08114>.
 - [143] Y. Zhang, Y. Zhang, Q. Xu, and R. Zhang. Learning robust shape-based features for domain generalization. *IEEE Access*, 8:63748–63756, 2020.
 - [144] K. Zhou, Y. Yang, T. Hospedales, and T. Xiang. Deep domain-adversarial image generation for domain generalisation. *AAAI*, 2020.
 - [145] J.-Y. Zhu, T. Park, P. Isola, and A. A. Efros. Unpaired image-to-image translation using cycle-consistent adversarial networks. In *International Conference on Computer Vision (ICCV)*, 2017.